M.P. Tuitjer

Effect of Flexural Cracks on web-shear cracking of prestressed concrete continuous members

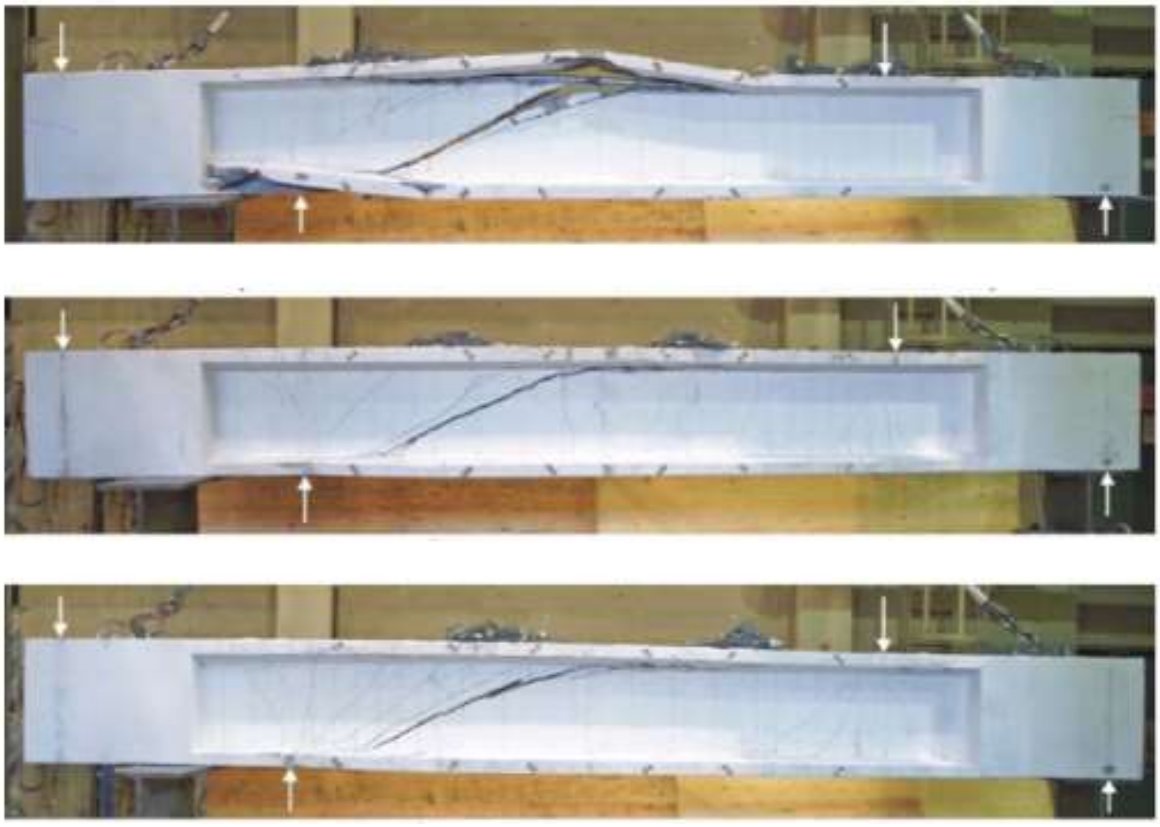

TU Delft

Effect of Flexural Cracks on web-shear cracking of prestressed concrete continuous members

By

M.P. Tuitjer
4416023

in partial fulfilment of the requirements for the degree of

Master of Science,

at the Delft University of Technology,
to be defended publicly on 16-08-2019

Thesis committee:	Dr. ir. M. A. N. Hendriks	TU Delft
	Ir. M. A. Roosen	TU Delft
	Dr. Ir. Y. Yang	TU Delft
	Ir. L. J. M. Houben	TU Delft

TU Delft

Abstract

Shear tension failure in thin-webbed prestressed concrete elements is yet to be predicted in an accurate manner. The analytical method uses assumptions to simplify the theory. This makes it less accurate. The calculated resistance to web-shear cracking is based on the principle tensile stress reaching the tensile strength of concrete. Failing in shear tension is more risky than failing in bending, since it often happens abruptly without any warnings. Previous research shows however that shear tension failure often occurs before the principle tensile stress reaches the assumed tensile strength of concrete. This means that the resistance is being overestimated. Comparisons between experimental results and theoretical models have shown that the coefficient of variation for the shear force at web-shear cracking for experiments including flexural cracks is significantly larger than for experiments without flexural cracks. It is assumed that flexural cracks are present when principle tensile stress in the outer fiber is higher than tensile strength in the flange. This indicates that the presence of flexural cracks influence the stress distribution in the areas where web-shear cracking occurs.

To find the influence of flexural cracks on web-shear cracking a well documented experiment about continuous prestress concrete members failing in shear tension is used for a case study. Namely the thesis ''The Influence of Axial Load and Prestress on The Shear Strength of Web-Shear Critical Reinforced Concrete Elements'' written by Liping Xie in 2009. Three of the specimen are chosen to be researched, between these three the only changing variable is the amount of prestress. All three fail under shear tension, however one has no observed flexural cracks, one has the flexural cracks and the web-shear cracks occur simultaneously and the last one shows flexural cracks before web-shear cracking.

Three analyses are performed per specimen: analytical analysis, linear finite element analysis (LFEA) and a non-linear finite element analysis (NLFEA). These analyses are compared to each other and to the experimental results. An outstanding result is that for every load in every specimen it holds that: $\sigma_{1\_ana} > \sigma_{1\_LFEA} \geq \sigma_{1\_NLFEA}$. The maximum principle tensile stresses calculated with an analytical method are consistently higher than principle tensile stresses that follow from a LFEA and NLFEA. This means that performing a simple analytical analyses gives a lower shear resistance than the LFEA and the NLFEA. All three analyses indicated flexural cracks for the beam in which no flexural cracks were observed. However the NLFEA showed that these were cracks of a maximum crack width of $\frac{9}{1000}$ mm at the moment of web-shear cracking. These widths are not visible by eye. All specimen showed web-shear cracks under a shear load lower than predicted, meaning all analyses overestimate the shear tension resistance.

A sensitivity analysis is performed to find the influence of shear reinforcement and of the tensile strength of the concrete. Conclusions are that the shear reinforcement has little to no influence up until the moment of web-shear cracking.

All analysis overestimate the resistance to web-shear cracking. In this thesis a sensitivity analysis is performed to the influence of the tensile strength of concrete. It is concluded that if the tensile strength of the concrete is reduced by 40% the NLFEA still results in shear forces larger than the shear force at web-shear cracking during the experiments.

Another conclusions of this research is that the presence of micro flexural cracks reduce the principle tensile stresses in the adjacent web areas. The specimen in which no flexural cracks were observed

during testing shows flexural cracks conform all analyses it is impossible to compare specimen uncracked in bending with specimen cracked in bending. Up until reaching the tensile strength of the concrete the LFEA and the NLFEA are logically equal. When the load is further increased differences between the LFEA and the NLFEA occur. It is assumed that this difference is the result of the presence of the flexural micro cracks. The specimen with the smallest flexural micro cracks showed also the smallest difference between σ_{1_LFEA} and σ_{1_NLFEA}. From this it can be concluded that larger cracks result in a larger reduction of σ_1. It is expected that if the micro flexural cracks evolve to significant flexural cracks that the principle stresses are reduced even more, resulting in a underestimation of the actual shear tension resistance.

Content

1 Introduction

Many bridges in the Netherlands are re-evaluated. Due to the fact that their original service life time is reached or due to the changes in the design standards. During the reassessment these bridged have to suffice the new regulations, the Eurocode 2. The Eurocode 2 has some big changes compared to the old standards. First of all the Eurocode 2 prescribes a heavier live load modal with heavier axle loads. This is a consequence of the ever enlarging traffic, especially the trucks with multiple axes. The second change, which is of huge interest for this thesis, is the fact that the Eurocode 2 prescribes a smaller shear capacity for shear stresses in the cross-section. Another huge influence on the reassessment on shear of old bridges is that these bridges often have none, poorly designed or not enough shear reinforcement.

The result is that during the reassessment a lot of old bridges seem to have insufficient shear resistance. It is well known that it is riskier to have an inadequate shear design than flexural design, because shear failures usually give way less signs of distress and warning before failing than flexural failure. That being said it is also known that the classical beam theory, plain sections remain plain, gives accurate results for flexural design. This allows for a rational and relatively simple flexural design for cracked and uncracked concrete members. For the determination of shear strength of prestressed or reinforced concrete members this is not the case. In this case there is no clear method yet. That shear-behavior is more complicated than flexural behavior is a consequence of all the different load-transfer mechanisms involved.

1.1 Background

1.1.1 Shear cracking

Two typical ways of shear cracking in reinforced or prestressed concrete are inclined flexure-shear cracking and inclined web-shear cracking. Flexural shear cracking occurs in areas where there is a high bending moment in combination with a high shear force. In these areas bending cracks will occur in the most outer fiber, since the bending stress will be the highest at that point following the well known $\sigma = \frac{My}{I}$. When the force is further increased some of these vertical bending cracks will evolve to inclined flexure-shear cracks. The angle of flexure-shear cracks are approximately 20 to 45 degrees.

Web-shear cracking occurs in uncracked areas, where the bending moment is small and the shear force is high. These specific cracks will originate in the web of the concrete member when the principal stress transcends the cracking strength of the concrete. When the force further increases the web-shear crack will extend towards the flanges, this can happen very rapidly. Web-shear cracks often occur in prestressed concrete beams with thin webs near the infliction point or near the end supports. Infliction points are the points where the beams deformations changes from convex to concave or the other way around, thus where the moment line crosses zero. The angle of web-shear cracks is in the range of 15 to 40 degrees.

Figure 1-1 shows the location where web-shear cracking (blue cracks) is expected and where flexure-shear cracking (red cracks) is expected in a single span. As stated before flexure-shear cracking always starts as a flexural crack, also known as bending crack. For almost all prestressed single span members the prestress is asymmetric which results in inflection points. At these points and close to the support web-shear cracking can occur.

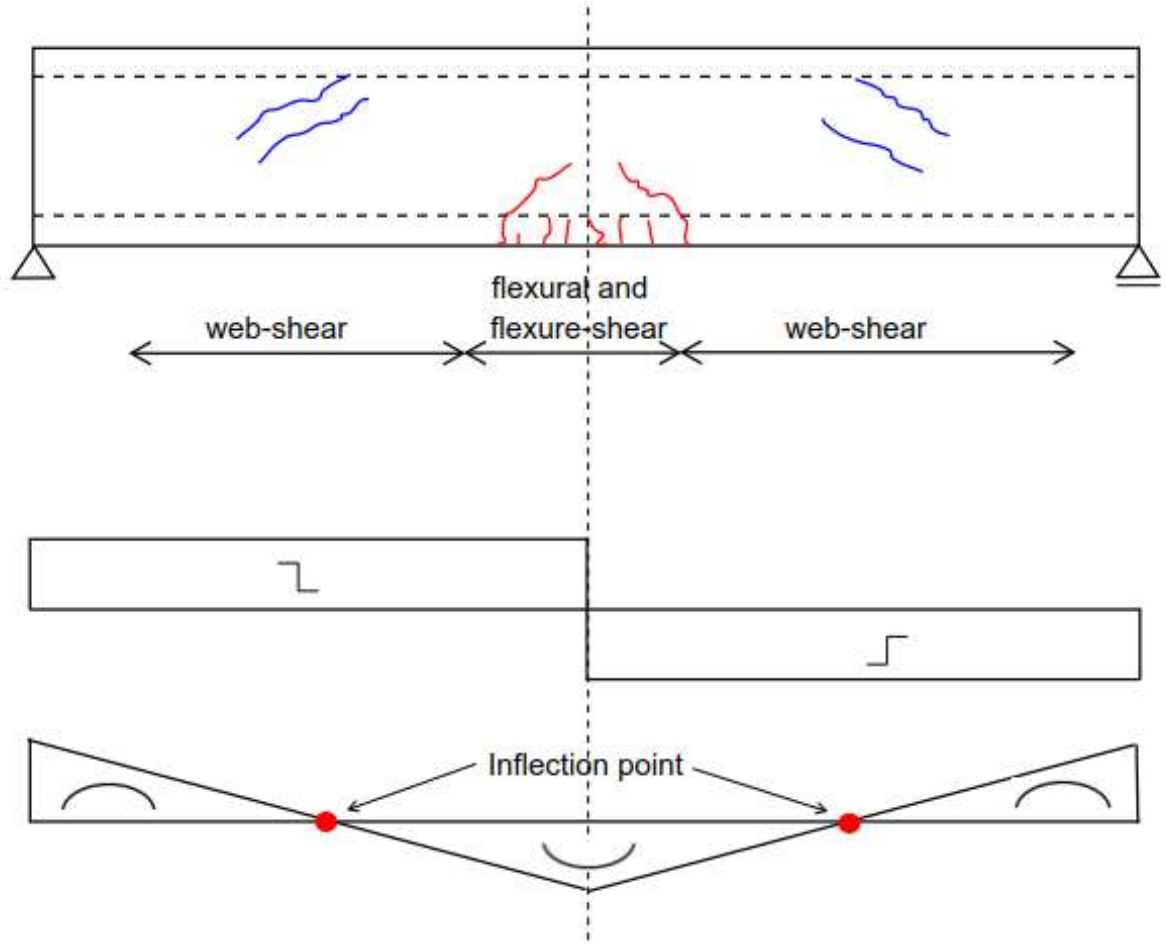

Figure 1-1 Crack patterns for prestressed single span members

In Figure 1-2 a continuos beam is schemetically shown with two point loads. Just as for the single span the locations of web-shear (blue cracks) and flexure-shear craking (red cracks) are indicated. In contrast to the single span there are inflection points in the continuos beam, see moment line. Therefore web-shear cracking can not only occur at the end supports, but also at the inflection points.

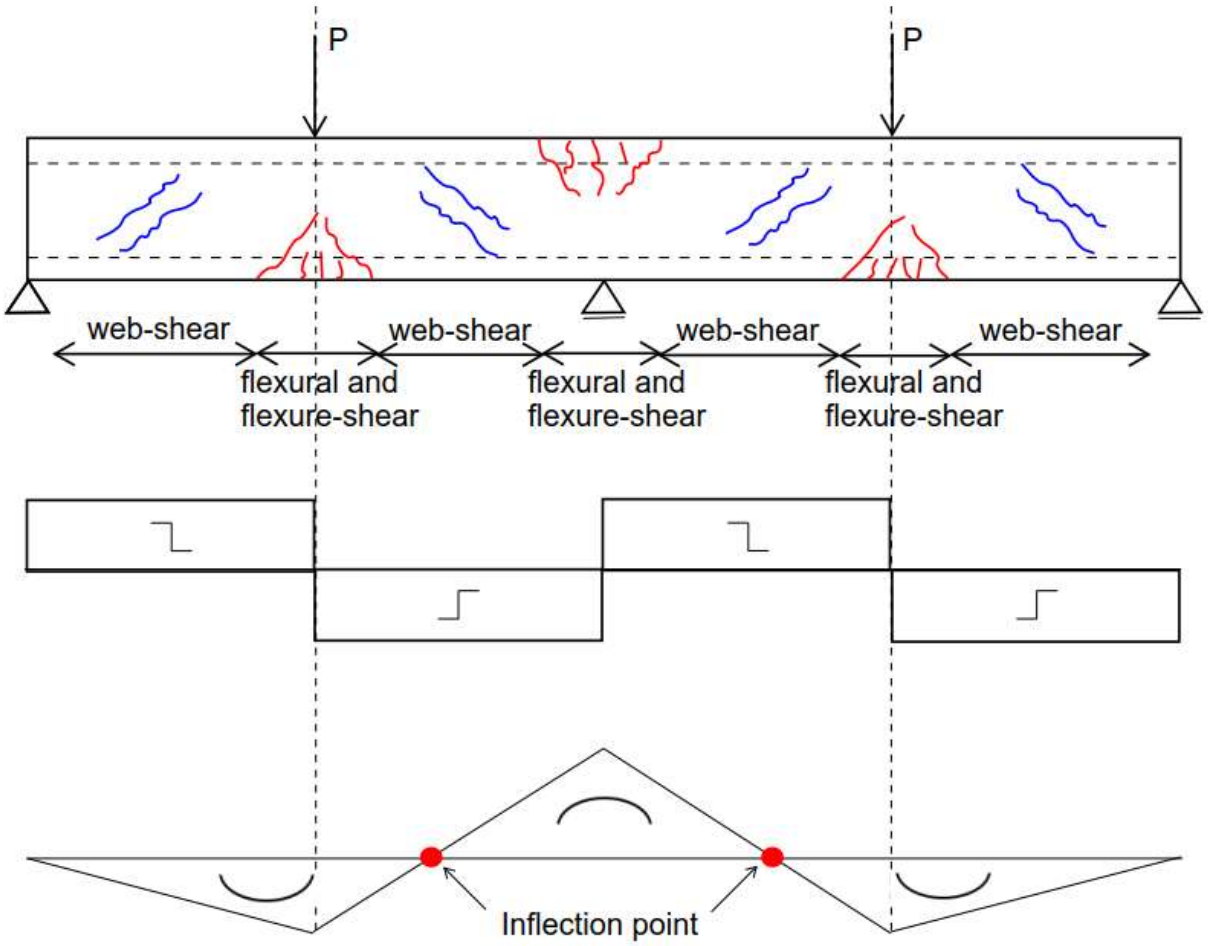

Figure 1-2 Crack patterns for prestressed continuous concrete members

1.2 Problem description

For reinforced and or prestressed thin webbed concrete members like I-beams, T-beams and box girder structures shear tension failure is of huge importance. This is due the fact shear tension failure for concrete members without or with insufficient shear reinforcement is a brittle failure mode and brittle failure modes are the most dangerous since these kind of failures give no warning before failing. If enough stirrups are present the failure is ductile.

As explained before, a lot of bridges are insufficient in the reevaluation in the shear requirements. Therefore it is highly interesting to know how conservative the codes really are. The codes seems especially conservative with the presence of flexural cracks. During reassessment it is assumed that concrete members for the regions uncracked in bending that the principle tensile stress can determined as a linear elastic stress distribution. There are doubts if this is really the case. It can be possible that the stress distribution in the regions without cracks in bending gets disturbed by the bending cracks. This might be the reason why previously done research shows that the resistance to web-shear cracking is conservative when there are bending cracks present in the specimen.

In previous research it is shown that the web-shear cracking does not always originates from the highest principle stress in the specimen. It is not quite clear why this is the case. Three reasons are being researched: size effects, additional strength of the flanges and the influence of bending cracks on the stress distribution. Size effect takes into consideration that a web-shear crack would emerge in an area where the principle tensile stress is above a certain percentage of the tensile strength rather than a single peak stress above the tensile strength. Because in a area where the neighboring elements also have a high stress there is less room for redistribution of the stresses and in bigger areas imperfections are more likely to be present. When the highest principle stress is found near the flanges it could be the case that the flanges provide extra strength and therefore counteract web-shear cracking. The last reason is the influence of present bending cracks in the specimen. This thesis is focused on finding the influence of bending cracks. It is highly interesting to get a good insight on how the stress distribution is influenced by flexural cracks and if this can be predicted and implemented in the requirement codes to get a less conservative approach.

1.2.1 Single span beams

A distinction can be made between single span and continuous beams. Single span beam are the natural starting point for requirement codes and experiments due to the simplicity.

Previous research to the resistance to diagonal tension cracking in prestressed beams [SJ Kroeze, 2018] concludes that the experiments without flexural cracks and without exceeding the uniaxial tensile strength in the ultimate fiber gives the most consistent outcome. For specimen with flexural cracks the outcome varies significantly more. The results are shown in Table 1-1. In this table the specimen are divided into two groups: all specimen and only the specimen without flexural cracks. Kroeze uses multiple methods of finding the maximum principle stress, in this table the method of checking for the highest principle stress over the height and only checking at the center of gravity are presented. These methods are both used in several requirement codes. This table shows that the specimen without flexural cracks have a lower $\frac{\sigma_1}{f_{ctm}}$ and a much lower coefficient of variation. The magnitude of the coefficient of variation for all specimen, and thus including specimen with flexural cracks, is with 16 and 12 percent still acceptable. However this does imply a decent influence of flexural cracks. To come to this conclusion only linear elastic finite element analysis were performed. A short overview of this thesis and the conclusions is given in the literature review, chapter 2.3.1.

Table 1-1 Single span mean and C.o.V. for uncracked and cracked specimen. Source: Kroeze (2018)

Single span		**all specimen**	**only specimen without flexural cracks**
	Number of experiments	29	11
Checking for σ_1 over height	*mean*	1.18	1.09
	C.o.V	0.16	0.06
Checking for σ_1 only at center of gravity	*mean*	0.81	0.79
	C.o.V	0.12	0.06

Suitability of shear tension code requirements for assessment of existing structures [Roosen, 2011] confirms that there is an influence of bending cracks. In this paper the experimental shear resistance of 15 beams without flexural cracks and 36 beams with flexural cracks are compared with the shear resistance confirm three different requirement codes. It should be noted that the experiments used by the paper includes the experiments that SJ Kroeze used. The codes used are Eurocode 2, ACI and de fib Modelcode 2010. It was concluded that the mean, experimental found resistance to web-shear cracking divided by the predicted mean shear tension capacity, for specimen cracked in bending is above 1.2 to even 1.45. Where a value of 1 would mean that the prediction is exact, therefore the requirement codes seem quite conservative. The coefficient of variation is also larger for specimen cracked in bending with a value approximately 0.14. This is three times as large as the coefficient of variation for specimen uncracked in bending, but still an acceptable value. The mean for the specimen uncracked in bending match the predictions conform the codes quite accurate with values between 1.05 and 1.2.

1.2.2 Continuous beams

For continuous beams a lot less research is found. There is however a well-documented test report of the influence of axial load and prestress on the shear strength of web-shear critical reinforced concrete members [Xie, 2009], a summary of this this can be found in paragraph 2.3.1. Table 1-2 shows the experimental research compared to checking the for the max principle stress over the height and checking only at the center of gravity. The result is comparable to the results of single span. The coefficient of variation is again notably larger for all specimen, thus including specimen with bending cracks. Also it can be noted that the method which checks only at the center of gravity seems to have less influence of the presence of bending cracks. Furthermore it can be seen that the mean drops below 1, which indicates an overestimation of the resistance to web-shear cracking.

Table 1-2 Continuous mean and C.o.V. for uncracked and cracked specimen. Source: Xie (2009)

Continuous beams		**all specimen**	**only specimen without flexural cracks**
Number of experiments		11	3
Checking for σ_1 over height	$\frac{V_{exp}}{V_{height}}$	1.12	0.95
	C.o.V	0.47	0.08
Checking for σ_1 only at center of gravity	$\frac{V_{exp}}{V_{CoG}}$	0.71	0.77
	C.o.V	0.18	0.05

1.3 Research question and scope

The aim of this thesis is to find a way to improve the predictions of the resistance of web shear cracking for concrete members without shear reinforcement. Therefore the main question is as follows:

How can the shear tension resistance of concrete members without shear reinforcement be predicted in the most accurate way?

To answer this main question the following sub questions will be addressed:

- What is the influence of the presence of bending cracks on the stress distribution in the uncracked zones?
- What is the influence of the presence of bending cracks on shear tension failure?
- To which extend can the requirement codes be applied to continuous prestressed reinforced members?

The first and second sub questions follows from previous research, as specified in the problem description, where it is predicted that the safety factor is more conservative and the coefficient of variation is higher with the presence of bending cracks. To answer these two sub questions a comparison between experimental, analytical and numerical will be made, this is described in depth in chapter 3. To really get a good insight of how the stress distribution in concrete member with flexural cracks are influenced a non-linear finite element analysis will be performed.

The codes requirement are written for single span beams. However in practice continuous beams are used on a regular basis. Therefore it is interesting to research if or how the requirement codes can be applied to continuous beams. This explains the third sub question.

1.4 Outline

In chapter 2 it is described how the ACI building codes, Eurocode 2 and the fib Model Code 2010 deal with web-shear failure. Also a literature review is performed on previous theses about web-shear cracking. In chapter 3 the methodology of this thesis is described. Chapter 4 includes a description of the test set-up, the properties of the materials and the experimental results. The analytical method and results are given in chapter 5. In chapter 6 a linear finite element analysis (LFEA) is described. This includes the model, the results and the comparison to the analytical analysis and the experimental results. In chapter 6 a non-linear finite element analysis is performed. In which the model and the results are given. Also a comparison to the LFEA, the analytical analysis and the experimental results is made. Finally in chapter 8 the conclusions of this research are made.

2 Literature study

2.1 Requirement codes

As stated in the problem description it is suspected that the requirement codes are conservative on the shear tension failure. The discussed codes in this thesis are the ACI building codes (ACI), Eurocode 2 (EC2) and the fib Model Code 2010 (MC2010). All these codes use the same concept, namely if the principle tensile stress in the web is higher than the tensile strength of the concrete. The EC2 and the MC2010 assume that a region cracked in flexure shear is governing over web-shear. The ACI makes no distinction between regions with and without bending cracks. The principle tensile stress is calculated using the Mohr's circle, see Figure 2-1. The Mohr's circle is a two-dimensional graphical representation of the transformation law for the Cauchy stress tensor. The first figure shows the element stress state, this is the ratio of shear and normal stresses on an element of the concrete. These can be transformed to a stress state in which the shear stresses are zero and the normal stresses are at their maximum using Mohr's circle.

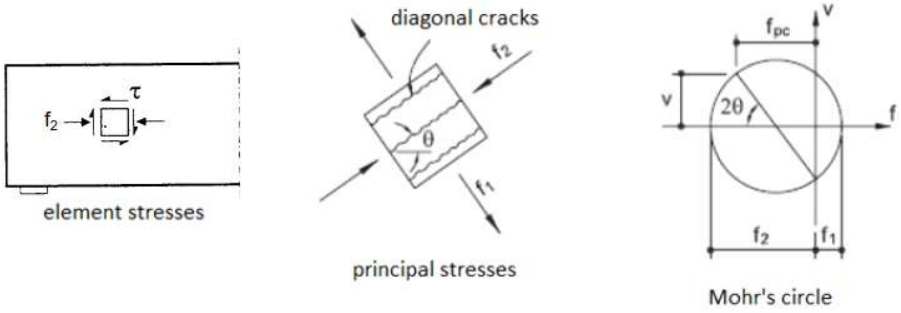

Figure 2-1 Principal stresses conform Mohr's circle

From the Mohr's circle a formula for the principals tensile stress can be found:

$$\sigma_1, \sigma_2 = \frac{\sigma_x + \sigma_y}{2} \pm \sqrt{\left(\frac{\sigma_x - \sigma_y}{2}\right)^2 + \tau^2} \tag{2.1}$$

In which σ_x is the normal stress in the concrete, σ_y is the perpendicular stress to the normal stress and τ is the shear stress at the same point. This formula can be rewriting by using the following equations for the shear and the normal stress:

$$\tau = \frac{V_{Rd,ct} S}{b_w I} \tag{2.2}$$

$$\sigma_x = \alpha_1 \sigma_{cp} \tag{2.3}$$

Where $V_{Rd,ct}$ is the shear resistance of the concrete, S is the first moment of area, I is the second moment of area also known as the moment of inertia, b_w is the width of the cross-section, σ_{cp} is the normal stress in the concrete, which is calculated with the formula 2.4 for prestressing beams. This formula is based on a Euler-Bernoulli beam, which uses the hypotheses that plane sections remain plane and normal to the axis of the beam during deformation.

$$\sigma_{cp}(x,y) = \frac{N}{A(x)} + \frac{M(x)y}{I} \tag{2.4}$$

In which N is the normal force, this is equal to the prestressing force in most cases. The area of the cross-section is denoted as A. M(x) is the bending moment varying over x. The height of the coordinated is given by y and I is the well known moment of inertia. There is no clear way to calculate the vertical stress σ_y and in practice the vertical stress is often neglected.

After substitution the stress limit can be expressed in a formula 2.2:

$$V_{R,ct} = \frac{I_c b_w}{S_c}\sqrt{f_{ct}^2 + \alpha_1 \sigma_{cp} f_{ct}} \tag{2.5}$$

Although the EC2, ACI and MC2010 all start from the same principle they have different assumptions and conditions for when and how to apply formula 2.5.

2.1.1 Eurocode

The Eurocode divides shear requirements into two categories namely with and without shear reinforcements. It's already stated that many of the old concrete structures have none or badly designed shear reinforcement, it is therefore difficult to choose which category some concrete members belong to.

Elements without shear reinforcement

For single span concrete members without shear reinforcement the member is divided in different regions. The regions are cracked and uncracked in bending. In figure 1 for single span and in figure 2 for continuous beam these regions are indicated. It is also shown which failure modes are expected in each zone. As explained before shear tension failure is expected in regions with a small moment, a high normal force and a large shear force. Whereas flexural shear failure is expected in the regions with a large moment, a low normal force and a high shear force. Therefore shear flexural cracking is expecting in the zone with bending cracks.

According to the Eurocode formula 2.5, this is equation 6.4 from the Eurocode, is feasible for the uncracked regions of single span concrete members without shear reinforcement. There are some conditions set for this formulae. First of all the stress in the outer fibre needs to be lower than the mean tensile strength of the concrete, otherwise there would be bending cracks. Secondly for the set distance (x) of the support it is not required to fulfil the equation. This regions is called the disturbed region. It is assumed that in these regions the stress distribution is disturbed by reaction forces or concentrated loads. The distance for which this is the case is a line drawn with a 45° angle from the inner edge of the support until crossing the neutral axis of the beam. This is graphically presented in Figure 2-2.

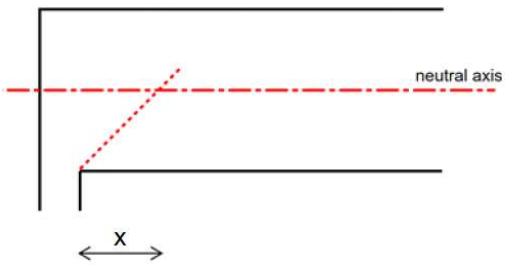

Figure 2-2 Disturbed region

There are two different methods of finding the governing principle stress: the first method is searching for the highest principle stress at various axis and the second method only considers the neutral axes. The Eurocode requires, when the width changes over the height, checks at various axis to find the maximum principle stress, see Figure 2-3. It is likely that the maximum shear force is found at the intersection between the web and the flanges.

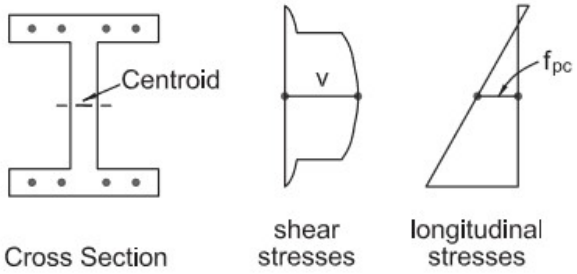

Figure 2-3 Stress at centroid axis

For regions with flexural cracks, thus the regions with a high moment and a relatively high shear force, the design shear resistance is calculated in a total different way.

2.1.2 Fib Modelcode 2010

According to the MC2010 the design shear resistance of single span prestressed hollow core slabs without shear reinforcement occurs when the principal tension stress demand in the web exceeds the tensile strength of the concrete. Although the MC2010 specifically states that the formulas are for hollow core slabs the formulas below are also used for beams without shear reinforcement.

The MC2010 gives approximations for calculating the design shear resistance. These two levels of approximations are the two methods in sub question 2. Namely only check for the highest tensile principle stress at the neutral axis with a reduction in the concrete tensile strength and check for the highest tensile principle stress at various axis without any reduction in the concrete tensile strength.

Approximation level 1 considers the principal tensile stress only at the centroidal axis and states that the design shear resistance is given by:

$$V_{R,ct} = 0.8\frac{I_c b_w}{S_c}\sqrt{f_{ct}^2 + \alpha_1 \sigma_{cp} f_{ct}} \tag{2.6}$$

This is exactly the same formula as formula 2.5, the only difference is the reduction factor of 0.8. Which is added due to only considering stresses at the centroidal axis.

Approximation level 2 considers the principal tensile stress at various axis. Therefore the parameters changing over the height are a function over the height. The design shear resistance is then given by:

$$V_{R,ct} = \frac{I_c b_w(y)}{S_c(y)} \left[\sqrt{f_{ct}^2 + \alpha_1 \sigma_{cp}(y) f_{ct}} - \tau_{cp}(y) \right] \tag{2.7}$$

Where:

$b_w(y)$ is the width of the cross section at the height y;

$S_c(y)$ first moment of area above y\height y and about the centroidal axis;

$\sigma_{cp}(y)$ is the concrete compressive stress at height y and distance l_x;

$\tau_{cp}(y)$ is the shear stress in the concrete due to transmission of prestress at height y and distance l_x;

The concrete compressive stress at height y and distance l_x can be determined as follows:

$$\sigma_{cp}(y) = \left[\frac{1}{A_c} + \frac{y_c - y}{I} \right] F_p(l_x) \tag{2.8}$$

And the shear stress in the concrete due to transmission of prestress at height y and distance l_x is given by:

$$\tau_{cp}(y) = \frac{1}{b_w(y)} \left[\frac{A_c(y)}{A_c} - \frac{S_c(y)(y_c - y_{pt})}{I} \right] \frac{dF_p(l_x)}{dx} \tag{2.9}$$

Where:

y_c is the height of the concrete centroidal axis;

A_c is the area of the concrete cross section;

$A_c(y)$ is the area of the concrete above height y;

y_{pt} is the height of centroidal axis of the prestress;

$F_p(l_x)$ is the prestressing force at distance l_x;

2.1.3 ACI building code 318-08

The ACI is based on the same concept as the MC2010, namely that the design shear resistance of the beam is the summation of the shear resistance of the concrete and the shear resistance of the shear reinforcement. Thus formula 2.28 holds for the ACI.

$$V_{Rd} = V_{Rd,c} + V_{Rd,s} \geq V_{Ed} \tag{2.10}$$

There is however a big difference in approach between the ACI and both the EC2 and MC2010. Namely that the ACI does not make a distinction between with and without shear reinforcement and also not between single span- and continuous beams. The ACI does however makes a distinction between non-prestressed and prestressed members. The formulas given for non-prestressed and prestressed members are not interchangeable by setting the prestress force to zero. This is a result of the fact that only the equations for designing web-shear cracking are based on the Mohr's circle. All other equations

are obtained by numerical curve fitting. The formulas for non-prestressing members are not included in this thesis, since the focus is on prestressing members only.

Web-shear cracking

The ACI only checks the maximum stresses at the centroidal axis, just like the MC2010 approximation level 1 for hollow core slabs. Since the stresses are not checked at different axes and to take shrinkage into account a reduction is applied, the permitted principal tensile stress are set to the cracking strength of concrete. This cracking strength follows from a split cylinder test and is a conservative approach. Since the cracking strength is found to be lower than the in the EC2 and MC2010 used tensile strength of concrete.

Prestressed members

For prestressed concrete members the shear resistance of the concrete is the minimum of the shear resistance to web-shear cracking and shear resistance to flexure-shear cracking. Thus given the shear resistance of concrete is given formula xx. This is differs from the MC2010 and the EC2.

The critical section differs from the critical section of non-prestressed members. For prestressed members the critical section is h/2 from the face of the support.

$$V_c = \min(V_{ci}, V_{cw}) \tag{2.11}$$

Where:

V_{ci} is the resistance to flexural-shear cracking;

V_{cw} is the resistance to web-shear cracking;

The resistance of the concrete to flexural shear cracking is giving in equation 2.37. In this equation describes the first term the force required for a flexural crack to develop to a flexural-shear crack.

$$V_{ci} = 0.0498\sqrt{f_c'}b_w d + \frac{V_u M_{ct}}{M_u} \tag{2.12}$$

With:

$$V_{ci} \leq 0.141\sqrt{f_c'}b_w d \tag{2.13}$$

$$M_{ct} = \left(\frac{I}{y_t}\right)\left(0.498\sqrt{f_c'} + f_{pe}\right) \tag{2.14}$$

Where:

M_{ct} as the total moment required to cause cracking at the extreme fiber in tension;

f_{pe} is the compressive stress in the concrete due to effective prestress force only at the extreme fiber of section where tensile stress is caused by externally applied loads. After allowance for all prestress losses;

y_t is the distance from centroid of gross section, neglecting reinforcement, to extreme fiber in tension;

The resistance of the concrete to web-shear cracking is a simplified version of equation 2.5 and is given by the following formula:

$$V_{cw} = \left(0.291\sqrt{f_c'} + 0.3f_{pc}\right) b_w d + V_p \tag{2.15}$$

Where:

f_{pc} is the compressive stress in the concrete (after allowance for all prestress losses) at centroid of cross section resisting externally applied loads;

V_p is the vertical component of the effective prestress force at section;

2.3 Literature review

In this paragraph the theses of L. Xie (2009), SJ. Koeze (2018) and A. Sugianto (2019). L. Xie performed several test on prestressed thin webbed beams. These test will be the base of this thesis and will be reconstructed with finite element program Diana. SJ. Kroeze and A.sugianto both performed a research on the failure mechanism web-shear cracking.

2.3.1 L. Xie

The thesis '' The influence of axial load and prestress on the shear strength of web-shear critical reinforced concrete elements'' written by Xie in 2009. She performed several beams and panel test and looked at the prediction of the resistance conform the ACI and Canadian Standards Association (CSA). It was concluded that beams subjected to very high compression resulted in an extremely violent way of failure. Even when more stirrups were added. Furthermore it is concluded that web-shear cracking is generously overestimated by traditional method. The influence of the flanges on the stiffness and strength is found. Beams with thick flanges are slightly stronger than the beams with thin flanges. The increase in shear strength is approximately 10% with flange thickness of 75 mm instead of 50 mm.

The shear strength is increased by prestressing and reduced by axial tension. The ACI underestimates the shear strength of beams subjected to tension and heavily overestimates the beams subjected to compression. The influence of the axial force on web-shear cracking was very different than the ACI predicted.

The predictions conform the ACI code agreed very poorly with the experiments and were very inconsistent. One of the reasons might be the treatment of tension and compression in the ACI. Not only the location was predicted wrong in most cases, but also the ultimate shear strength. The ACI predicts an almost linear increase in web-shear resistance with the increase of stirrups, this is also found in the tests.

In Table 1-2 a the C.o.V. and the mean of the results of Xie are shown. From this table it follows that the resistance to web-shear cracking is overestimated when bending cracks are present. This follow from the fact that the mean values, shear resistance of the experiment divided by the shear resistance according to the requirement codes, is 0.95 for specimen without bending cracks. The C.o.V. is significantly higher when the specimen with flexure are included. Indicating a influence of flexural cracks on the shear tension resistance.

2.3.2 SJ. Kroeze

The main purpose of this research is to determine which model predicts the resistance with respect to the formation of shear tension cracks in the most accurate way. This is done by performing an analytical- and a linear elastic FEM analysis of 29 single span beam experiments performed by Choulli (2005) and Elzanaty (1986).

One of the biggest conclusion indicates the problem of this thesis, namely that the experiments without flexural cracks and without exceeding the uniaxial tensile strength in the ultimate fibre give the most consistent outcome. This means that the influence of flexural cracks on the stress distribution can be significant. This conclusion followed from the LFEA.

Another conclusion of the research is that the proposed analytical model is only checking for the highest principle stress at the neutral axis, with a reduction to the uniaxial strength. A proposition is made that the reduction should be 20% of the uniaxial strength.

2.3.3 A. Sugianto

The aim of the thesis of Sugianto is to verify if there is a relation between the uniaxial tensile strength and the web-shear cracking of prestressed concrete beams. To achieve this goal the experiments of Hanson (1964), Choulli (2005), and Elzanaty (1986) were studied with a linear finite element analysis to get an insight of the more refined principle stress distribution at the location of the web-shear crack. Sugianto proposed two new methods to ensure the presence of size effect, the σ_1 area method and the ratio-of-distances method. These methods are introduced to make it possible to study size effect on experimental-size beams. Both methods confirm the presence of size effect. However Sugianto describes that several specimen were found to be unfit due to the presence of bending cracks. One of the recommendations is to perform a NLFEA on specimens with flexural cracks, which is done in this thesis.

3 Methodology

In this chapter an overview is given of the steps that are taken to get to answer the main and sub questions of this thesis. As already stated in the problem description experiments show that the coefficient of variation increased with the presence of flexural cracks, see Table 1-1 and Table 1-2. To capture the protentional influence of the bending cracks and to find the most accurate way of shear tension resistance of reinforced concrete members without shear reinforcement a comparison has to be made between experimental-, analytical-, and numerical results. Figure 3-1 gives a schematic overview of the comparisons that will be made.

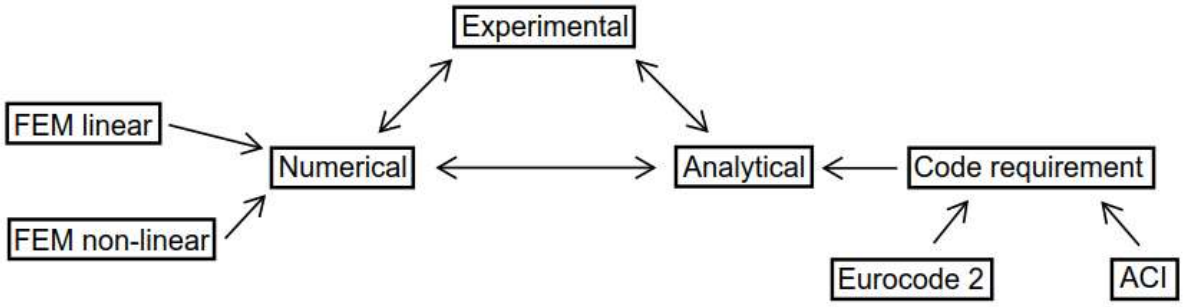

Figure 3-1 Schematic overview of the method

The experimental results act as a guideline for the comparison between all analyses. For this thesis no experiments are performed, therefore results of already executed experiments are used. The experiments used in this thesis are based on the those of L. Xie. Her detailed report perfectly describes the specimen, test-set up, material properties, as-built dimensions and results of eleven prestressed I-profiled beams.

The results of the EC2 analytical analysis includes the results of the ACI, since the EC2 requires the stress calculation of the height and over the longitudinal axis and the ACI only requires the stresses at the CoG along the longitudinal axis. The results of the analytical analysis can be compared to the experimental results. It can be observed if the principle tensile stresses calculated exceed the tensile strength of the concrete. This way the location of potential cracks can be compared to the actual cracking pattern found during testing.

Comparing the analytical results with the LFEA results gives an insight in the influence of the assumptions made in the analytical analysis. These assumptions are described in chapter 5.1. The LFEA is also compared to the experimental results. This is done in the same way as the analytical analysis, namely comparing the locations where $\sigma_1 > f_{ctm}$ with the crack pattern found in the experiments.

The NLFEA is firstly compared to the experimental results to see if or how far the crack patterns match. Furthermore a force displacement is compared.

To see the influence of bending cracks on the principle stress distribution of a NLFEA is needed. The shear force at which the principle tensile stress reaches f_{ctm} in the web indicated the originating of a web-shear crack. At this moment the NLFEA is compared to the LFEA. The difference in principle tensile stress is caused by the presence of bending cracks, since the model is the same except for the non-

linearity in the concrete. It is assumed that in the specimen without bending cracks the principle stress found in the NLFEA and in the LFEA are approximately equal. If this is the case than a cause for the high C.o.V. in experiments with bending cracks is found.

4 Experiment

4.1 Experimental set-up

The eleven beams are all thin webbed I-section beams under different axial force and shear force and are identified as LB1 to LB11. For easy reference the same labels are used. The applied axial force varies between $-800\ kN$ compression and $500\ kN$ tension. The specimens are all tested in the same setup, Figure 4-1. The beam is tested as a continuous beam, since the left support is not an end support. The middle part of the beams, with a length of $l_w = 3220\ mm$, is a thin webbed I-shaped cross-section. Both ends of the beams, a 700 mm long diaphragm block, are used to transfer the prestressing force from the end to the middle part of the beams. The test setup is designed in such a way that double bending and a constant shear force are introduced in the test region of 2400 mm long (the region between the left-hand support and the right-hand point load), this is shown in Figure 4-2. As explained in chapter before double bending happens with an inclination point. In this point web-shear cracking is expected.

The specimens are divided into two groups. Group 1 consists of beam LB1 to LB5 and have thick flanges of 75mm and group 2 consists of beam LB6 to LB11 and have thin flanges of 50mm, see Figure 4-1. The specimens are sorted to the axial force they were subjected to per group, thus LB1 highest compression force of group 1 and LB5 highest tension force of group 1.

Not all eleven specimens are useful for this thesis. LB1 is a pilot specimen and showed seven vertical shrinkage cracks due to the restraining of the wooden formwork and the longitudinal reinforcement. This is more than all the other specimens. After LB1 the formwork was changed from wood to Styrofoam, which was easier to demold. During testing LB1 behaved differently than the other specimens and is therefore neglected. Since this thesis is interested in prestressed beams the specimens with 0 prestress or even tension axial stresses are also neglected. The specimens that remain are LB2, LB3, LB6, LB7, LB8, LB10 and LB11. To do a complete analyses a selection of three is made, namely LB6-LB8. These specimens are chosen because these are very comparable. The prestressing force is the only variable that changes and at the moment of web shear cracking LB6 has no bending cracks, LB7 does have bending cracks and specimen LB8 the bending cracks and web shear cracking happens simultaneously.

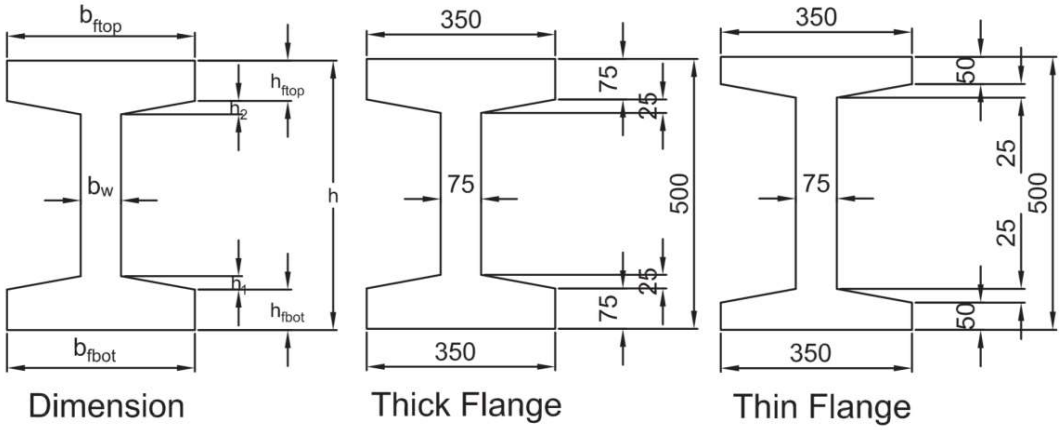

Figure 4-1 Cross-sections. Source: Xie (2009)

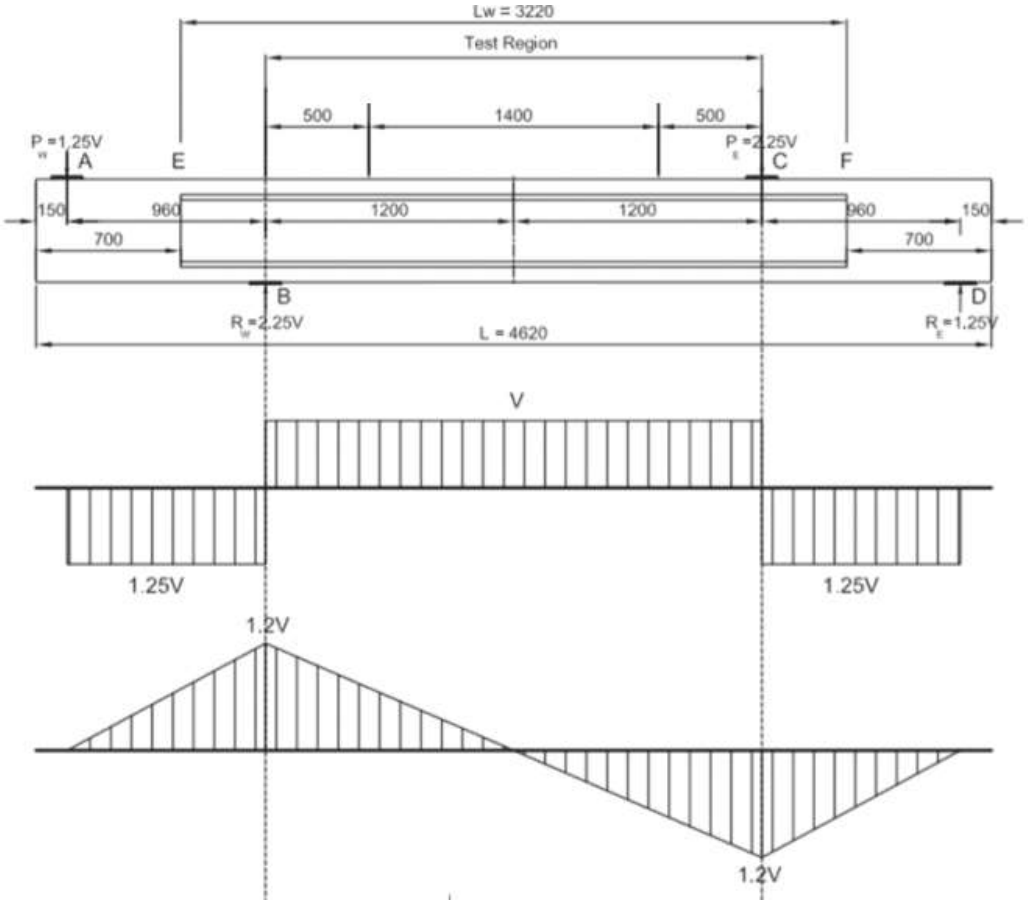

Figure 4-2 Overview beam and V-, M-line. Source: Xie (2009)

In Table 4-1, all as-built dimensions of the specimens of interest are given. The d is the distance from the extreme compression fiber to centroid of longitudinal tension reinforcement, but not less than 0.8h for prestressed members. The N is the normal force, which is the prestressing force. The prestressing force is applied on one side and is equally divided over the top and bottom prestressing ducts.

Table 4-1 As-built dimensions. Source: Xie (2009)

Specimen	**LB6**	**LB7**	**LB8**
h [mm]	506	506	504
b_w *[mm]*	73	73	73
b_{ftop} *[mm]*	350	353	352
h_{ftop} *[mm]*	55	55	51
b_{fbot} *[mm]*	350	353	352
h_{fbot} *[mm]*	51	51	53
h1 [mm]	25	25	25
h2 [mm]	25	25	25
d [mm]	473	471	473
A_{stop} *[mm²]*	934	934	934
A_{sbot} *[mm²]*	934	934	934
N [kN]	-797	-255/-319	-319

4.1.1 Reinforcement layout

The reinforcement is composed out of three parts. The longitudinal reinforcement, the transverse reinforcement and the unbonded prestressing bars within a conduit duct. The longitudinal reinforcement is designed not to yield at web-shear failure. Deformed 15M bars are used as longitudinal reinforcement. The transverse reinforcement is designed in such a way to ensure web-shear failure in the test region. D4 cold-drawn deformed wires are used as transverse reinforcement for all specimens. The transverse reinforcement in the test region is not the same for all specimens. Outside the test region the transverse reinforcement is the same for all specimens, namely 10M deformed bars spaced at 125 mm, approximately triple the reinforcement of the test region. This is done because the shear outside the test region is higher than within the test region, see Figure 4-2. The dimensions and reinforcement for LB6-LB8 are the same and shown in Figure 4-3.

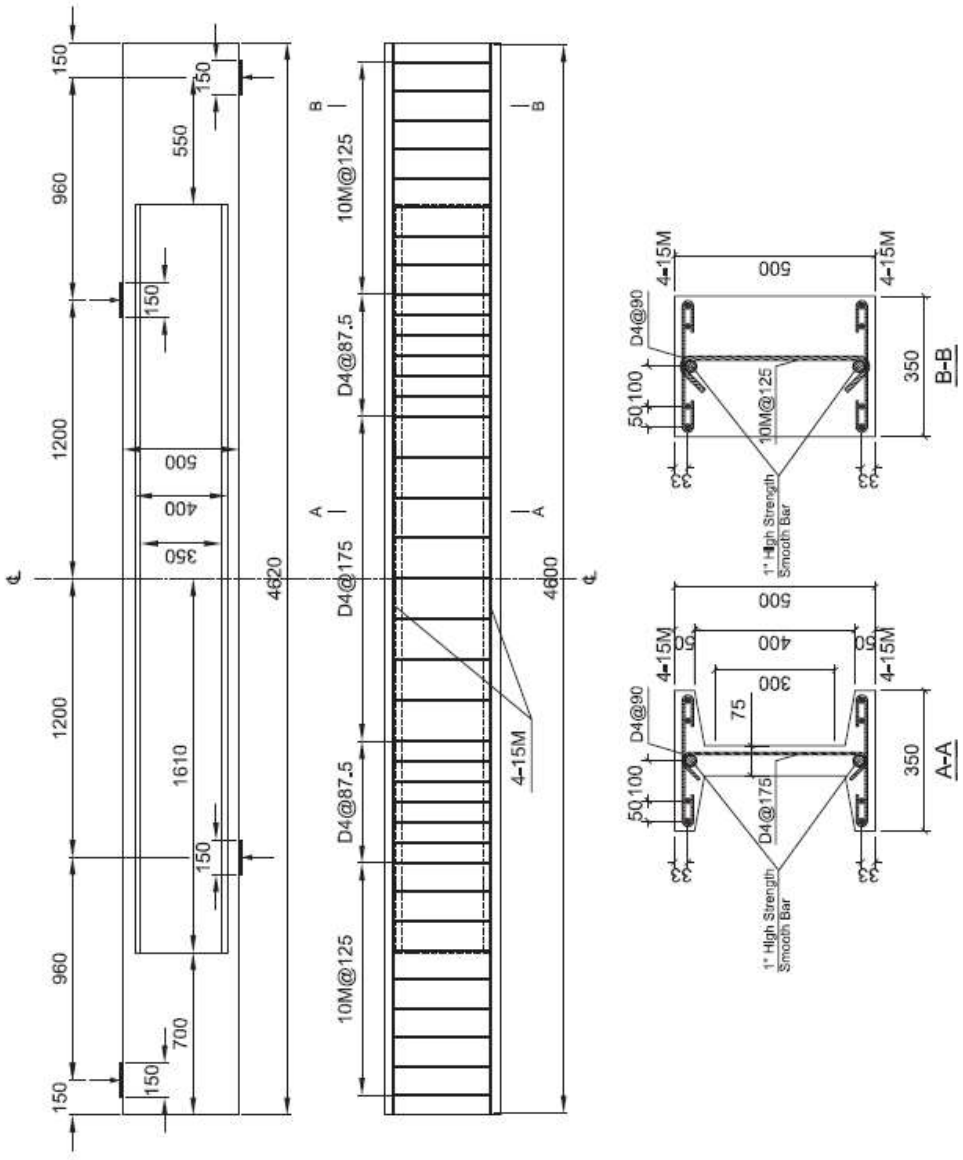

Figure 4-3 Reinforcement layout. Source: Xie (2009)

4.1.2 Material properties

4.1.2.1 Concrete

The used concrete is ready-mixed self-compacting concrete (SCC). The specified concrete strength was 35 MPa, but is tested more precisely at 7-day, 14-day, 28-day and at test day. The compressive strengths found are shown in the table below.

Table 4-2 Concrete properties. Source: Xie (2009)

Specimen	**LB7-LB8**
7-day [MPa]	50.7
14-day [MPa]	55.6
28-day [MPa]	56.2
Age at test [days]	62
At test [MPa]	63.5
E_c [MPa]	40300
f_t' [MPa]	2.63
ϵ_c' [mϵ]	2.47
f_r [MPa]	473

In the table is also the Young's modulus given. The Young's modulus is calculated conform the ASTM standard (the American Society for Testing Materials), the following equation is used:

$$E_c = \frac{\sigma_2 - \sigma_1}{\epsilon_2 - \epsilon_1} \tag{2.1}$$

In which σ_2 is equal to 40% of f_c' and ϵ_2 the corresponding strain and ϵ_1 is equal to $50 * 10^{-6}$ and σ_1 the corresponding stress.

Also the specified tensile strength (f_t') is given in the table. This is not a measured value, but calculated from the measured concrete compressive strength as shown in equation 2.1:

$$f_t' = 0.33\sqrt{f_c'} \tag{2.1}$$

Lastly the f_r is given, this is the modules of rupture. These values are obtained by test at test day.

In figure xx is the average concrete stress-strain relation is shown for LB6-LB9. This full stress-strain responses are obtained by test at test day.

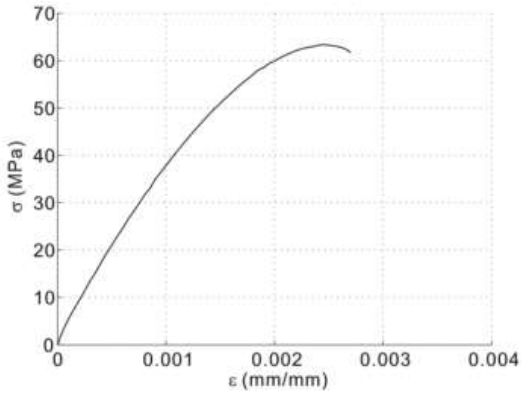

Figure 4-4 Stress strain relation of concrete. Source: Xie (2009)

4.1.2.2 Reinforcement

The table below all the specifications of the different reinforcement steel used is given. These are obtained by performing test conform ASTM standard.

Table 4-3 Reinforcement properties. Source: Xie (2009)

Size	d_b [mm]	A_s [mm^2]	f_y [MPa]	f_u [MPa]	ϵ_y [$m\epsilon$]	ϵ_u [$m\epsilon$]	Es [MPa]
D4	5.72	24.2	529	581	2.65	40	195800
10M	11.3	100	431	571	2.16	140	201880
15M	16	200	409	671	2.05	130	201100
Prestressing bar	25.4	507	972	1074	-	-	199400
Duct	-	134	300	400	1.50	100	200000

Figure 4-5 shows the stress-strain relation of 10M and 15M. The stress-strain relation of the smooth high-strength rod is given in Figure 4-6.

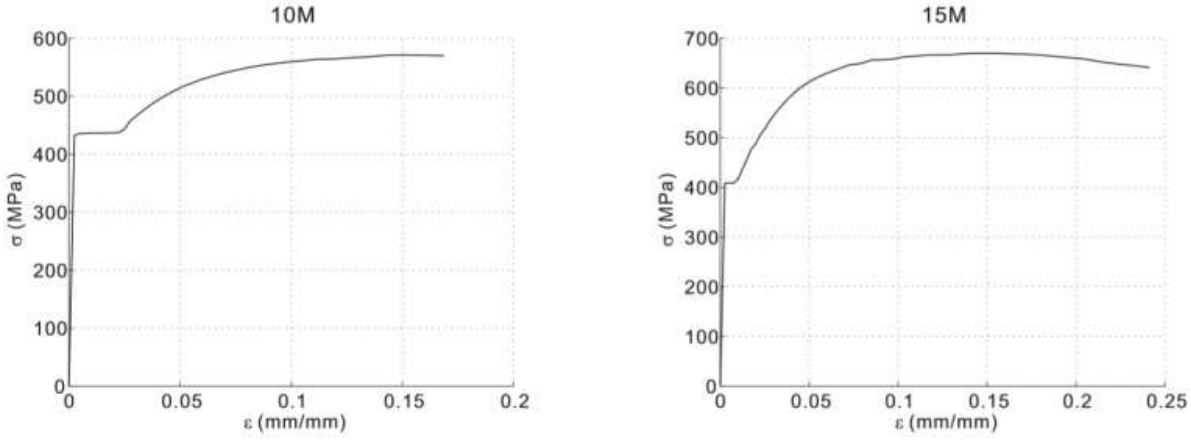

Figure 4-5 Stress strain relation longitudinal reinforcement. Source: Xie (2009)

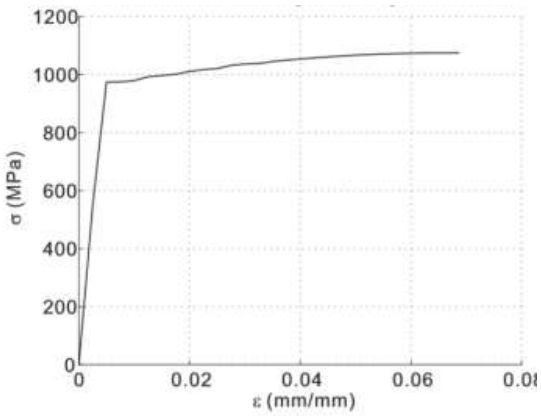

Figure 4-6 Stress strain relation prestress bar. Source: Xie (2009)

4.2 Test set-up

The prestress is applied through two unbonded one-inch high-strength smooth bars, one in the top- and one in the bottom flange. Several decisions are made to keep the friction loss at a minimum: smooth bars are used, prestressing bars were kept in the ducts during the casting process to keep the ducts straight and grease was used.

The prestressing was applied through post-tensioning at one end. This was done in a conventional way. With prestressing bars longer than the specimen which were connected to steel plates using nuts at one end and were connected to the jacking apparatus at the other end. This is shown in Figure 4-7.

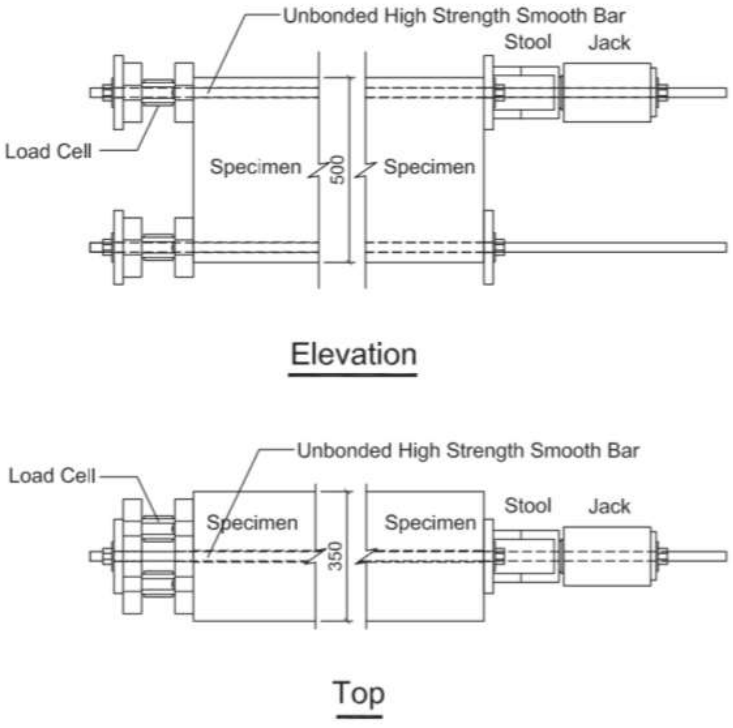

Figure 4-7 Prestressing set-up. Source: Xie (2009)

The point loads are introduced with the help of a spreader beam to get the right ratio between the forces, because the left-hand load is 1.25v and the right-hand load is 2.25v. This is shown in Figure 4-8.

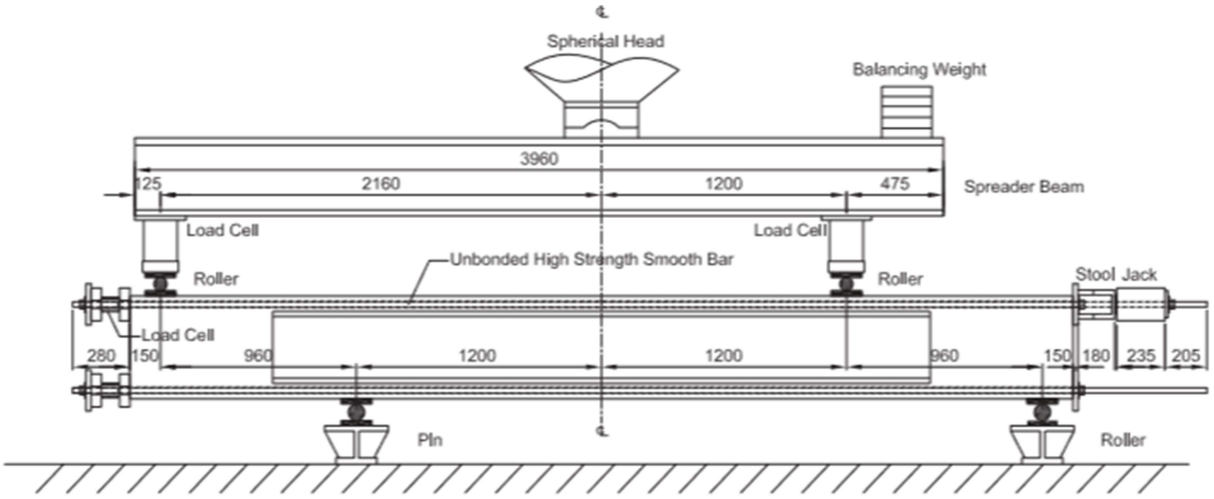

Figure 4-8 Test set-up (including spreader beam). Source: Xie (2009)

4.3 Experimental results

In this paragraph the experimental results are shown of specimens LB6-LB8. The main goal is to find the web shear resistance of prestressed beams without shear reinforcement. Since old bridges often have not enough of insufficient shear reinforcement. It is assumed that the presence of shear reinforcement is neglectable on the moment of originating of the first web-shear crack. Due to the fact the shear reinforcement is only activated when shear cracks are present. Therefor an important point of interest is the load at which the web shear crack occurs, this would be the failure load for web-shear cracking if there was no shear reinforcement at all.

Another interesting moment is failure. The moment of failure can be compared with the FEM non-linear analysis. The table below shows the shear force and shear stress for the moment of web shear cracking and for failure at the junction of web and top flange. Subscript cr for cracking and u for ultimate. It can be noted that LB7 two prestresses are present. During the testing of LB7 the axial load varied a lot. It is assumed that the axial load of -255 kN corresponds with the web-shear cracking load and that the axial load of -319 kN corresponds to the axial load during failure.

Specimen	N [kN]	V_{cr-exp} [kN]	v_{cr-exp} [MPa]	V_{u-exp} [kN]	v_{u-exp} [MPa]
LB6	-797	148.1	3.81	155.8	5.01
LB7	-255/-319	80.1	2.06	137.8	4.43
LB8	-512	111.2	2.92	134.3	4.34

LB6

In specimen LB6 no flexural nor flexure-shear cracks occurred. The first set of web-shear cracks appeared at a shear force of 148.1 kN with an inclination of 27° to 36° and a crack width of maximal 1.0 mm, see Figure 4-9. These first web-shear cracks came with small cracks at the joint between the web and the top flange. As the load increased no new cracks appeared. The existing web-shear crack increased an the

horizontal cracks continued to extend along the junction of the web and the top flange. The specimen failed at a load of 155.8 kN due to opening of one major shear crack and buckling of the flanges.

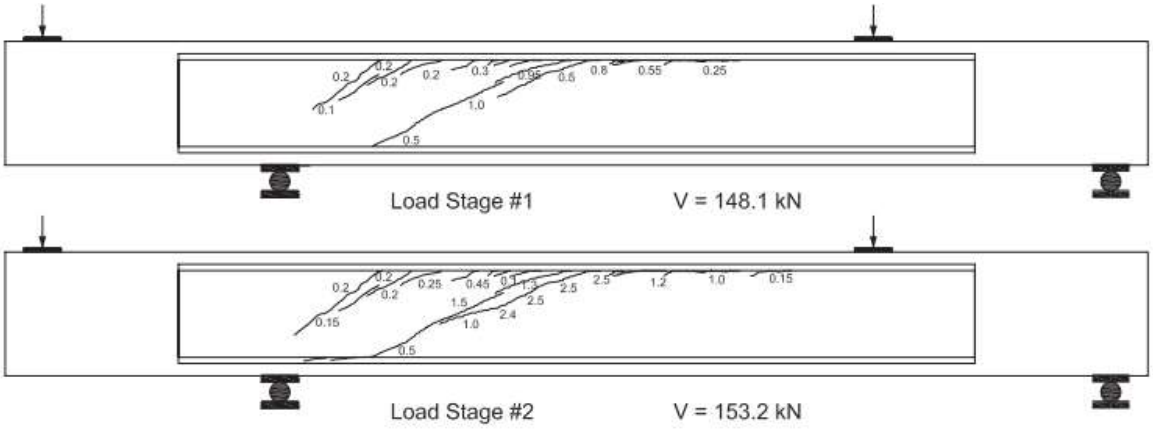

Figure 4-9 Experimental results LB6. Source: Xie (2009)

LB7

Specimen LB7 showed bending cracks before the web shear cracking occurred. This happened at a shear force of 72.7 kN and is shown in Figure 4-10. It can be seen that these cracks occur above the western support, which makes sense since there the moment is at the maximum. The first web shear crack occurred at a shear force of 80.1 kN. The inclination of this crack was about 35° and had a width of 0.35 mm. With increasing the load more web-shear cracks of lower inclination developed. The width of the web shear cracks was larger than the width of the flexural cracks. Finally the specimen failed at a shear force of 137.8 kN due to opening of the major web-shear crack and rupture of the stirrups.

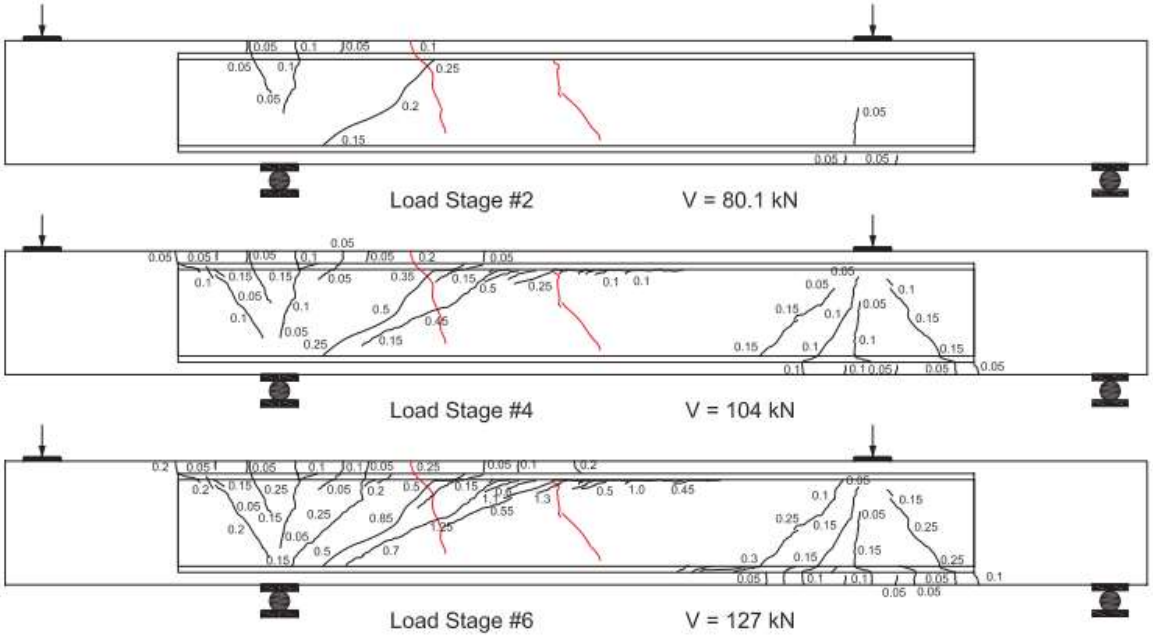

Figure 4-10 Experimental results LB7. Source: Xie (2009)

LB8

Specimen LB8 showed no bending cracks before web shear cracking occurred, however bending cracks were originated simultaneously with the originating of the web shear crack, see Figure 4-11. This happened at a shear force of 111.2 kN. The bending cracks appear above the western support. As the loads increased more web-shear cracks with smaller inclination appeared. Only one or two flexural cracks developed in flexural-shear cracks. The specimen failed at a shear force of 134.3 kN due to opening of the major shear crack and the shear crack thrusting through the flanges.

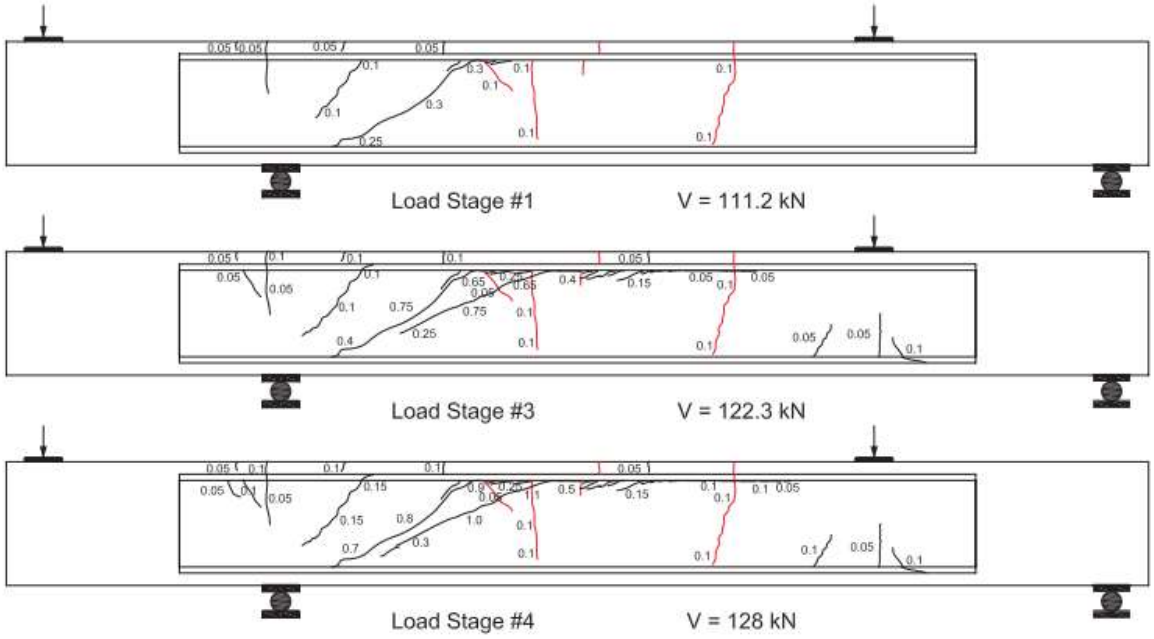

Figure 4-11 Experimental results LB8. Source: Xie (2009)

5 Analytical Analysis

5.1 Analytical method

As described in chapter 2 there are two different methods to check for the highest principle tensile stress. These are only checking for the highest principle stress at the CoG and checking for the highest principle stress over the height of the beam, both over the axial axes of the beam. It is interesting to see the different results of these methods. The EC2 and ACI are chosen as the requirement codes.

To calculate the axial-, vertical-, shear- and principle stresses the built-as dimensions are used. With these dimensions the first and second moment of area calculated. First calculations show that the reinforcement has a decent influence on the axial stress which are introduced by the prestress. Therefore the moment of area and second moment of area includes the stiffness of concrete and the stiffness of steel. This is done by replacing the reinforcement with concrete and multiply the area of the reinforcement by factor α. Factor α is the ratio between the E_{steel} to $E_{concrete}$. This can include the prestress bar, this is the case for pretensioned prestress bars.

The self-weight of the beam is converted to a distributed load or distributed loads. This depends on the shape of the beam and if this changes over the axial axes. These distributed loads are converted to moment- and shear force diagram with the help of MatrixFrame 5.3.

The point loads are set to the moment of web-shear cracking given in chapter.

The prestress also creates a moment: $M_p = Ny$ with N equal to the prestressing force and y the distance of the prestressing bars to the CoG.

With the information above the total moment- and shear force diagram can be computed. The beams are considered as an Euler-Bernoulli beam, a simplification that assumes that perpendicular planes to the neutral plane remain plane and perpendicular to the neutral plane after bending. This means that the axial stress, σ_{xx}, is easily calculated with the formula below. This is the most used method in practice.

$$\sigma_{xx}(x,y) = \frac{N}{A_c + (\alpha - 1) * A_s} + \frac{M_{total}(x)y}{I_{total}} \tag{2.1}$$

M_{total} is the sum of the prestressing moment, the moment due to the loads and the moment due to self weight. The moment is obviously a function of x. In the second moment of area (I_{total}) the steel is neglected.

The vertical stress, σ_{yy}, is only present directly under and close by the reaction forces and loads. In practice σ_{yy} is often neglected and therefore it will also be neglected in the analytical calculations of this this report.

The shear stress, σ_{xy}, is calculated with the formula 2.2. In which the shear force is a function of the x-coordinate, the moment of area a function of the y-coordinate and t dependent of y-coordinate. With the obtained σ_{xx}, σ_{yy} and σ_{xy} the principle stresses can be calculated conform formula 2.1.

5.2 Analytical results

The stresses are calculated at several vertical plains, namely cross-section A-A to I-I as shown in Figure 5-1. These are positioned at the beginning and end of the test region, the points where 60°, 45° and 30°

angles lines out of the inner part of the load-/support plate crosses the CoG and at middle of the test region.

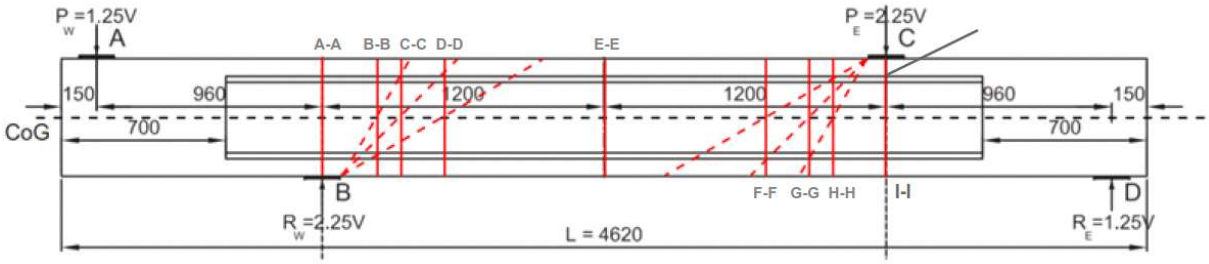

Figure 5-1 Indication of cross-sections

LB6

Figure 5-2 shows the moment diagram. It can be observed that the influence of the moment of the dead load and the prestress are almost neglectable in comparison to the moment of the point loads. The moment line of the self-weight is found with MatrixFrame 5.3.

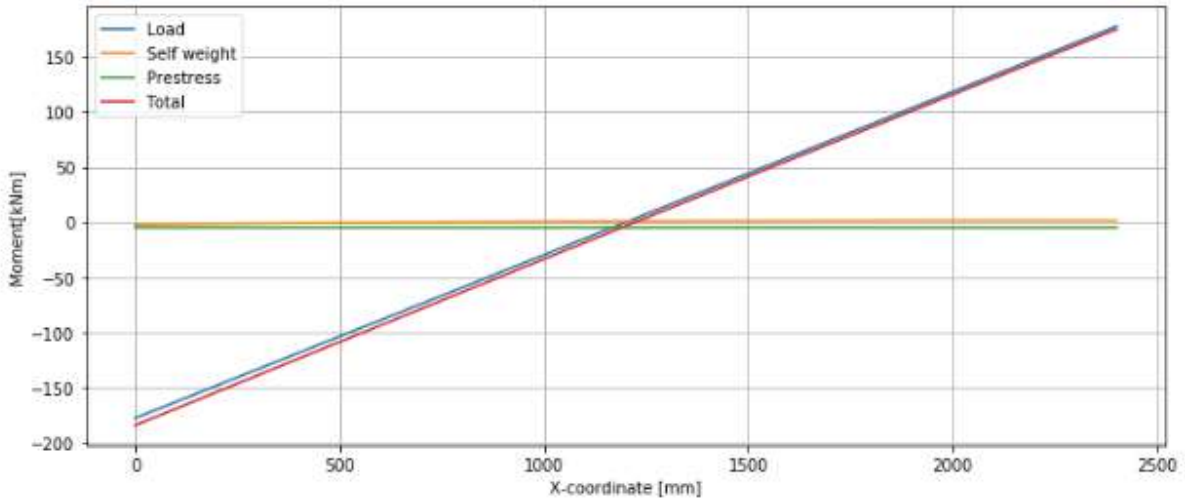

Figure 5-2 Moment diagram LB6

Figure 5-3shows the shear force diagram. It can be noted that just as for the moment diagram the influence of self-weight is almost neglectable.

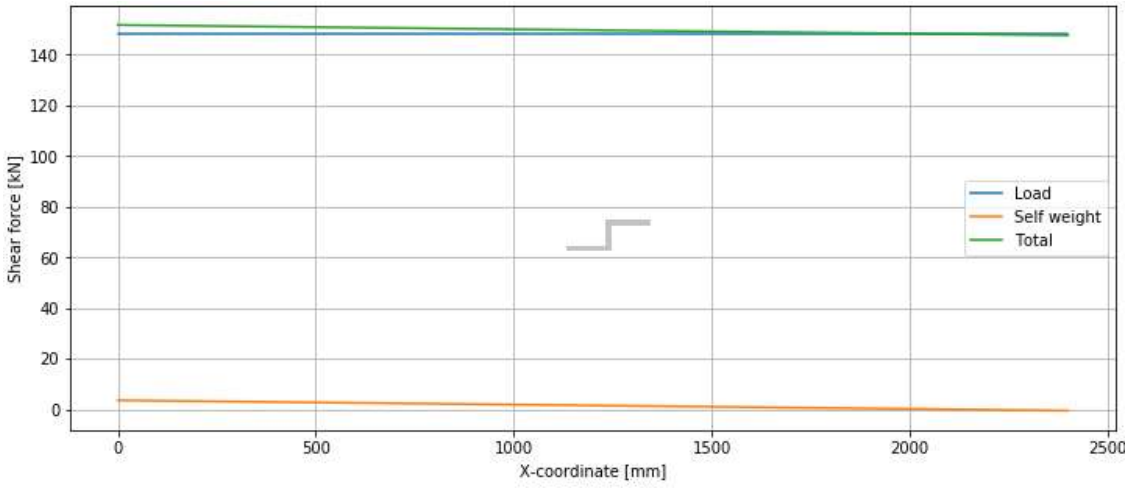

Figure 5-3 Shear force diagram LB6

The first and second moment of inertia are calculated and given in the table below. The first moment of area is simply the area times the distance of the CoG of that specific area to the CoG of the whole cross-section. The second moment of area of A1,A3 and A5 are calculated with the well known $\frac{1}{12}bh^3$. For the trapezoid A2 and A4 the moment of inertia is calculated as $\frac{h^3(a+4ab+b^2)}{36(a+b)}$ in which h is the height, a is the width on top and b is the width on the bottom, respectively b_{web} and b_{flange}.

Table 5-1 First and second moment of area (LB6)

	A	z_{top}	S per area	I
	$[mm^2]$	$[mm]$	$[mm^3]$	$[mm^4]$
A1	1.71E+04	25.5	3.92E+06	9.07E+08
S1	3.97E+03	33.0	8.84E+05	1.98E+08
A2	5.29E+03	60.8	1.03E+06	2.01E+08
A3	2.56E+04	251.0	1.18E+05	2.61E+08
A4	5.29E+03	441.2	-9.81E+05	1.82E+08
S2	3.97E+03	473.0	-8.63E+05	1.88E+08
A5	1.85E+04	478.5	-4.11E+06	9.21E+08
Total	**7.96E+04**		**0.00E+00**	**2.86E+09**

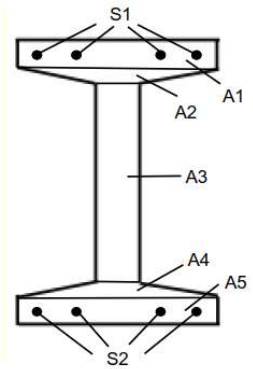

Figure 5-4 Cross-section divided in areas

As described in chapter 2 with the now known shear force- and moment distribution the stresses σ_{xx}, σ_{xy} and the principle stresses σ_1 and σ_2 can be calculated. This is done at different levels of the hieght of the beam. These levels include the top of the beam, start of inclination of the flange, top of the web, bottom of the web. In the table below the values of σ_{xx} in N/mm^2 are given over the vertical and axial axes of the beam.The height is given relative to the CoG. The cross-secction are shown in Figure 5-1. As a sanity check it can be noted that σ_{xx} does not change at the CoG, which obviously makes sense.

Table 5-2 σ_{xx} in N/mm^2 over the height per cross-section (LB6)

	Height	A-A	B-B	C-C	D-D	E-E	F-F	G-G	H-H	I-I
Top of beam	**256**	2.71	1.26	0.99	-10.47	-21.81	-22.08	-24.33	-26.42	2.71
Start of inclined	**205**	0.17	-0.99	-1.20	-10.38	-19.46	-19.67	-21.48	-23.15	0.17
Top of web	**180**	-1.07	-2.09	-2.28	-10.33	-18.31	-18.49	-20.08	-21.54	-1.07
	150	-2.55	-3.40	-3.56	-10.28	-16.94	-17.10	-18.42	-19.64	-2.55
	100	-5.04	-5.60	-5.71	-10.19	-14.63	-14.74	-15.62	-16.43	-5.04
	50	-7.53	-7.81	-7.86	-10.10	-12.32	-12.38	-12.82	-13.23	-7.53
CoG	**0**	-10.02	-10.02	-10.02	-10.02	-10.02	-10.02	-10.02	-10.02	-10.02
	-50	-12.51	-12.22	-12.17	-9.93	-7.71	-7.66	-7.22	-6.81	-12.51
	-100	-15.00	-14.43	-14.32	-9.84	-5.40	-5.30	-4.42	-3.60	-15.00
	-150	-17.49	-16.64	-16.48	-9.75	-3.09	-2.94	-1.62	-0.39	-17.49
Bottom of web	**-170**	-18.50	-17.54	-17.36	-9.72	-2.15	-1.98	-0.48	0.91	-18.50
Start of inclined	**-195**	-19.75	-18.64	-18.43	-9.67	-1.00	-0.80	0.92	2.52	-19.75
Bottom of beam	**-250**	-22.48	-21.07	-20.80	-9.58	1.54	1.80	4.00	6.05	-22.48

The table below gives the values of σ_{xy} in N/mm^2 over the vertical and axial axes of the beam. These are calculated with the well known shear force $\frac{VS}{bI}$. As a sanity check it can be seen that there is no shear stress in the outer fibers and maximum shear stress at the CoG. The shear stress changes barely over the different plains. This is the case because, as can be seen in the shear force diagram in Figure 5-3, the shear also barely changes in axial direction.

Table 5-3σ_{xy} in N/mm^2 over height per cross-section (LB6)

	Height	A-A	B-B	C-C	D-D	E-E	F-F	G-G	H-H	I-I
Top of beam	**256**	0.00	0.00	0.00	0.00	0.00	0.00	0.00	0.00	0.00
Start of inclined	**205**	-0.73	-0.73	-0.73	-0.73	-0.72	-0.71	-0.71	-0.71	-0.71
Top of web	**180**	-4.24	-4.23	-4.23	-4.23	-4.19	-4.15	-4.15	-4.14	-4.13
	150	-4.50	-4.49	-4.49	-4.49	-4.44	-4.40	-4.40	-4.39	-4.38
	100	-4.84	-4.82	-4.82	-4.82	-4.77	-4.72	-4.72	-4.71	-4.71
	50	-5.03	-5.02	-5.02	-5.02	-4.97	-4.92	-4.92	-4.91	-4.90
CoG	**0**	-5.10	-5.09	-5.08	-5.08	-5.03	-4.98	-4.98	-4.97	-4.96
	-50	-5.03	-5.02	-5.02	-5.02	-4.97	-4.92	-4.92	-4.91	-4.90
	-100	-4.84	-4.82	-4.82	-4.82	-4.77	-4.72	-4.72	-4.71	-4.71
	-150	-4.50	-4.49	-4.49	-4.49	-4.44	-4.40	-4.40	-4.39	-4.38
Bottom of web	**-170**	-4.33	-4.32	-4.31	-4.31	-4.27	-4.23	-4.23	-4.22	-4.21
Start of inclined	**-195**	-0.75	-0.75	-0.75	-0.75	-0.74	-0.74	-0.74	-0.74	-0.73
Bottom of beam	**-250**	0.00	0.00	0.00	0.00	0.00	0.00	0.00	0.00	0.00

And lastly the principle tensile stresses are given below, also in N/mm^2. As described in chapter 2 the principle tensile stress can be calculated when the shear stress and axial stress are known with the simplified equation: $\sigma_1 = \frac{\sigma_{xx}}{2} + \sqrt{\frac{\sigma_{xx}^2}{2} + \sigma_{xy}^2}$. Which is equation 2.1 without vertical stresses and is

derived from the Mohr circle. It is logical that the highest principle tensile stresses are found at the junction between web and flange, since the width is small and the distance to the CoG is large.

It is remarkable that the maximum principle tensile stress is higher than f_{ctm} only at the outer fibre at cross-sections A-A and I-I. These cross-sections are located respectively above the western support and the below the eastern load, Figure 5-1. This would indicate flexural cracks, however no flexural cracks occurred during testing of LB6. At the location of the web-shear crack, approximately at C-C, the principle tensile stress stays well below f_{ctm}. Namely 3.31 N/mm^2 and $f_{ctm} = 4.25\ N/mm^2$.

Table 5-4 σ_1 in N/mm^2 over the height per cross-section (LB6)

	Height	A-A	B-B	C-C	D-D	E-E	F-F	G-G	H-H	I-I
Top of beam	**256**	5.71	2.71	1.26	0.99	0.00	0.00	0.00	0.00	0.00
Start of inclined	**205**	2.76	0.82	0.38	0.34	0.05	0.03	0.03	0.02	0.02
Top of web	**180**	4.79	3.73	3.31	3.24	1.48	0.90	0.89	0.82	0.76
	150	4.13	3.40	3.10	3.05	1.65	1.07	1.07	0.99	0.93
	100	3.27	2.92	2.77	2.74	1.88	1.39	1.38	1.31	1.25
	50	2.64	2.51	2.45	2.44	2.03	1.72	1.72	1.66	1.62
CoG	**0**	2.14	2.13	2.13	2.13	2.09	2.06	2.06	2.05	2.04
	-50	1.71	1.77	1.79	1.80	2.06	2.39	2.40	2.48	2.56
	-100	1.34	1.42	1.46	1.47	1.93	2.74	2.77	3.00	3.24
	-150	1.00	1.09	1.13	1.14	1.72	3.12	3.17	3.66	4.19
Bottom of web	**-170**	0.88	0.96	1.00	1.01	1.61	3.29	3.36	3.99	4.70
Start of inclined	**-195**	0.03	0.03	0.03	0.03	0.06	0.39	0.44	1.33	2.72
Bottom of beam	**-250**	0.00	0.00	0.00	0.00	0.00	1.54	1.80	4.00	6.05

LB7

The as-built dimensions of LB7 compared to LB6 only differ in the width of the bottom flange of 3 mm. This results in an almost equal first and second moment of area to LB6. The method is exactly the same as described at LB6. The used areas are also the same and given in Figure 5-4.

Table 5-5 First and second moment of area (LB7)

	A	z_{top}	S per area	I
Area	$[mm^2]$	$[mm]$	$[mm^3]$	$[mm^4]$
A1	1.71E+04	25.5	3.93E+06	9.11E+08
S1	3.97E+03	33.0	8.86E+05	1.99E+08
A2	5.29E+03	60.8	1.03E+06	2.02E+08
A3	2.56E+04	251.0	1.32E+05	2.62E+08
A4	5.33E+03	441.2	-9.85E+05	1.83E+08
S2	3.97E+03	473.0	-8.61E+05	1.87E+08
A5	1.86E+04	478.5	-4.14E+06	9.25E+08
Total	**7.98E+04**		**0.00E+00**	**2.87E+09**

The moment diagram and shear force diagram are again calculated with help of MatrixFrame 5.3 and are shown in respectively Figure 5-5 and Figure 5-6. Just like LB6 the influence of self-weight is neglectable as can the moment created by the prestress.

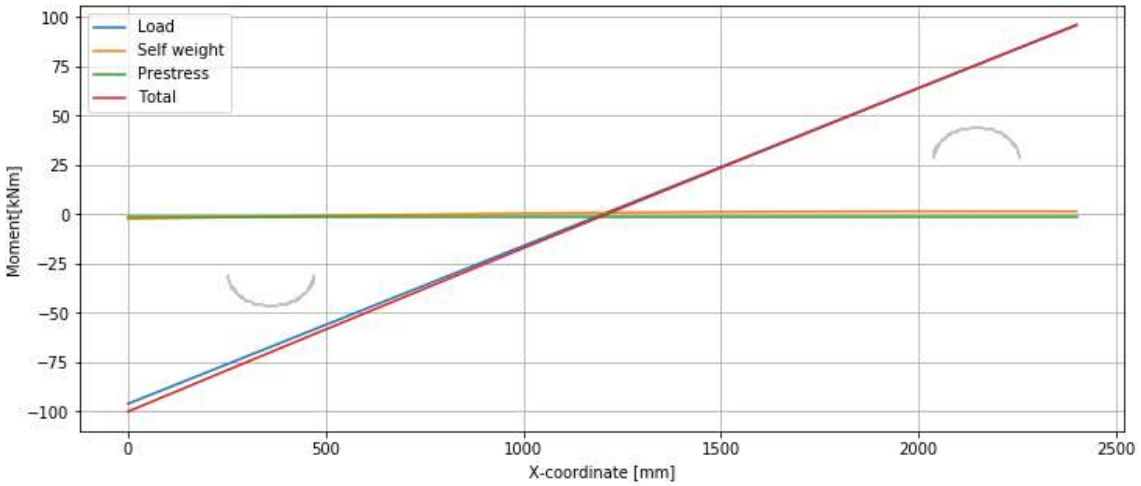

Figure 5-5 Moment diagram LB7

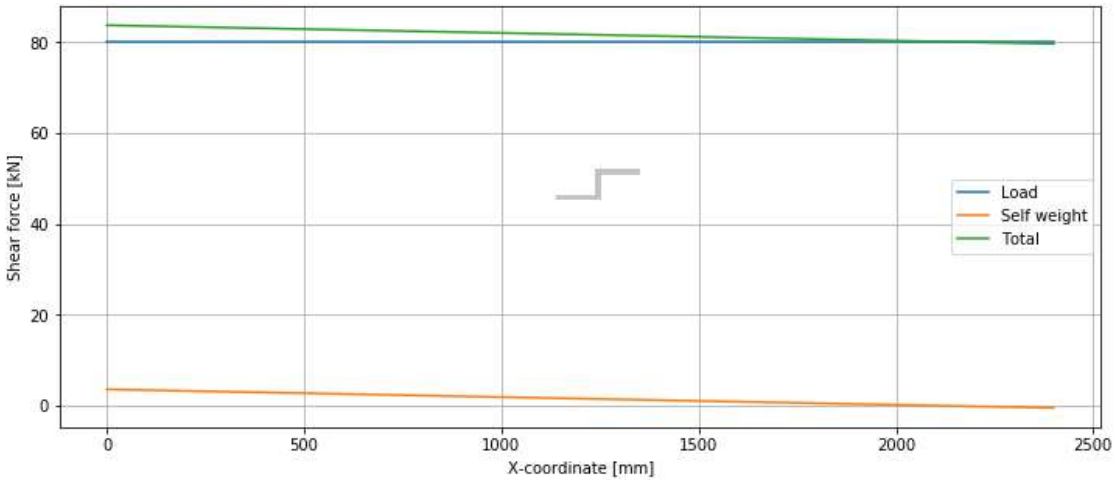

Figure 5-6 Shear force diagram LB7

The table below gives σ_{xx} at different height and at different plains. As a sanity check it can be noted that the stress at the CoG does not change between different cross-sections, which is logical since the prestress is assumed to be equally distributed throughout the test region and pure bending is assumed which results in zero horizontal stress due to the moments. Furthermore it can be noticed that the highest horizontal stresses are found above the support and the eastern load. Which makes sense with the M-line given in Figure 5-5.

Table 5-6 σ_{xx} in N/mm^2 over the height per cross-section (LB7)

	Height	A-A	B-B	C-C	D-D	E-E	F-F	G-G	H-H	I-I
Top of beam	**256**	5.45	3.17	3.01	1.63	-3.42	-8.39	-9.72	-10.94	-12.06
Start of inclined	**205**	3.73	1.90	1.77	0.67	-3.37	-7.36	-8.42	-9.40	-10.30
Top of web	**180**	2.88	1.28	1.17	0.20	-3.35	-6.85	-7.78	-8.64	-9.43
	150	1.87	0.53	0.43	-0.37	-3.32	-6.24	-7.02	-7.73	-8.39
	100	0.18	-0.71	-0.78	-1.31	-3.28	-5.22	-5.74	-6.22	-6.66
	50	-1.51	-1.95	-1.99	-2.25	-3.24	-4.21	-4.47	-4.71	-4.93
CoG	**0**	-3.20	-3.20	-3.20	-3.20	-3.20	-3.20	-3.20	-3.20	-3.20
	-50	-4.88	-4.44	-4.41	-4.14	-3.15	-2.18	-1.92	-1.69	-1.47
	-100	-6.57	-5.68	-5.62	-5.08	-3.11	-1.17	-0.65	-0.18	0.26
	-150	-8.26	-6.92	-6.83	-6.03	-3.07	-0.15	0.62	1.33	1.99
Bottom of web	**-170**	-8.93	-7.42	-7.31	-6.40	-3.05	0.25	1.13	1.93	2.68
Start of inclined	**-195**	-9.77	-8.04	-7.91	-6.87	-3.03	0.75	1.76	2.69	3.54
Bottom of beam	**-250**	-11.63	-9.40	-9.24	-7.91	-2.98	1.87	3.16	4.35	5.45

Table 5-7 show the shear stresses which are present in the test region conform the analytical analysis. Again the outer fiber has zero shear stress and the maximum shear stress is found at the CoG. The magnitude of the shear stress compared to LB6 is almost half, this is due to the big difference at which load web-shear cracking occurs. The shear force used in the analytical analysis for LB6 is 148.2 kN and for LB7 it is 80.1 kN.

Table 5-7 σ_{xy} in N/mm^2 over the height per cross-section (LB7)

	Height	A-A	B-B	C-C	D-D	E-E	F-F	G-G	H-H	I-I
Top of beam	**256**	0.00	0.00	0.00	0.00	0.00	0.00	0.00	0.00	0.00
Start of inclined	**205**	-0.40	-0.40	-0.40	-0.40	-0.39	-0.39	-0.39	-0.38	-0.38
Top of web	**180**	-2.34	-2.33	-2.32	-2.32	-2.28	-2.25	-2.24	-2.23	-2.23
	150	-2.49	-2.47	-2.47	-2.46	-2.43	-2.39	-2.38	-2.37	-2.36
	100	-2.67	-2.65	-2.65	-2.64	-2.60	-2.57	-2.56	-2.55	-2.54
	50	-2.78	-2.76	-2.76	-2.75	-2.71	-2.67	-2.66	-2.65	-2.64
CoG	**0**	-2.81	-2.80	-2.80	-2.79	-2.75	-2.71	-2.70	-2.69	-2.68
	-50	-2.78	-2.76	-2.76	-2.75	-2.71	-2.67	-2.66	-2.65	-2.64
	-100	-2.67	-2.65	-2.65	-2.64	-2.60	-2.57	-2.56	-2.55	-2.54
	-150	-2.49	-2.47	-2.47	-2.46	-2.43	-2.39	-2.38	-2.37	-2.36
Bottom of web	**-170**	-2.39	-2.38	-2.38	-2.37	-2.34	-2.30	-2.29	-2.28	-2.28
Start of inclined	**-195**	-0.41	-0.41	-0.41	-0.41	-0.40	-0.40	-0.40	-0.39	-0.39
Bottom of beam	**-250**	0.00	0.00	0.00	0.00	0.00	0.00	0.00	0.00	0.00

The principle tensile stresses are given of LB7 are given in the table below. It can be noted that the maximum principle tensile stress is equal above the support and below the load. This would indicate that flexural cracks are as likely to occur on both sides of the test region. During testing flexural cracks occurred above the support first.

At the 45° plain out of the support at the junction between the web and flange, corss-section C-C, the principle tensile stress is higher than at the same location at the opposite side of the test region. Which would suggest that if web-shear cracking occurred it would be above the support, as it did during testing. However σ_1 at the junction between web and flange stays below f_{ctm}.

The stress in the outer fiber above the support and below the load are exceeding f_{ctm}. This would indicate flexural cracks on both side. During testing flexural cracks were observed, first above the support and later also under the load.

Table 5-8 σ_1 in N/mm^2 over the height per cross-section (LB7)

	Height	A-A	B-B	C-C	D-D	E-E	F-F	G-G	H-H	I-I
Top of beam	**256**	5.45	3.17	3.01	1.63	0.00	0.00	0.00	0.00	0.00
Start of inclined	**205**	3.77	1.98	1.86	0.86	0.05	0.02	0.02	0.02	0.01
Top of web	**180**	4.19	3.05	2.98	2.42	1.16	0.67	0.60	0.54	0.50
	150	3.59	2.75	2.70	2.28	1.28	0.81	0.73	0.67	0.62
	100	2.76	2.32	2.29	2.07	1.44	1.05	0.97	0.91	0.86
	50	2.12	1.95	1.94	1.84	1.54	1.30	1.24	1.19	1.15
CoG	**0**	1.64	1.62	1.62	1.61	1.58	1.54	1.54	1.53	1.52
	-50	1.26	1.32	1.33	1.37	1.56	1.79	1.87	1.94	2.01
	-100	0.95	1.05	1.05	1.12	1.48	2.05	2.25	2.46	2.67
	-150	0.69	0.79	0.80	0.88	1.34	2.31	2.71	3.13	3.56
Bottom of web	**-170**	0.60	0.70	0.71	0.78	1.26	2.43	2.92	3.45	3.98
Start of inclined	**-195**	0.02	0.02	0.02	0.02	0.05	0.93	1.85	2.75	3.59
Bottom of beam	**-250**	0.00	0.00	0.00	0.00	0.00	1.87	3.16	4.35	5.45

LB8

The small difference in the as-built measurements result in a slightly different location of the CoG, first- and second moment of area. These are given in the Table 5-9.

Table 5-9 First and second moment of area (LB8)

	A	z_{top}	S per area	I
	$[mm^2]$	$[mm]$	$[mm^3]$	$[mm^4]$
A1	1.79E+04	26.5	4.00E+06	9.02E+08
S1	3.97E+03	33	8.65E+05	1.89E+08
A2	5.31E+03	62.76470588	9.99E+05	1.88E+08
A3	2.56E+04	253	-5.70E+04	2.61E+08
A4	5.31E+03	443.2352941	-1.02E+06	1.97E+08
S2	3.97E+03	473	-8.82E+05	1.97E+08
A5	1.72E+04	478.5	-3.91E+06	8.93E+08
Total	**7.91E+04**		**0.00E+00**	2.83E+09

As for LB6 and LB7 the moment and shear force diagrams are computed, see respectively Figure 5-7 and Figure 5-8. The moment line due to self-weight is calculated in Matrix Frame. It is logical that just as for LB6 and LB7 the influence of the self-weight is neglectable compared to the moment of the load. The moment of prestress due to slightly asymmetrical tendons is also close to nothing.

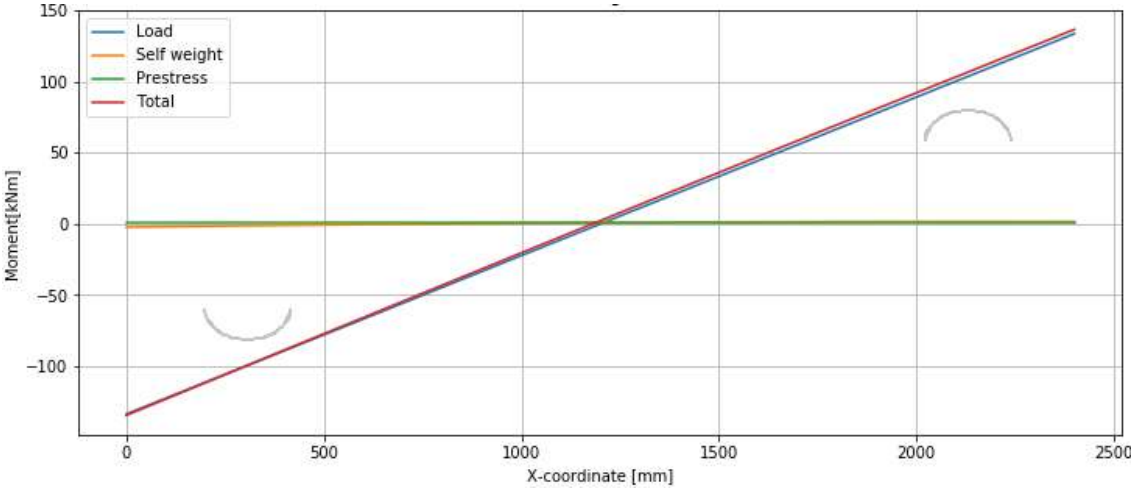

Figure 5-7 Moment diagram LB8

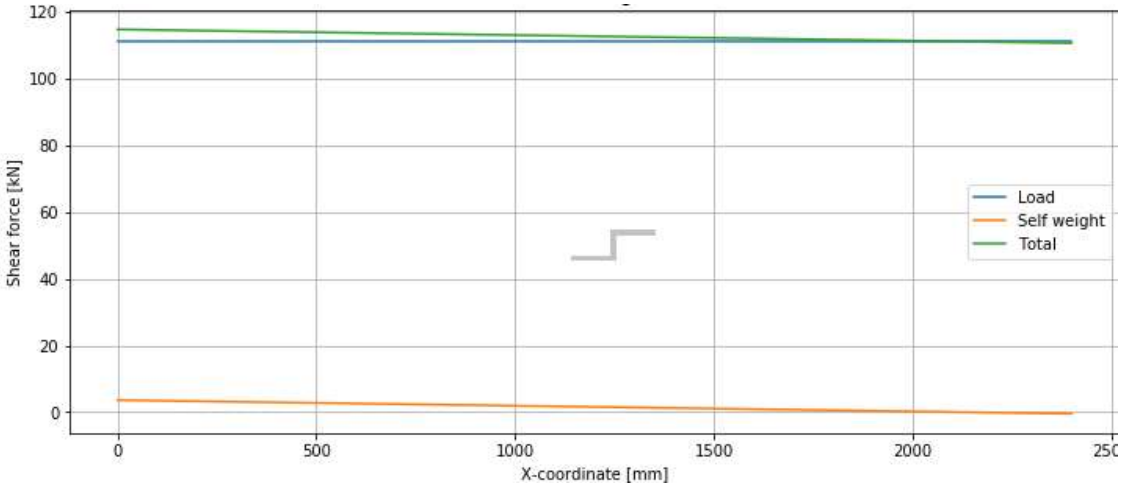

Figure 5-8 Shear force diagram LB8

The σ_{xx} of LB8 are given in the table below. These are calculated in the same as LB6 and LB7 and show comparable results with high tensile stresses above the support and below the load in the outer fiber.

Table 5-10 σ_{xx} in N/mm^2 over the height per cross-section (LB8)

	Height	A-A	B-B	C-C	D-D	E-E	F-F	G-G	H-H	I-I
Top of beam	**250.8**	8.13	5.24	4.80	3.24	-3.98	-11.12	-12.64	-14.32	-15.87
Start of inclined	**197.8**	5.56	3.28	2.93	1.71	-3.99	-9.62	-10.82	-12.15	-13.37
Top of web	**172.8**	4.35	2.35	2.05	0.98	-3.99	-8.92	-9.96	-11.12	-12.19
	150.0	3.25	1.51	1.25	0.32	-4.00	-8.27	-9.18	-10.19	-11.11
	100.0	0.82	-0.34	-0.51	-1.13	-4.01	-6.86	-7.47	-8.13	-8.75
	50.0	-1.61	-2.18	-2.27	-2.58	-4.02	-5.45	-5.75	-6.08	-6.39
CoG	**0.0**	-4.03	-4.03	-4.03	-4.03	-4.03	-4.03	-4.03	-4.03	-4.03
	-50.0	-6.46	-5.88	-5.79	-5.48	-4.04	-2.62	-2.31	-1.98	-1.67
	-100.0	-8.88	-7.73	-7.55	-6.93	-4.05	-1.20	-0.60	0.07	0.69
	-150.0	-11.31	-9.57	-9.32	-8.38	-4.06	0.21	1.12	2.12	3.05
Bottom of web	**-179.2**	-12.73	-10.66	-10.34	-9.23	-4.07	1.04	2.12	3.32	4.43
Start of inclined	**-204.2**	-13.94	-11.58	-11.23	-9.96	-4.08	1.74	2.98	4.35	5.61
Bottom of beam	**-255.2**	-16.41	-13.46	-13.02	-11.44	-4.09	3.18	4.73	6.44	8.02

The shear stresses are in line with the results of LB6 and LB7 and are given below. The main influence on shear stresses is the load. Since the load of LB8 is in between the load of LB6 and LB7 the shear stresses are also in between those of LB6 and LB7. Furthermore the maximum shear stress is located at the CoG and the shear stress is zero in the outer fiber.

Table 5-11 σ_{xy} in N/mm^2 over the height per cross-section (LB8)

	Height	A-A	B-B	C-C	D-D	E-E	F-F	G-G	H-H	I-I
Top of beam	**250.8**	0.00	0.00	0.00	0.00	0.00	0.00	0.00	0.00	0.00
Start of inclined	**197.8**	-0.56	-0.56	-0.56	-0.56	-0.55	-0.55	-0.54	-0.54	-0.54
Top of web	**172.8**	-3.26	-3.25	-3.25	-3.24	-3.21	-3.17	-3.16	-3.16	-3.15
	150.0	-3.41	-3.40	-3.40	-3.39	-3.35	-3.32	-3.31	-3.30	-3.29
	100.0	-3.67	-3.65	-3.65	-3.64	-3.60	-3.56	-3.55	-3.55	-3.54
	50.0	-3.82	-3.80	-3.80	-3.79	-3.75	-3.71	-3.70	-3.69	-3.68
CoG	**0.0**	-3.87	-3.85	-3.85	-3.84	-3.80	-3.76	-3.75	-3.74	-3.73
	-50.0	-3.82	-3.80	-3.80	-3.79	-3.75	-3.71	-3.70	-3.69	-3.68
	-100.0	-3.67	-3.65	-3.65	-3.64	-3.60	-3.56	-3.55	-3.55	-3.54
	-150.0	-3.41	-3.40	-3.40	-3.39	-3.35	-3.32	-3.31	-3.30	-3.29
Bottom of web	**-179.2**	-3.22	-3.20	-3.20	-3.20	-3.16	-3.13	-3.12	-3.11	-3.10
Start of inclined	**-204.2**	-0.55	-0.55	-0.55	-0.55	-0.54	-0.54	-0.54	-0.53	-0.53
Bottom of beam	**-255.2**	0.00	0.00	0.00	0.00	0.00	0.00	0.00	0.00	0.00

The principle tensile stresses of LB8 are given below. Unlike LB6 and LB7 the calculated σ_1 at the junction between web and flange is larger than f_{ctm}, which would indicate web-shear cracking. The highest principle tensile stress is however found above the support. This stress is almost double the magnitude

of the stress at the junction at the 45° plain. This would suggest that flexural cracks should occur well before web-shear cracking. Experimental results show however that flexural cracks and web-shear cracks occurred simultaneously.

Table 5-12 σ_1 in N/mm^2 over the height per cross-section (LB8)

	Height	A-A	B-B	C-C	D-D	E-E	F-F	G-G	H-H	I-I
Top of beam	**250.8**	8.13	5.24	4.80	3.24	0.00	0.00	0.00	0.00	0.00
Start of inclined	**197.8**	5.62	3.37	3.04	1.87	0.07	0.03	0.03	0.02	0.02
Top of web	**172.8**	6.10	4.63	4.43	3.77	1.78	1.01	0.92	0.83	0.77
	150.0	5.40	4.24	4.08	3.55	1.90	1.17	1.07	0.98	0.90
	100.0	4.10	3.49	3.40	3.12	2.12	1.52	1.42	1.33	1.25
	50.0	3.10	2.87	2.83	2.72	2.25	1.88	1.81	1.74	1.68
CoG	**0.0**	2.35	2.33	2.33	2.32	2.29	2.25	2.24	2.23	2.23
	-50.0	1.77	1.87	1.88	1.94	2.24	2.63	2.72	2.83	2.94
	-100.0	1.32	1.45	1.48	1.56	2.11	3.01	3.27	3.58	3.90
	-150.0	0.95	1.08	1.11	1.20	1.89	3.42	3.92	4.53	5.15
Bottom of web	**-179.2**	0.77	0.89	0.91	1.00	1.72	3.69	4.36	5.19	6.03
Start of inclined	**-204.2**	0.02	0.03	0.03	0.03	0.07	1.89	3.08	4.41	5.66
Bottom of beam	**-255.2**	0.00	0.00	0.00	0.00	0.00	3.18	4.73	6.44	8.02

6 Linear finite element analysis

6.1 Model

The prestressed concrete reinforced beams are modelled with the non-linear finite element program Diana FEA. The Guidelines for non-linear finite element analysis of reinforced concrete structures (Hendriks, de Boer, & Belletti, 2017) is used.

In Figure 6-1 the model is shown. A 2D model is chosen to keep the model as simple as possible. The 3D effects are neglected, this is possible due to the fact that the beam is slender. The element class is for all shapes, except the reinforcement and prestress, the same namely regular plane stress. The thickness is set to the in-built dimensions as given in Table 4-1. The thickness of the inclined part of the flanges are added with the use of functions.

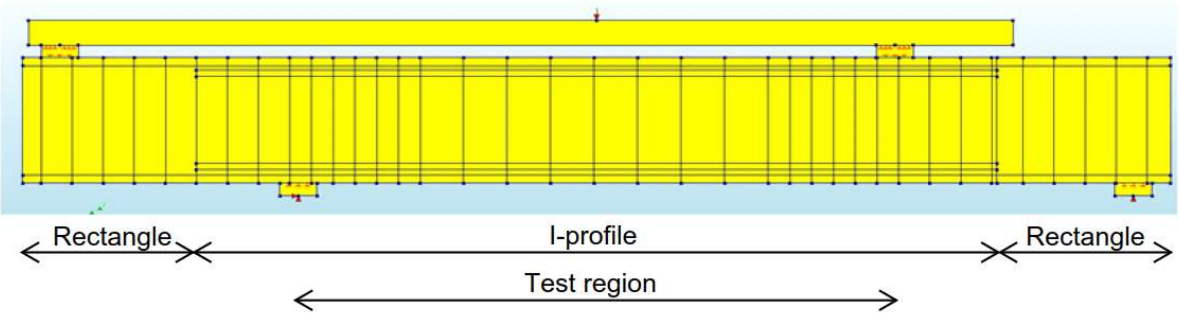

Figure 6-1 Model overview

The figure below shows the mesh. The mesh is kept the same over the whole model to make sure that the mesh is built up out of a well divided square mesh and the running time of a analysis is still within proportions. The mesh order is quadratic and linear interpolation mid-side node location is used. The mesh size is set to 20 mm.

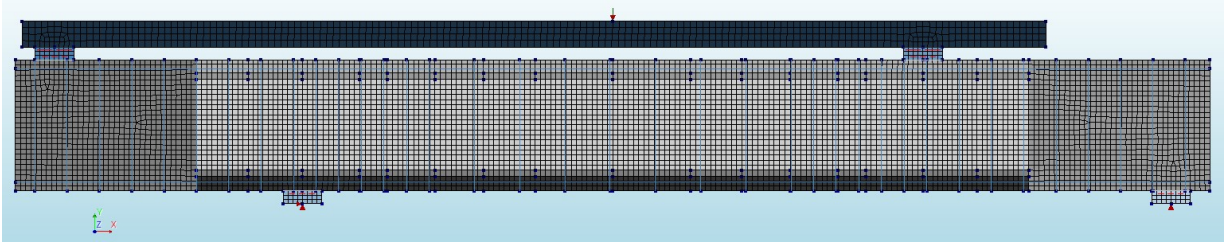

Figure 6-2 Mesh overview

The material properties of the concrete are given in the table below.

Table 6-1 Concrete properties LFEA

	Concrete
E [MPa]	40300
v [-]	0.2
ρ [T/mm³]	2.4E-09

The vertical lines in Figure 6-1 are the stirrups and the horizontal lines close to the top and the bottom is the longitudinal reinforcement. The longitudinal reinforcement, stirrups, and prestress are implemented as wire, with properties specified in Table 6-2. These followed from the thesis of Xie.

Table 6-2 Reinforcement properties LFEA

	Young's modulus [MPa]
Longitudinal bars	210000
Prestress	2E+11
Stirrups	195800

Just as in the experiment load- and support plates are used to reduce peak stresses. These plates are modeled as steel. The specifications of these plates are given in the table below.

Table 6-3 Load- and support plate properties LFEA

	load- and support plate
E [MPa]	210000
v	0.2
t [mm]	350

The spreader beam on top, Figure 6-1, is added to make it possible to perform a displacement controlled load in the non-linear analysis, however the spreader beam is also added in the linear analysis to keep both models similar. It is given the same material properties as the load- and support plates.

Between the load-, support plates and the beam a 2D line interface is implemented to recreate the experiment. This means that the shear stresses that are transformed are limited. The specifications are given in the table below. The thickness is equal to the width of the flanges.

Table 6-4 Interface properties LFEA

	interface
Normal stiffness [N/mm^3]	2.015E+06
Shear stiffness [N/mm^3]	2.015
t [mm]	350

The prestress is implemented as load. Post tensioning load, prestressed from one side with half the prestressing force per duct. The friction coefficient is kept zero, since it is a straight cable and as specified in chapter 4 a lot of measurements are taken to reduce friction. The wobble effect is neglected.. The self-weight is implemented as a load. The mass of the reinforcement is neglected.

As explained before the load is modeled as a prescribed displacement. To find the value of the prescribed displacement (u) which matches with the shear force that occurs during web-shear cracking in the experiment a simple linear interpolation is performed. First the shear force is calculated with a prescribed displacement of 1 mm and then the ratio between the calculated shear force and the shear force during web-shear cracking is used to find the proper displacement.

Table 6-5 Linear interpolation of prescribed displacement

Specimen	N [kN]	V_{cr-exp} [kN]	$V_{u=1mm}$ [kN]	u [mm]
LB6	-797	148.1	153.7	0.963
LB7	-255	80.1	152.9	0.524
LB8	-512	111.2	149.9	0.742

The model is checked based on the ratio between the shear forces. This is shown in the table below. Where R_E and R_W stand for respectively reaction force east and reaction force west. It shows that the model with the spreader beam does indeed divide the load in the correct ratio between the reaction forces. The ratio follows from the statically determined beam given in Figure 4-2.

Table 6-6 Ratio check of reaction forces

	R_E	$V = \frac{R_E}{2.25}$	R_W	$V = \frac{R_W}{1.25}$
	[kN]	[kN]	[kN]	[kN]
LB6	333.5	148.2	185.3	148.2
LB7	180.2	80.1	100.1	80.1
LB8	250.2	111.2	139.0	111.2

6.3 Results

In this chapter the results of the linear elastic finite element model per experiment will be shown and discussed.

LB6

Figure 6-3 to Figure 6-10 give an overview of the results of the linear elastic analysis of specimen LB6. The displacement field on Figure 6-3 shows the expected displacement, left end moves in negative y-direction and right end in positive y-direction. The inclination point of the moments is in the middle of the beam is visible. The displacement changes from concave to convex. It can be seen that the spreader beam does not move purely vertically, but also rotates. This is logical, since the prescirbed dispalcement is not located in the middle of the spreader beam.

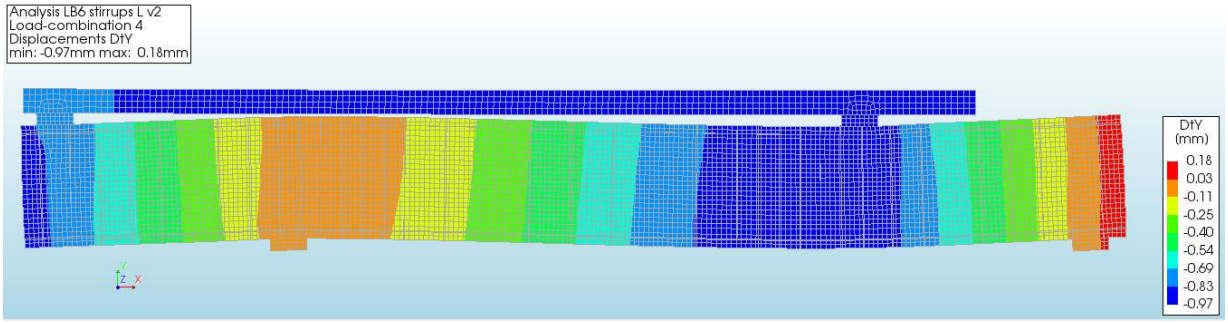

Figure 6-3 Displacement in y-direction under web-shear cracking load (LB6)

Figure 6-4 shows the stress in x-direction in the reinforcement. Obviously the σ_{xx} is 0 in the vertical stirrups. In Figure 6-4 it looks like there is only prestress located on the top side, but this is illusion due the same height of the prestress and the longitudinal reinforcement. In Figure 6-5 the prestress is moved 2 mm outwards and the longitudinal reinforcement is moved 2 mm inwards. This shows that the prestress and longitudinal reinforcement are both present in the bottom and top of the beam and both functional. The maximum σ_{xx} in the reinforcement of $786\ N/mm^2$ follows from the prestress, since this stress multiplied by the area of the unbonded high stress smooth bar equals half of the total prestressing force: $786 * 507 = 398.5\ kN$. The compression stress of $193\ N/mm^2$ occurs at the beginning and the end of the beam. This probably is the result of the fact that the prestress and longitudinal reinforcement are located at the same height. The stress in the bottom longitudinal reinforcement above the western support reaches a maximum stress of $107\ N/mm^2$ and $117\ N/mm^2$ below the eastern load. These values stay well below the yield stress of steel.

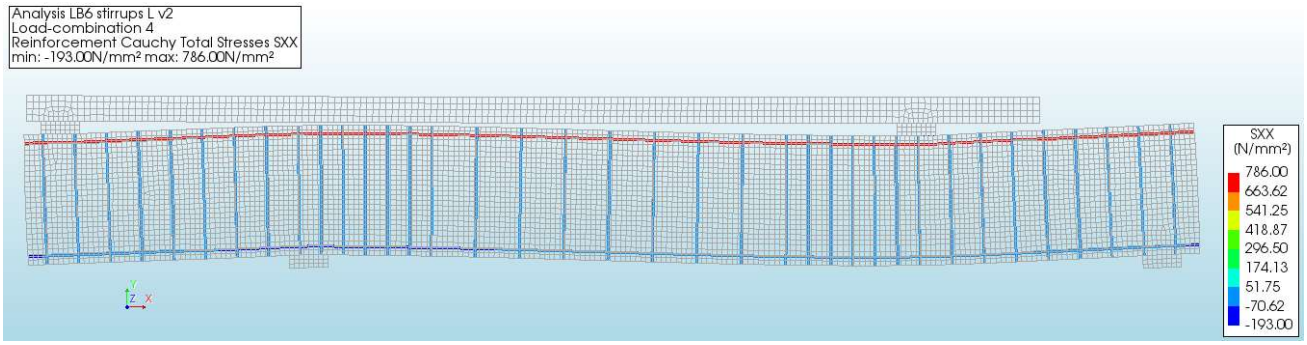

Figure 6-4 σ_{xx} in reinforcement under web-shear cracking load (1)

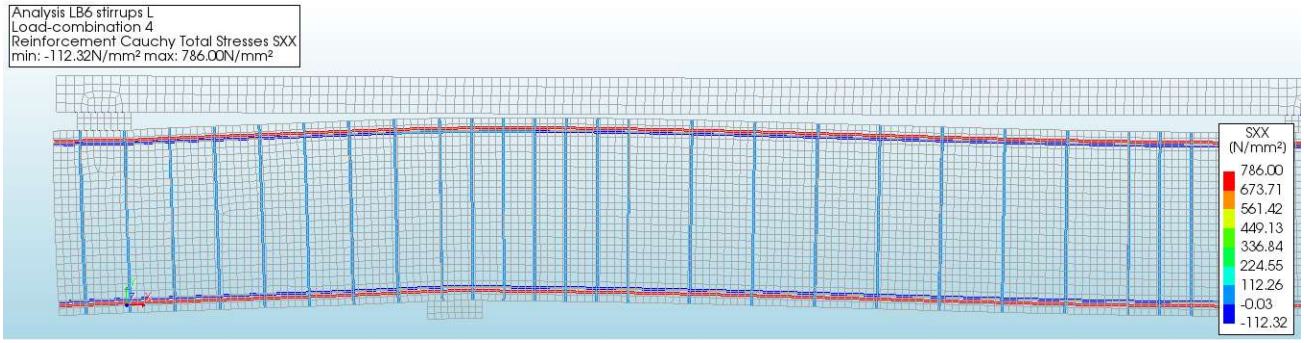

Figure 6-5 σ_{xx} in reinforcement under web-shear cracking load (2)

Figure 6-6 shows the vertical stress in the reinforcement. Obviously the stress in y-direction is zero in the longitudinal reinforcement and in the prestress. Normally it is assumed that the shear reinforcement only contributes when shear cracks are present. However the vertical stress in the stirrups varies between $-40\ N/mm^2$ and $-25\ N/mm^2$. These values are are probably the result of shear deformation.

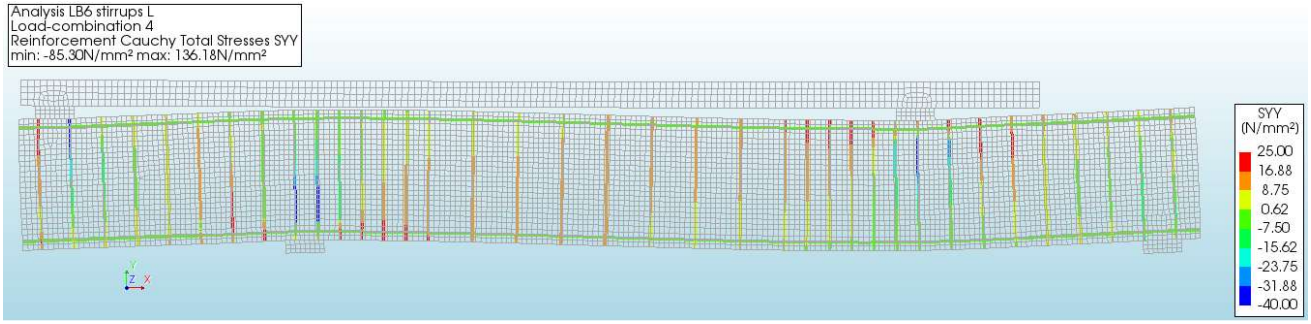

Figure 6-6 σ_{yy} in stirrups under web-shear cracking load (LB6)

Figure 6-7 shows the σ_{xx} distribution over the beam. Firstly it can be noted that peak compression stresses occur at the western support and the eastern load. These peaks occur due the interface material. It can also be noted that the beam behaves symmetrical, the western support shows practically same stress contours as the eastern load. This is the case because the because the σ_{xx} is built up out of three loads. The point loads generate a opposite moment of the same value at the western support compared to the eastern load. Thus create the same stresses in σ_{xx}. The prestress creates the same σ_{xx} over the whole height at both places. The small differences follow from the influence of the self-weight. However the analytical results already have shown that these influence are neglectable small. Further the moment inclination point in the middle of the beam is observable.

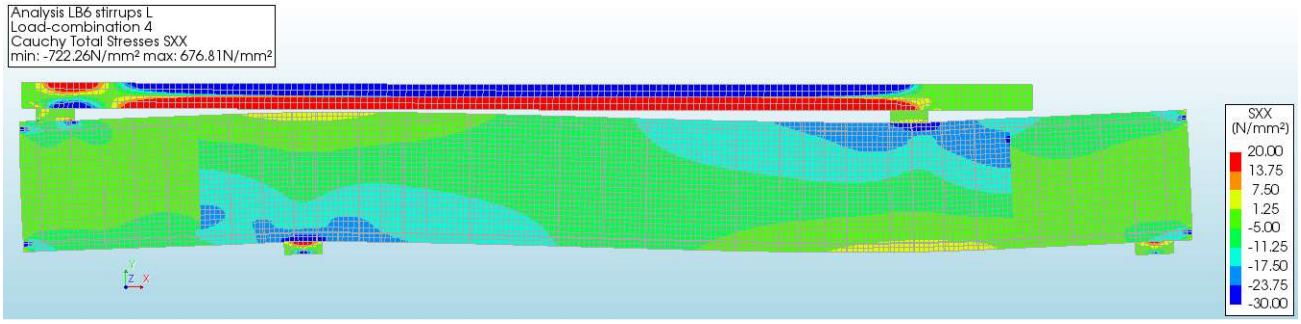

Figure 6-7 σ_{xx} in specimen LB6 under web-shear cracking load

The figure below shows the contours of σ_{yy}. A few things are noticeable, first of all it can be seen that the stress in y-direction is just as the stress in x-direction mirrored. This contour plot also shows the disturbed areas above the supports and below the loads. The area of the disturbed zone is approximately as Eurocode 2 expects: $45°$ from the inner part of the support-/load plate to the CoG. Outside the disturbed zone the maximum value of $\sigma_{yy} = 0.5\ N/mm^2$. Further away from the support the stress will go to zero.

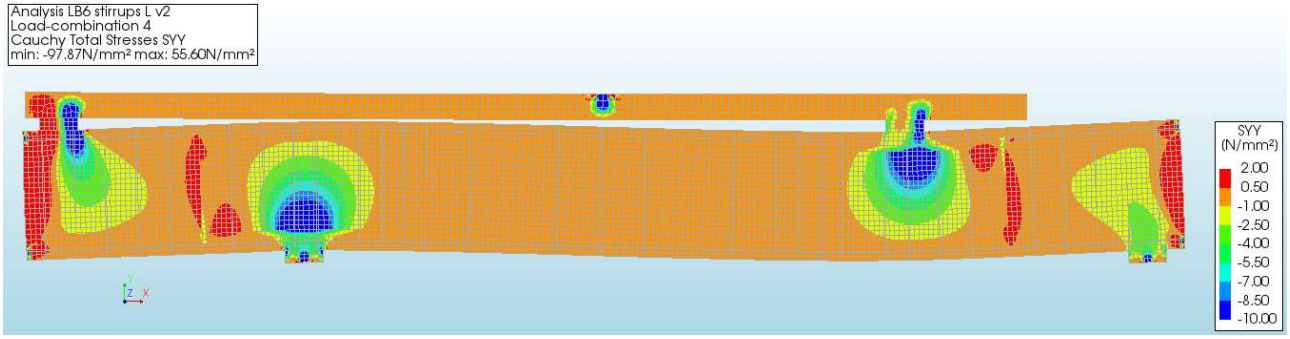

Figure 6-8 σ_{yy} in specimen LB6 under web-shear cracking load

Figure 6-9 shows the contours of the principle tensile stress. Just like the distribution of σ_{yy} the disturbed areas near the supports and loads are clearly visible in the distribution of σ_1. In this disturbed area both principle stresses are compression. The highest principle tensile stresses occur at both ends of the beam and in the junction between the rectangular cross-section and the I-beam cross-section. Further high stresses are found above the western support and under the eastern load, these locations are potential flexural cracking areas. Finally the location for potential web-shear cracks show high principle stresses, these are located at the cross-section approximately $45°$ out of the support-/ load plate to the CoG.

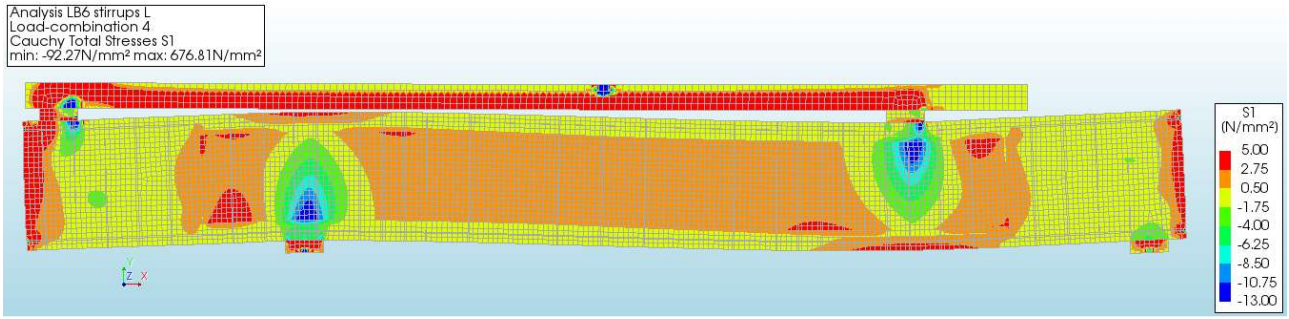

Figure 6-9 σ_1 in specimen LB6 under web-shear cracking load

In the figure below the limits are set in such a way that red zones indicate that the concrete tensile strength of $4.23\frac{N}{mm^2}$ is exceeded. It can be seen that that both ends of the beam exceed the tensile strength of the concrete. This is due the way of prestressing in the model, because no anchoring length is used. The junction between the rectangular cross-sections and the I-beam cross-section also shows exceeding of the concrete tensile strength, however during the experiments no cracks were found at this location. Furthermore it can be noted that in the top flange above the western support and in the bottom flange below the eastern load the tensile stresses are higher than the stresses in the tensile stresses at the critical cross-sections at $45°$ out of the support-/ load plates to the. This indicates that flexural cracks would appear before web-shear cracking while LB6 showed no flexural cracks during testing. This was also seen in the analytical analysis.

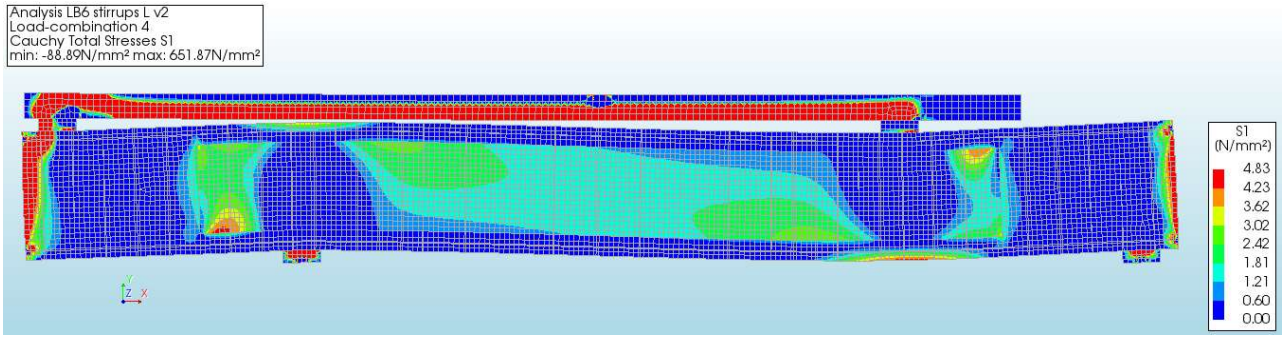

Figure 6-10 σ_1 in specimen LB6 under web-shear cracking load with f_{ctm} set as a limit

LB7

The results of the linear finite element analysis of LB7 are given below. The load is set to 80.1 kN, this is the load level at which first web-shear cracks occurred during testing. Figure 6-11 shows the displacement in y-direction, positive y is pointed upwards. The displacements are smaller than LB6 simply due the smaller load. Just like in LB6 a rotation in the spreader beam can be noticed, this creates two point loads on the specimen with the correct ratio.

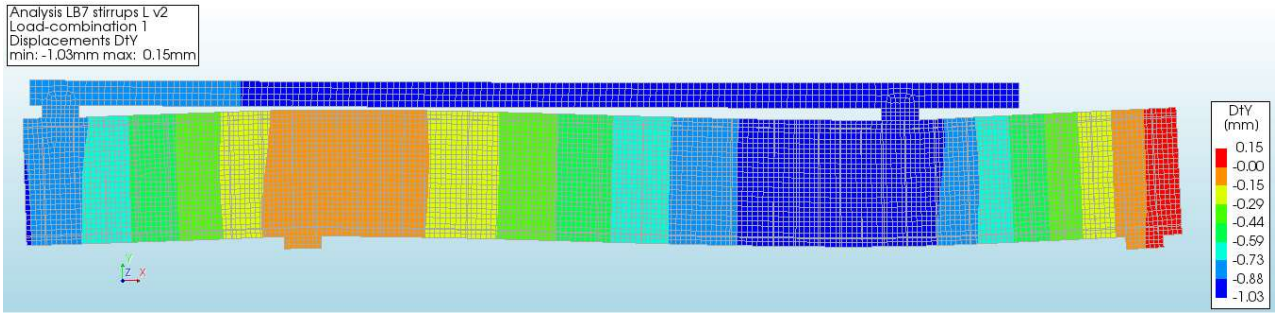

Figure 6-11 Displacement in y-direction under web-shear cracking load (LB7)

Figure 6-12 shows the σ_{yy} in the reinforcement. The stress in y-direction is logically zero in the longitudinal reinforcement. In the stirrups the stress differs between 20 and -40 N/mm^2. A peak stress is found near the west end of the specimen. This is a result of the interface conditions and rotation of the loading plate.

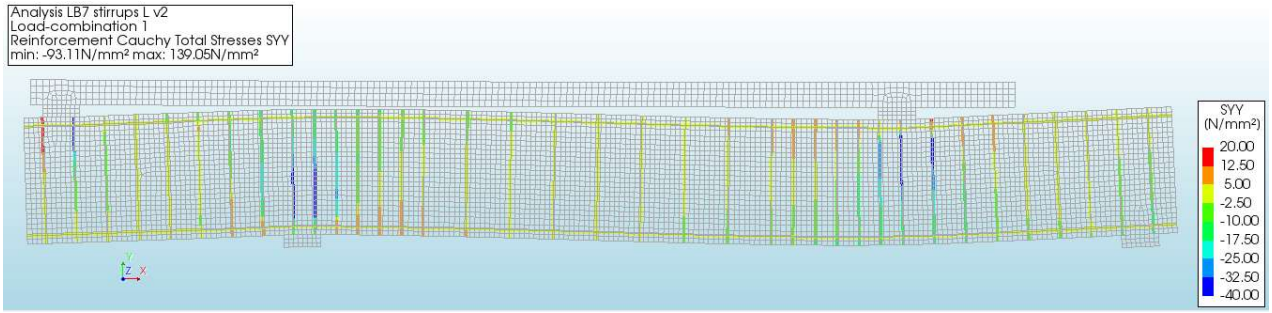

Figure 6-12 σ_{yy} in stirrups under web-shear cracking load (LB6)

The stress in the longitudinal reinforcement and in the prestress, σ_{xx}, is shown in Figure 6-13. Just like LB6 one side shows the stress in the longitudinal reinforcement and one side shows the stress in the prestressing bar, respectively top side and bottom side. This is due the fact that the longitudinal reinforcement is exactly places at the same height as the longitudinal reinforcement. Just like LB6 is the model check by moving the reinforcement and the prestress apart and it is found that both the longitudinal reinforcement as the prestress is implemented correctly. The found stress of $251.48\ N/mm^2$ is exactly half the prestressing force divided by the area of the strand. The compression stress in the reinforcement is the result of bending.

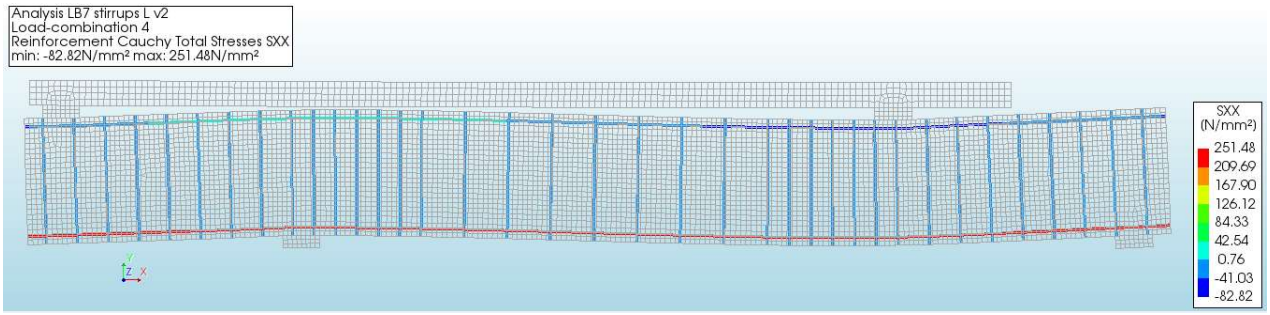

Figure 6-13 σ_{xx} in reinforcement under web-shear cracking load (LB7)

The figure below shows σ_{xx} in the specimen. As expected the highest stresses are found at the eastern load and at the western support since those are the locations of the maximum moment. Just like in LB6 the inclination point of the moment is clearly visible in the middle of these locations. The influence of the interface is also noticeable. The difference between the maximum and the minimum stress is the result of prestressing. Since the prestressing is a lot lower than in LB6, namely 255 kN compared to 797 kN, σ_{xx} has higher tension stresses in LB7.

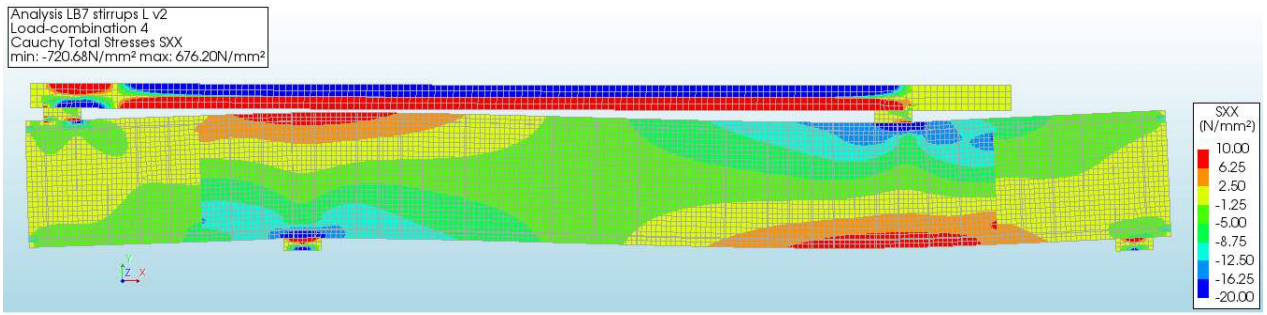

Figure 6-14 σ_{xx} in specimen LB7 under web-shear cracking load

The vertical stresses in LB7 are shown in Figure 6-15. The disturbed areas are clearly visible. Furthermore in the junction between I-profile and the rectangular cross-sections peak stresses are created. Just as near both ends of the beam. These fall outside the test region.

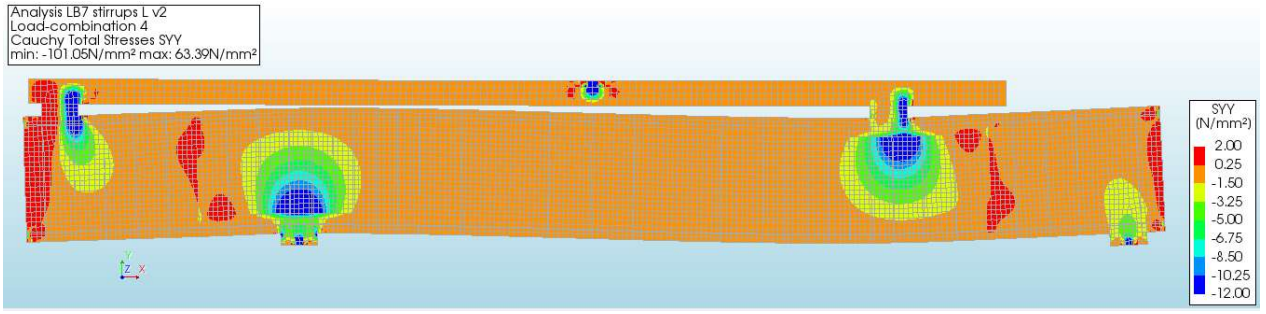

Figure 6-15 σ_{yy} in specimen LB7 under web-shear cracking load

Figure 6-16 and Figure 6-17 show σ_1 in the beam. Principle stresses are found up to approximately $9\ N/mm^2$, which is more than double the tensile strength of the concrete. Although bending cracks were present during testing at this load stage and thus values higher than the tensile strength are expected. The found values are higher than expected, since only a few minor cracks were present and these results show a whole area with higher principle tensile stresses than f_{ctm}.

In Figure 6-17 the red contour in the beam indicates the locations where $\sigma_1 > f_{ctm}$. During testing the first web-shear crack occurs at this load, but these results show that at this load a whole area in the web and in the flanges should be cracking. A clear difference with LB6 is found, LB6 shows smaller areas where σ_1 exceeds f_{ctm}. This indicated that more bending cracks were present at LB7 compared to LB6, which is also the found during testing. Also LB6 showed that the principle stress does not exceed f_{ctm} in the web, while LB7 clearly had an area where $\sigma_1 > f_{ctm}$ in the web.

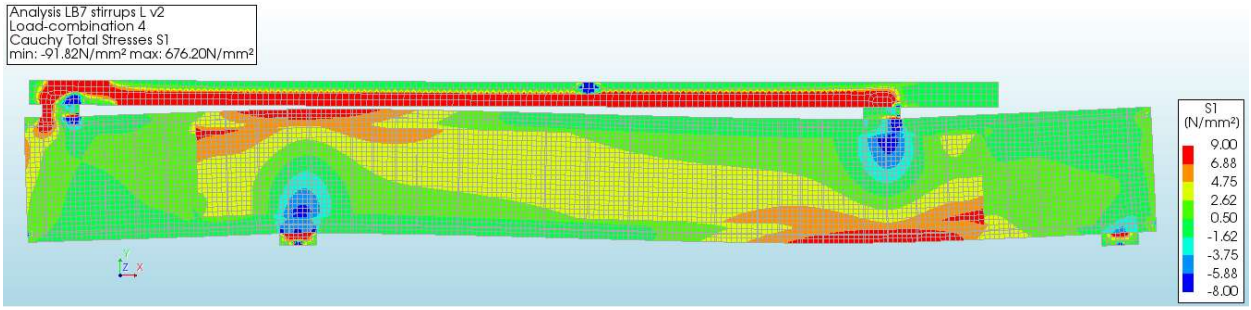

Figure 6-16 σ_1 in specimen LB7 under web-shear cracking load

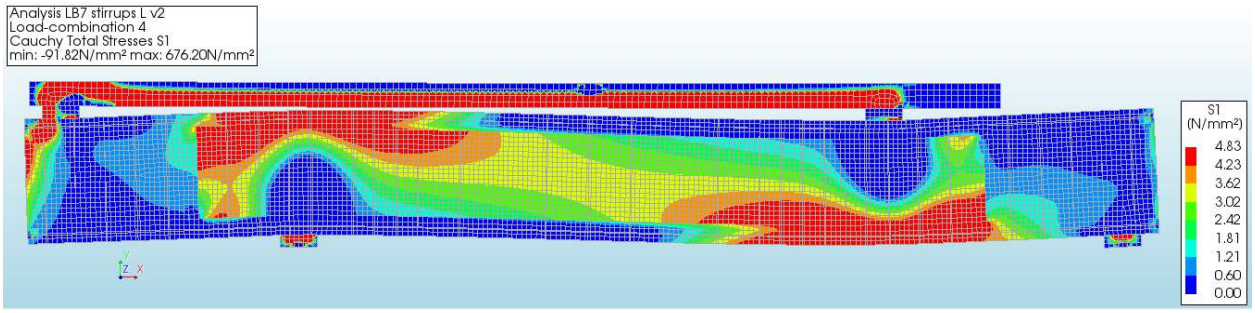

Figure 6-17 σ_1 in specimen LB7 under web-shear cracking load, f_{ctm} set as a limit

LB8

The results of LB8 are given in Figure 6-18 to Figure 6-24. The figure below shows the displacement in vertical direction, in which positive is upwards. Just like the other two experiments the shape of the deflection is as expected and a rotation is present in the spreader beam. The values are in between LB6 and LB7, just like the load of 111.2 kN is between the loads of LB6 and LB7.

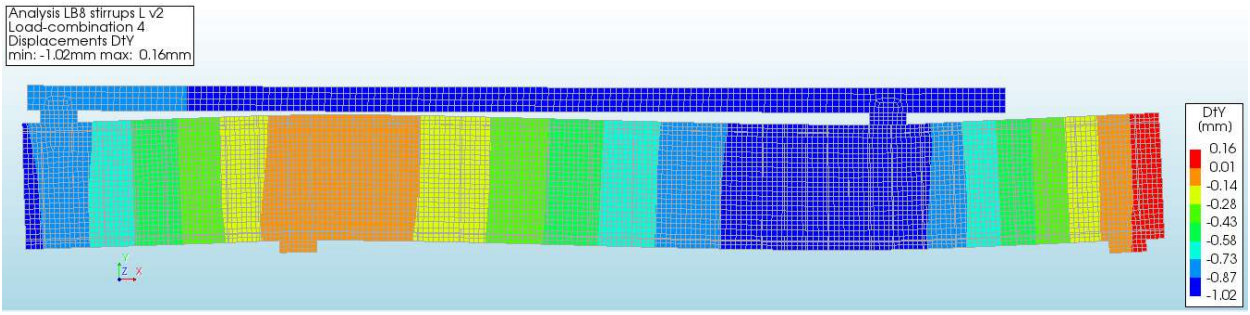

Figure 6-18 Displacement in y-direction under web-shear cracking load (LB8)

Just as in the results of LB6 and LB7 the horizontal stresses in the reinforcement shows the stress in the prestress tendon (bottom) and in the longitudinal reinforcement (top), Figure 6-19. The stress in the prestress is exactly half the prestressing force divided by the area of the unbonded tendon. The stress in the longitudinal reinforcement is a result of the moment and therefore maximum at the eastern load. However this maximum stress is also found in the bottom layer above the western support. This is logical since at both locations the moment is maximum and opposite of each other.

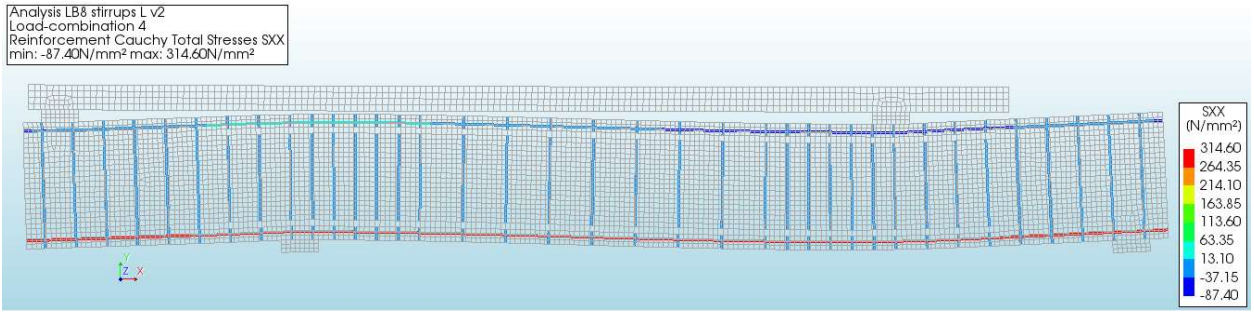

Figure 6-19 σ_{xx} in reinforcement under web-shear cracking load

The stresses in y-direction in the reinforcement are comparable to those of LB6 and LB7, Figure 6-20. With the maximum σ_{yy} found at the eastern load and the western support due to the presence of maximum moment and shear deformation.

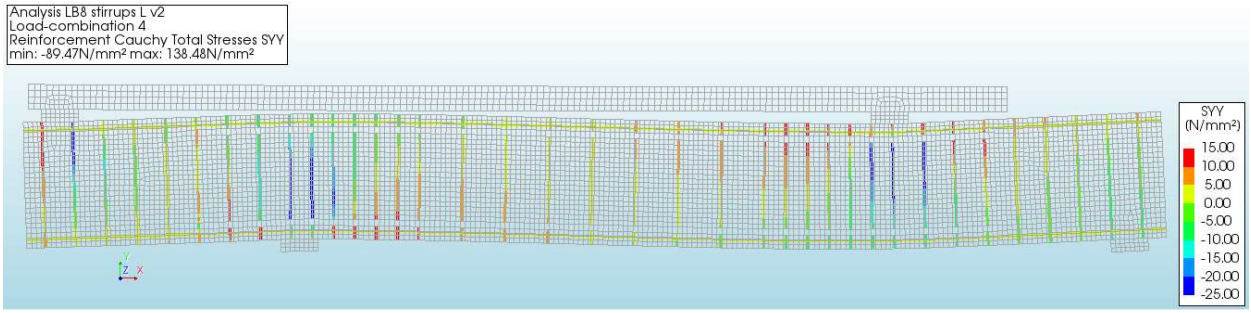

Figure 6-20 σ_{yy} in stirrups under web-shear cracking load

Figure 6-21 shows σ_{xx} in the beam. The shape of the contours is like those shown in LB6 and LB7. The values are comparable to those of LB7. This is due the fact that the prestressing force is almost double and thus a shift in σ_{xx} is expected towards compression. However the load is set to the load at which the first web-shear crack occurs and that is almost 50% higher for LB8 and thus the moment from which the σ_{xx} follows is also almost 50% higher. These two cancel each other out and this results in approximately the same horizontal stresses in LB8 as in LB7. Furthermore the moment inclination point is clearly visible again at the center of the beam.

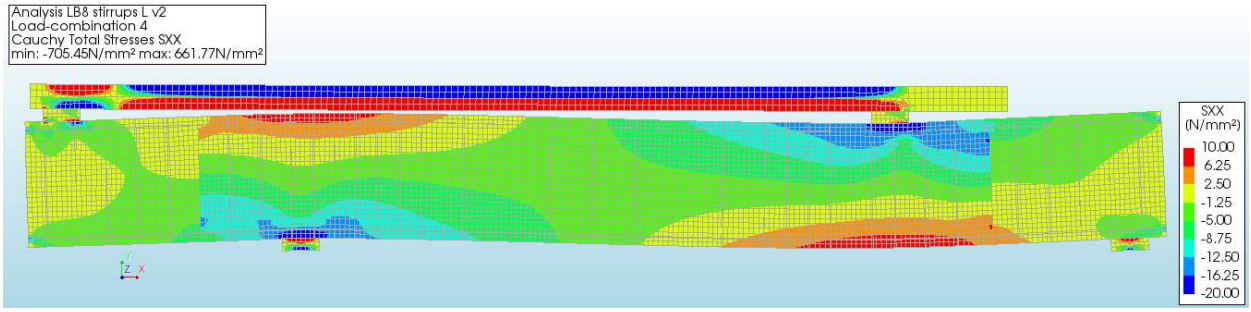

Figure 6-21 σ_{xx} in speciment LB8 under web-shear cracking load

Figure 6-22 shows σ_{yy} in specimen LB8. The contour plot is similar to that of LB6 and LB7, with a clear disturbed area under the eastern load and above the western support and peak stresses at the junction between the I-profile and the rectangular cross-sections and near both ends of the beam. The values of σ_{yy} are comparable to those of LB7, even though the load is approximately 50% higher.

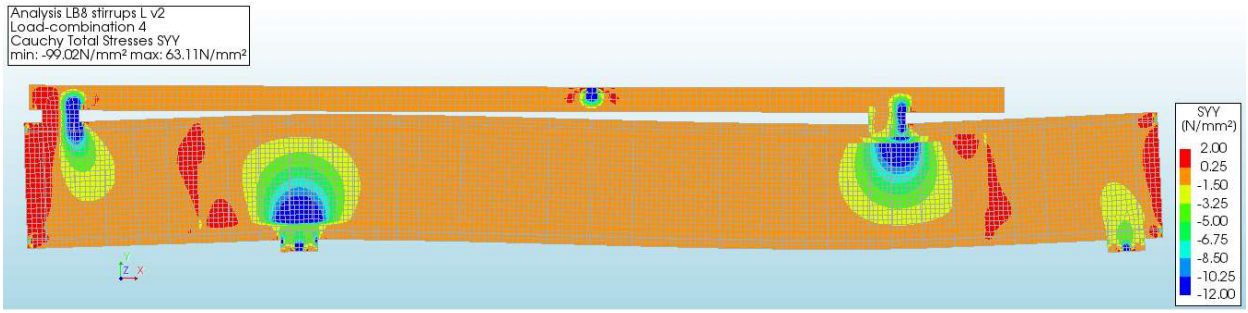

Figure 6-22 σ_{yy} in specimen LB8 under web-shear cracking load

Figure 6-23 shows the principle stress. The contour plot is similar to LB7. Both western load and eastern support show peak stresses at the outer fiber. These stresses have a maximum of approximately $9\ N/mm^2$. Figure 6-24 displays the same principle stress, however the limits are changed. In this figure the red areas are the areas in which $\sigma_1 > f_{ctm}$. The areas are comparable to LB7 even though LB7 showed flexural cracks before web-shear cracking and LB8 these cracks occurred simultaneously.

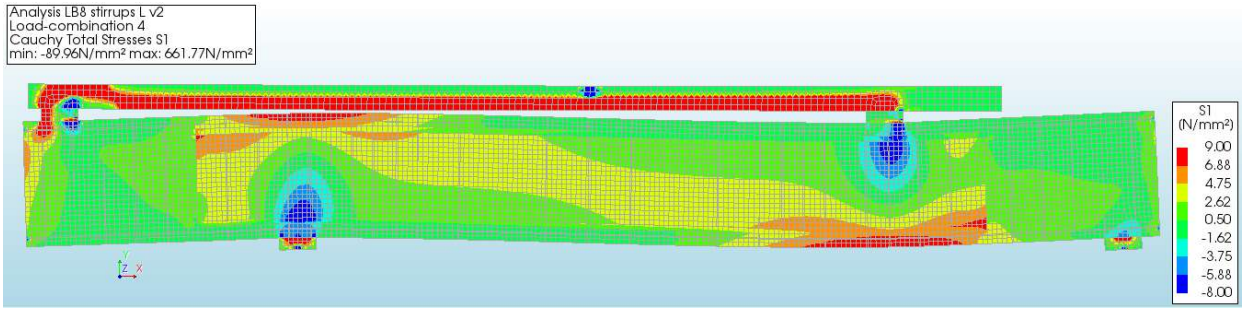

Figure 6-23 σ_1 in specimen LB8 under web-shear cracking load

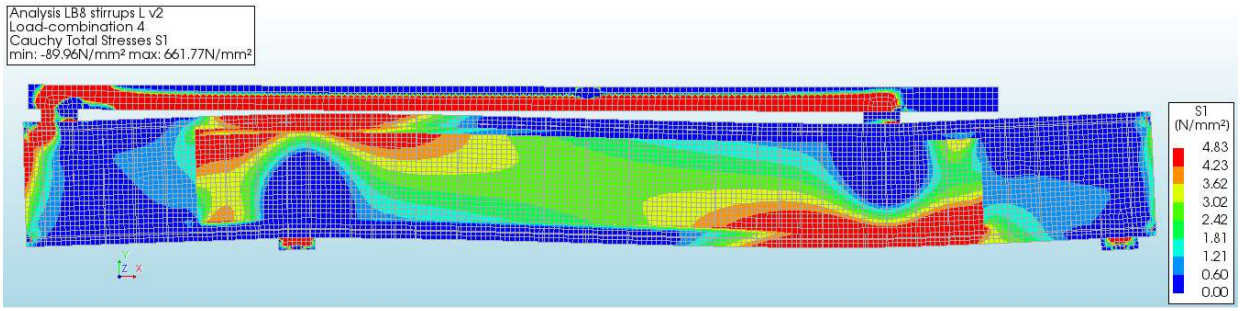

Figure 6-24 σ_1 in specimen LB8 under web-shear cracking load, f_{ctm}set as a limit

6.4 Comparison of results

As explained in chapter 3 it is very interesting to compare the analytical solution with the LFEA, because a LFEA can be performed rather quick compared to a NLFEA. Therefore it might be lucrative to perform LFEA over NLFEA and over analytical methods. In this paragraph the results of LFEA and analytical analysis will be compared to each other per specimen.

LB6

Table 6-7 Maximum principle tensile stresses (LB6)shows the maximum principle tensile stress of specimen LB6. The figure on the right hand side of the table indicate the locations, the highlighted area is the area that is checked conform EC2. This area is $45°$ out of the inner part of the support to the CoG. Location A is the location in where $\sigma_{1\_EC2\_\max}$ is found. For all specimen $\sigma_{1\_EC2\_\max}$ is found at this location, since the maximum moment in the area conform the EC2 is found in the this plain and the shear force does not change within the test region. At location A $\sigma_{1\_\mathrm{LFEA}\_A}$ is 20% lower than the $\sigma_{1\_EC2\_\max}$.

Location B is the location where $\sigma_{1\_\mathrm{LFEA}\_\max}$ is found. The results of LB6 show that the maximum principle stress in the LFEA is found within the area of the EC2, namely 40 mm to the right. The $\sigma_{1\_\mathrm{LFEA}\_\max}$ found in location B is only 1 percent higher than σ_{1_LFEA} at location A.

It can be concluded that if the EC2 is followed an analytical analysis results in a principle tensile stress of 3.31 N/mm^2 and a finite linear analysis would result in 2.68 N/mm^2. This is a reduction of 19 percent.

If ACI is followed only the values at CoG are checked. Two locations are interesting here, namely the location which shows maximum principle stress conform the analytical solution and the location which shows the maximum principle stress conform LFEA. Location C is the location where $\sigma_{1\_ACI\_\max}$ is found. $\sigma_{1\_ACI\_\max}$ is found to be 2.13 N/mm^2 which is 63 percent higher than $\sigma_{1\_\mathrm{LFEA}\_C}$, which is 1.31 N/mm^2. The maximum principle tensile stress according to the LFEA at the CoG is found 226 mm to the right, location D. At this location $\sigma_{1\_ana\_D} = 2.12\ N/mm^2$ compared to $\sigma_{LFEA\_max\_CoG} = 1.85\ N/mm^2$. The difference between $\sigma_{1\_ACI\_\max}$ and $\sigma_{LFEA\_max\_CoG}$ is a reduction of 13%.

Table 6-7 Maximum principle tensile stresses (LB6)

LB6	Location	Ana	LFEA	x
	[-]	$[\frac{N}{mm^2}]$	$[\frac{N}{mm^2}]$	[mm]
Over height	A	3.31	2.65	0
	B	3.17	2.68	41
At CoG	C	2.13	1.31	0
	D	2.12	1.85	226

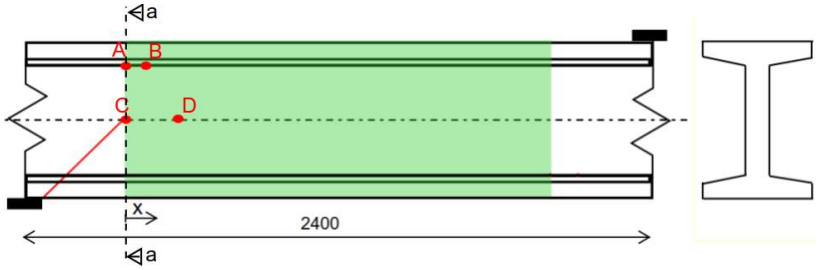

Figure 6-25 Locations of maximum principle stresses (LB6)

It is well known that the principle tensile stresses are a result of σ_{xx}, σ_{yy} and σ_{xy}. To find where the previously discussed differences in σ_1 between the LFEA and the analytical analysis come from the stresses distributions are plotted in Figure 6-26 to Figure 6-29. In these figures on the y-axis the height is given in mm and on the x-axis the magnitude of the stress in N/mm^2. The horizontal dotted blue lines indicate from top to bottom: top of the beam, start of inclined part, start of web, end of web, end of inclined part and bottom of beam.

These stress distributions are located at cross-section a-a. The analytical and numerical stress distribution of σ_{xx} match well, apart from the stress in the bottom flange. This difference in the bottom is most likely a result of the interface in the support and the fact that the analytical analysis assumes pure bending. The found values at location A are: $\sigma_{xx\_ana} = -3.1\ N/mm^2$ and $\sigma_{xx\_ana} = -2.1\ N/mm^2$.

An obvious difference between the analytical analysis and the LFEA is that σ_{yy} is neglected in the analytical analysis, this is also done in practice. At the junction between the flanges and the web the magnitude of σ_{yy} is approximately -0.1 N/mm^2.

The difference in the shear stress is found to be quite small, Figure 6-28. At the junction between the web and top flange the calculated shear stress analytically and numerical are respectively -4.2 and -4 N/mm^2. This is a difference of just 5%.

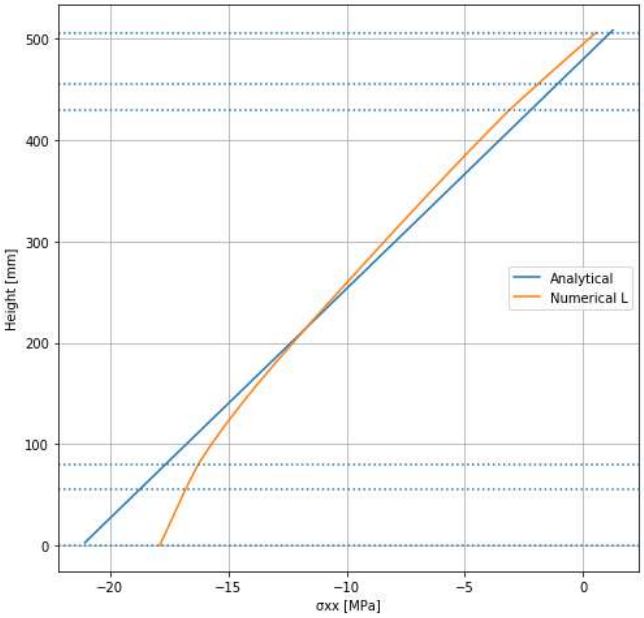

Figure 6-26 σ_{xx} distribution at a-a (LB6)

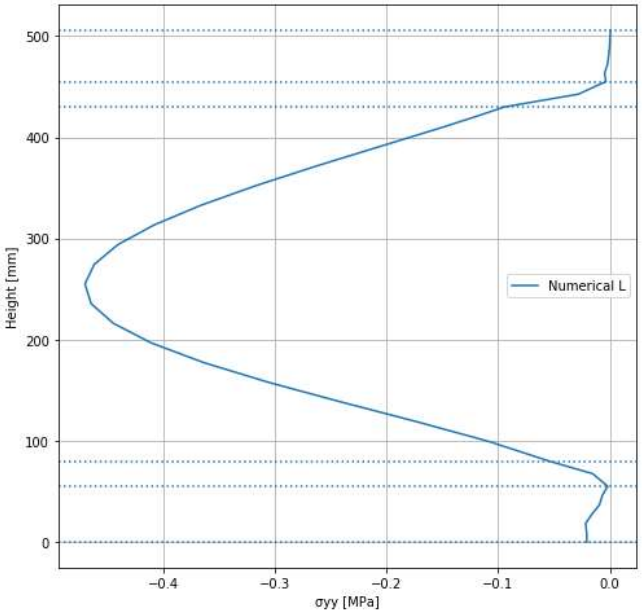

Figure 6-27 σ_{yy} distribution at a-a (LB6)

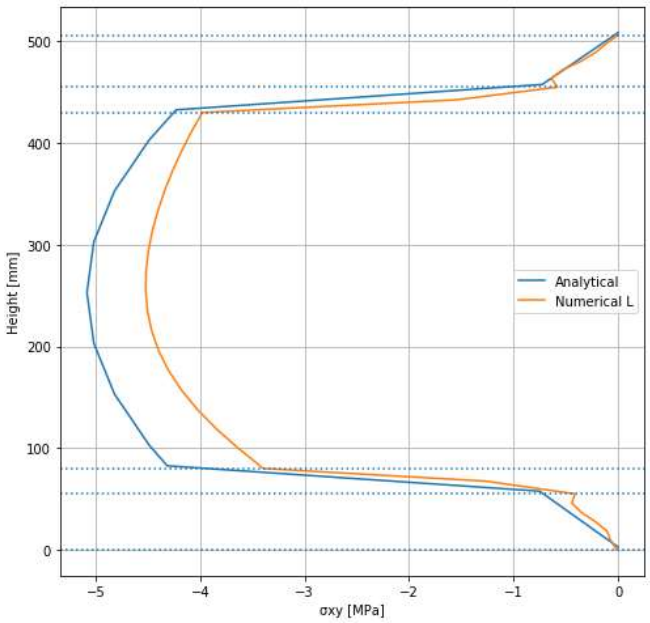

Figure 6-28 σ_{xy} distribution at a-a (LB6)

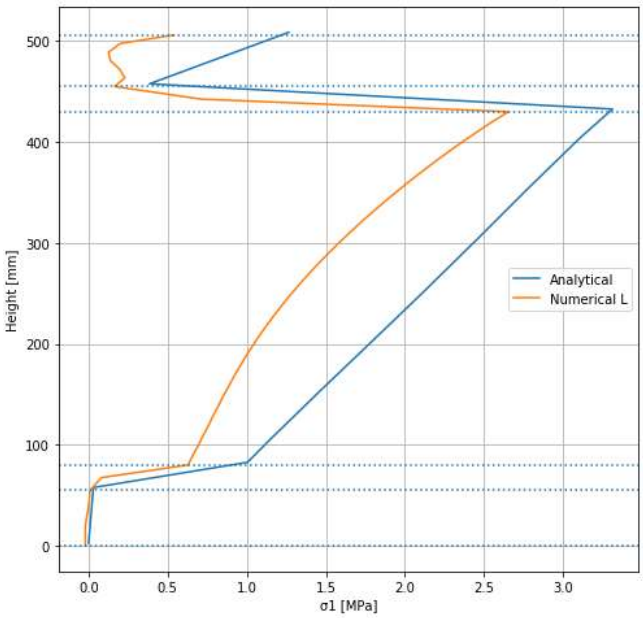

Figure 6-29 σ_1 distribution at a-a (LB6)

The table below shows what influence the differences in stresses have on σ_1. The first two rows indicate how the principle stresses are built up in the analytical analysis and in the LFEA. In the last three rows one of the stresses of the analytical solution is changed to the value of the LFEA and σ_1 is calculated conform equation 2.1. The last column shows the change in σ_1 due to the changed value of σ_{xx}, σ_{yy} or σ_{xy}.

Since all values in the last column are negative all differences in σ_{xx}, σ_{yy} and σ_{xy} result in a reduction of σ_1. It can be concluded that neglecting σ_{yy} is only a very small part of the difference between σ_{1_ana} and σ_{1_LFEA}. Furthermore the difference in σ_{xx} contributes most to the difference in σ_1.

Table 6-8 Influence of difference in σ_{xx}, σ_{xx} and σ_{xx} on σ_1

LB6	σ_{xx} $[N/mm^2]$	σ_{yy} $[N/mm^2]$	σ_{xy} $[N/mm^2]$	σ_1 $[N/mm^2]$	**Influence on σ_1** $[N/mm^2]$
Analytical	-2.09	-	-4.23	**3.31**	-
LFEA	-3.10	-0.09	-3.97	**2.65**	-
Ana - with σ_{xx} of the LFEA	**-3.10**	-	-4.23	**2.96**	-0.36
Ana - with σ_{yy} of the LFEA	-2.09	**-0.09**	-4.23	**3.28**	-0.03
Ana - with σ_{xy} of the LFEA	-2.09	-	**-3.97**	**3.06**	-0.25

LB7

Table 6-9 Maximum principle stresses (LB7)shows the maximum principle tensile stresses at critical locations. Location A is the location where both $\sigma_{1\_EC2\_\max}$ and $\sigma_{1\_LFEA\_max}$ are located. The maximum principle tensile stress is calculated with LFEA is 21% lower than the analytically found value. The values are respectively 2.98 N/mm^2 and 2.35 N/mm^2.

As explained before the ACI only check for the maximum tensile stress at the CoG this results in $\sigma_{1\_ACI\_\max} = 1.62\ N/mm^2$ at location B. At that location $\sigma_{1\_LFEA\_B} = 1.11\ N/mm^2$. This is a difference of 31%. The maximum principle stress at the CoG according to the LFEA is found at C, located 226 mm towards the center of the test region. The value for $\sigma_{1\_LFEA\_\max\_C.o.G} = 1.38\ N/mm^2$. This means that the maximum σ_1 found with the ACI is $1.62\ N/mm^2$ and with LFEA it is $1.38\ N/mm^2$, this is a reduction of 14%.

Table 6-9 Maximum principle stresses (LB7)

LB7	Location	Ana	LFEA	x
	[-]	$[\frac{N}{mm^2}]$	$[\frac{N}{mm^2}]$	[mm]
Over height	A	2.98	2.35	0
At CoG	B	1.62	1.11	0
	C	1.61	1.38	226

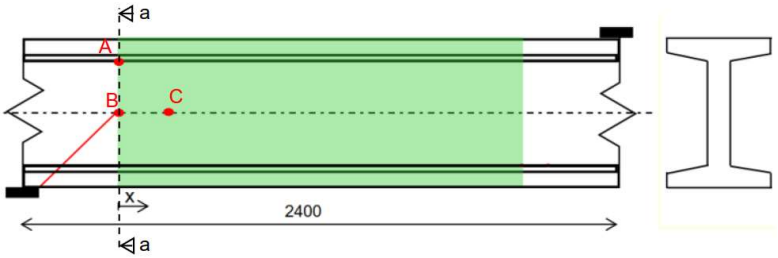

Figure 6-30 Locations of maximum principle stress (LB7)

The stress distributions of $\sigma_{xx}, \sigma_{yy}, \sigma_{xy}$ and σ_1 at cross-section a-a are given in Figure 6-31 to Figure 6-34. The stress distribution of σ_{xx} is similar to the one of LB6, again the influence of the interface at the bottom is noticeable. At the location A the difference is approximately 0.6 N/mm^2, $\sigma_{xx_ana} = 1\ N/mm^2$and $\sigma_{xx\_LFEA} = 0.4\ N/mm^2$.

The vertical stresses are once again neglected in the analytical analysis. The vertical stress in the LFEA at A is with $-0.03\ N/mm^2$only 7.5% of σ_{xx} at that location. This shows that the contribution of σ_{yy} to σ_1 is minimal compared to σ_{xx} and thus neglecting σ_{yy} in the analytical analysis does not explain the big difference in σ_{1_ana} and σ_{1_LFEA}.

Just like in LB6 the difference in shear stresses at location A between analytical analysis and LFEA is rather big with 35%. However it is just $0.8\ N/mm^2$difference, which is almost equal to the difference in σ_{xx} and in formula 2.1 it can be seen that σ_{xx} has a larger influence on σ_1 than σ_{xy}.

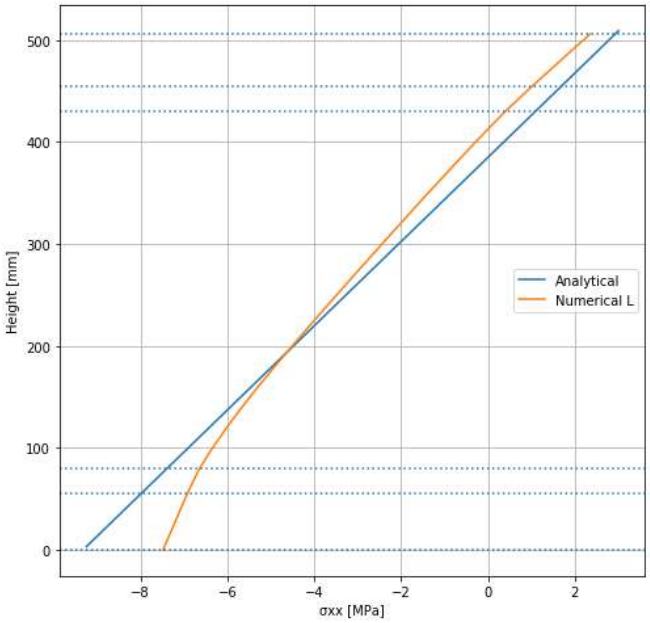

Figure 6-31 σ_{xx} distribution at a-a (LB7)

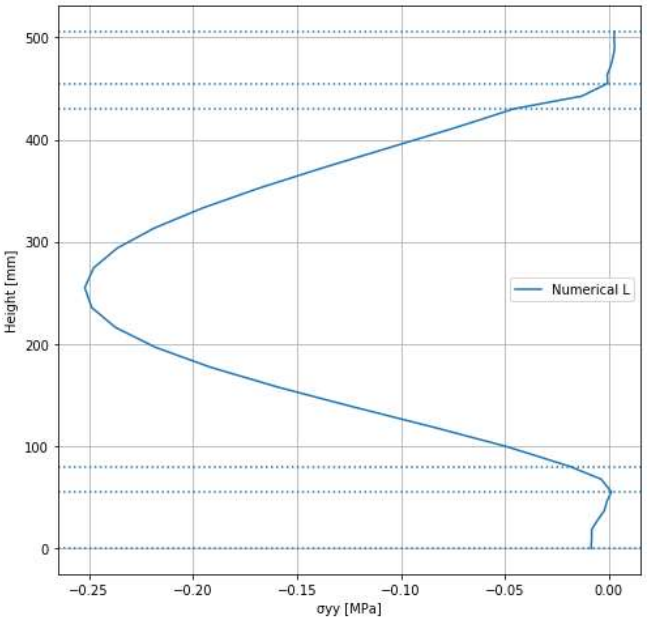

Figure 6-32 σ_{yy} distribution at a-a (LB7)

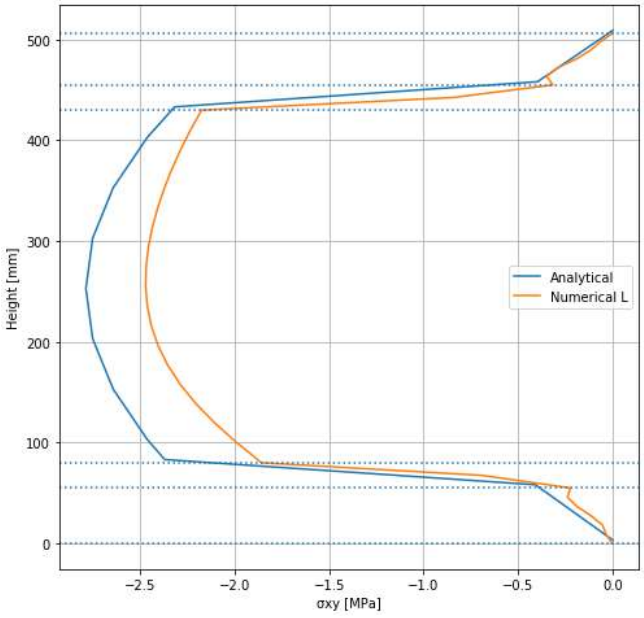

Figure 6-33 σ_{xy} distribution at a-a (LB7)

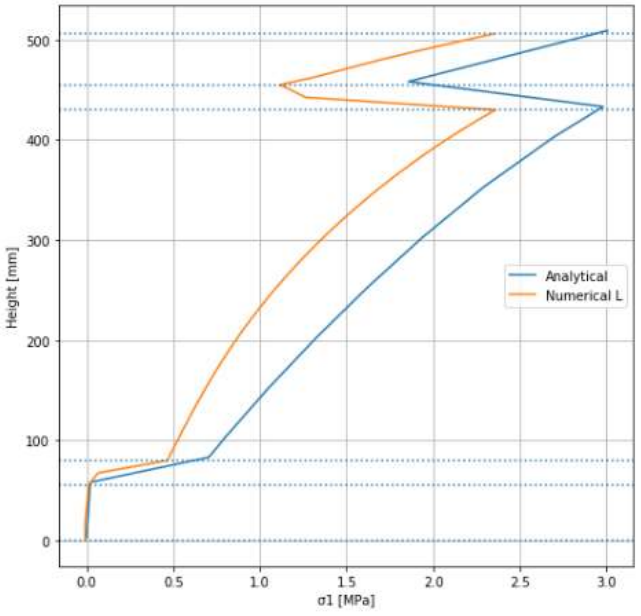

Figure 6-34 σ_1 distribution at a-a (LB7)

Table 6-10 shows what influence the differences in stresses have on σ_1. Just like LB6 all values in the last column are negative, meaning all differences in σ_{xx}, σ_{yy} and σ_{xy} result in a reduction of σ_1. It can be concluded that neglecting σ_{yy} in the analytical analysis only result in a very slight difference in σ_1. Furthermore it can be concluded that the biggest difference in σ_1 between the analytical analysis and the LFEA follows from the difference in σ_{xx}. This influence is three times as big as the influence of the difference in σ_{xy}.

Table 6-10 Influence of difference in σ_{xx}, σ_{xx} and σ_{xx} on σ_1

LB7	$\boldsymbol{\sigma_{xx}}$ $[N/mm^2]$	$\boldsymbol{\sigma_{yy}}$ $[N/mm^2]$	$\boldsymbol{\sigma_{xy}}$ $[N/mm^2]$	$\boldsymbol{\sigma_1}$ $[N/mm^2]$	**Influence on σ_1** $[N/mm^2]$
Analytical	1.17	-	-2.32	**2.98**	
LFEA	0.39	-0.05	-2.17	**2.35**	
Ana - with $\boldsymbol{\sigma_{xx}}$ of the LFEA	**0.39**		-2.32	**2.52**	-0.45
Ana - with $\boldsymbol{\sigma_{yy}}$ of the LFEA	1.17	**-0.05**	-2.32	**2.95**	-0.03
Ana - with $\boldsymbol{\sigma_{xy}}$ of the LFEA	1.17		**-2.17**	**2.83**	-0.15

LB8

Table 6-11 shows the crucial principle tensile stresses found with a analytical analysis and a LFEA for LB8. Just like LB7 locations A is where both $\sigma_{1\_EC2\_max}$ and $\sigma_{1\_LFEA\_max}$ are located. The maximum principle tensile stress conform the EC2 is with 4.33 N/mm^2 19% higher compared to the maximum principle stress which follows from the LFEA, which is 3.50 N/mm^2.

Conform the ACI, only checking CoG for maximum principle tensile stress, $\sigma_{1\_ACI\_max}$ is located at B with a value of 2.33 N/mm^2. At this location $\sigma_{1\_LFEA\_B} = 1.59\ N/mm^2$, which is 32 percent lower. However $\sigma_{1\_LFEA\_\max\_C.o.G.}$ is found in the LFEA at location C with a value of 1.94 N/mm^2. C is located 154 mm towards the center of the test region. The difference between the ACI and LFEA is thus 2.33 N/mm^2 and 1.94 N/mm^2, which is a reduction of 17 percent.

Table 6-11 Maximum principle stresses (LB8)

LB8	Location	Ana	LFEA	x
	[-]	$[\frac{N}{mm^2}]$	$[\frac{N}{mm^2}]$	[mm]
Over height	A	4.33	3.50	0
At CoG	B	2.33	1.59	0
	C	2.32	1.94	154

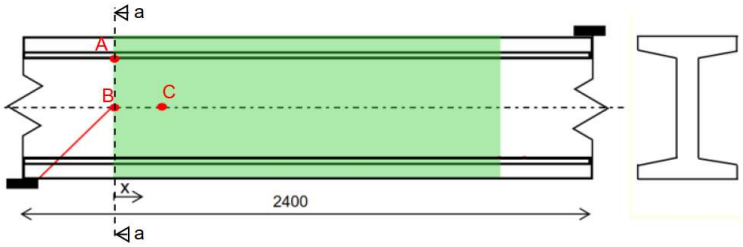

Figure 6-35 Locations of maximum principle stresses (LB8)

Figure 6-36 to Figure 6-37 show in order the stress distribution of σ_{xx}, σ_{yy}, σ_{xy} and σ_1 at cross-section a-a. The distributions have comparable shapes as LB6 and LB7. The distribution of σ_{xx} shows again a significant difference at the bottom fiber assumedly due to the presence of the support and due shear deformation.

The distribution of σ_{yy} shows that the value is approximately -0.02 N/mm^2 at location A. This is just as in LB6 and LB7 neglectable small. At the center of gravity it however contributes more to the difference between σ_{1_ana} and σ_{1_LFEA} with a value of -0.32 N/mm^2.

The shear stress at the junction between web and flange differs approximately 0.25 N/mm^2 between analytical analysis and LFEA. This is about 17 percent difference. At the CoG this difference increases to approximately 0.35 N/mm^2.

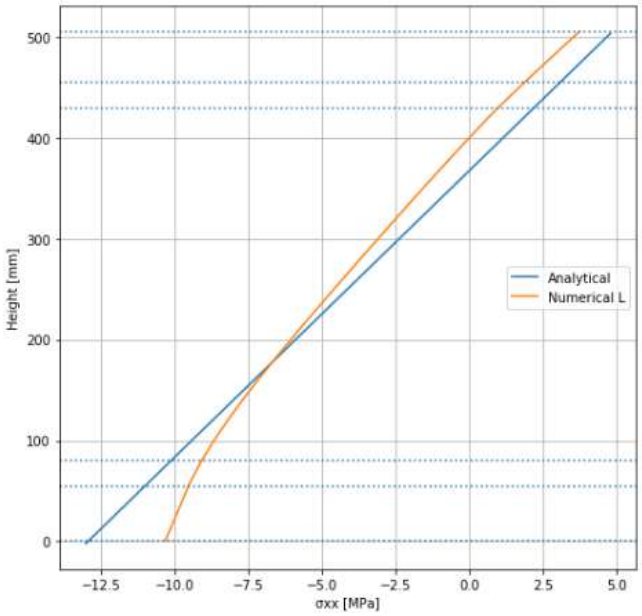

Figure 6-36 σ_{xx} distribution at a-a (LB8)

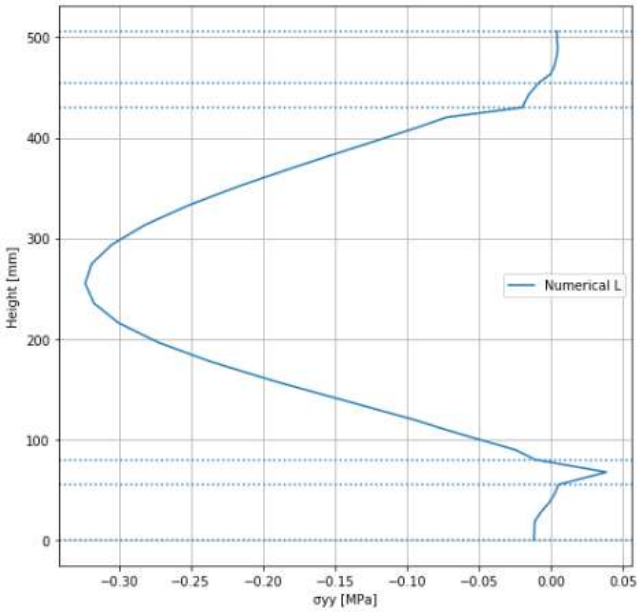

Figure 6-37 σ_{yy} distribution at a-a (LB8)

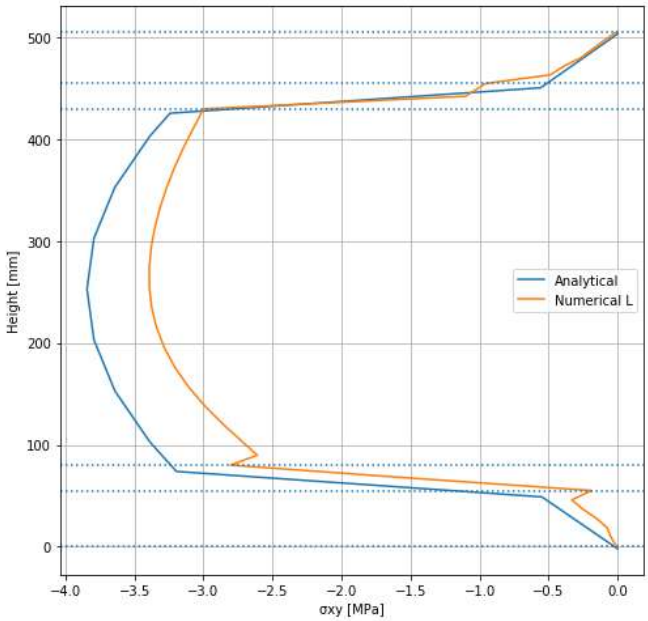

Figure 6-38 σ_{xy} distribution at a-a (LB8)

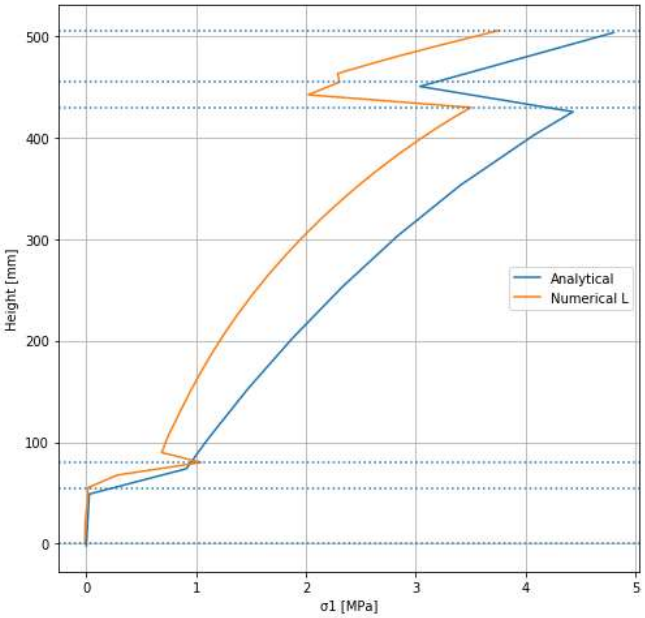

Figure 6-39 σ_1 distribution at a-a (LB8)

Table 6-12 shows just like in LB6 and LB7 the different built up of σ_1 at location A of the analytical analysis and the LFEA. The last three rows have the same values as the analytical analysis except for one stress, which is given the value of the LFEA. The principle stress is calculated with equation 2.1. This gives good insight to the influence of the difference in e.g. σ_{xx} to the difference in σ_1.

The results are similar to LB7, the influence of σ_{yy} is again neglectable. Meaning that the assumption of no vertical stresses at cross-section a-a which is made in the analytical analysis is justified. Again the stress with the most influence is σ_{xx} which results in 70 percent of the difference in σ_1. This means that the assumption of a Euler Bernoulli beam increases the principle stress by 0.66 N/mm^2.

Table 6-12 Influence of difference in σ_{xx}, σ_{xx} and σ_{xx} on σ_1

LB8	$\boldsymbol{\sigma_{xx}}$ $[\boldsymbol{N/mm^2}]$	$\boldsymbol{\sigma_{yy}}$ $[\boldsymbol{N/mm^2}]$	$\boldsymbol{\sigma_{xy}}$ $[\boldsymbol{N/mm^2}]$	$\boldsymbol{\sigma_1}$ $[\boldsymbol{N/mm^2}]$	**Influence on $\boldsymbol{\sigma_1}$** $[\boldsymbol{N/mm^2}]$
Analytical	2.05	-	-3.25	**4.43**	-
LFEA	0.98	-0.06	-3.00	**3.50**	-
Ana - with $\boldsymbol{\sigma_{xx}}$ of the LFEA	**0.98**	-	-3.25	**3.78**	-0.66
Ana - with $\boldsymbol{\sigma_{yy}}$ of the LFEA	2.05	**-0.06**	-3.25	**4.39**	-0.04
Ana - with $\boldsymbol{\sigma_{xy}}$ of the LFEA	2.05	-	**-3.00**	**4.20**	-0.24

7 Non-linear finite element analysis

7.1 Model

The geometry of the non-linear analysis is obvious similar to the geometry of the linear analysis. The differences lay in the non-linear behaviour of the concrete. Figure 7-1 shows that not the whole beam is modelled with the non-linear concrete. Both ends of the beam, the rectangular cross-sections and a small part of the I-profile, are modelled with linear material. This is done because when modelled with non-linear tensile behaviour the beams starts cracking at the end of the beam, the location where prestress in introduced. As well as in the junction between the rectangular cross-section and the I-profile. Figure 7-1 also shows that half of the test region is modelled with linear concrete material properties. This is done to reproduce the cracks in the same area as in the experiment. The analytical analysis and the LFEA already showed that the principle tensile stress under the eastern load is in some cases larger than the principle tensile stress above the western support.

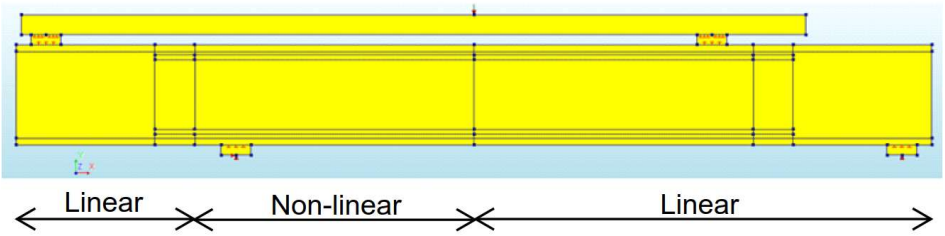

Figure 7-1 Indication of areas modelled with non-linear material

The concrete is modelled with the properties given in Table 7-1. The linear material properties are similar to the properties in the LFEA. The tensile strength is set to f_{ctm} conform EC2. The crack orientation is set to rotating to keep the spurious stress-locking to a minimum. The Poisson ratio is set to 0.2 and no reduction during cracking is applied.

Table 7-1 Concrete properties

Concrete			
Linear material properties			**Reference**
E	$[N/mm^2]$	40300	RTD
$\boldsymbol{\nu}$	[-]	0.2	RTD
$\boldsymbol{\rho}$	$[T/mm^3]$	2.4E-09	Xie
Non-linear material properties			
Tensile strength	$[N/mm^2]$	4.23	EC2
Tensile fracture energy	$[N/mm]$	0.1436	RTD
Compressive strength	$[N/mm^2]$	63.5	Xie
Compressive fracture energy	$[N/mm^2]$	36.9	RTD

The non-linear tensile behaviour is based on the Hordijk relationship, shown in Figure 7-2. This is an exponential-type softening diagram, which is preferred. The parameters are f_t is the tensile strength, G_f is the fracture energy and h is the equivalent length. The latter follows from mesh size. The area below the curve of Hordijk is the fracture energy divided by the equivalent length. The fracture energy is calculated with equation 7.1.

$$G_f = 0.073 f_{cm}^{0.18} \tag{7.1}$$

The model used for compression behaviour is the parabolic compression diagram, Figure 7-3. The parameters stand for: G_c compression fracture energy, h is once again equivalent length and f_c is the compressive strength. The compression fracture energy is 250 times the tensile fracture energy. The compressive strength is determined with tests.

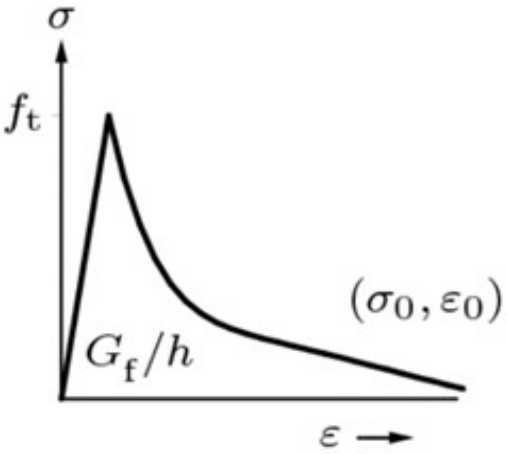

Figure 7-2 Hordijk softening

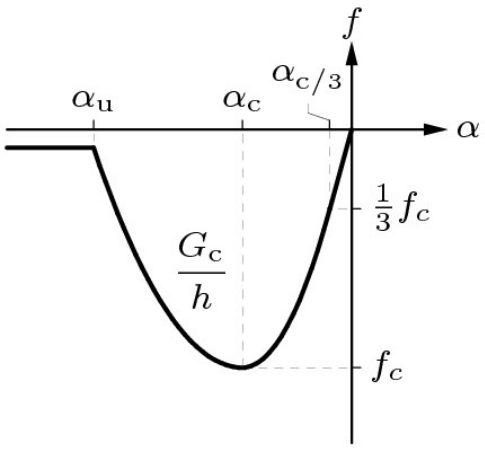

Figure 7-3 Parabolic compression diagram

The steel properties used in the support-, load plates and in the spreader beam are kept similar to the LFEA. The interface conditions are also kept the same.

The longitudinal reinforcement is checked and is found not reaching the plasticity and is therefore modelled linear with the same properties as in LFEA. Figure 7-4 shows the horizontal stresses in the reinforcement at failure in specimen LB7. Specimen LB7 shows the highest σ_{xx} in the reinforcement of the three specimen that are modelled. The stress reaches a maximum of 372 N/mm^2 below the eastern load and a maximum of 155 N/mm^2 above the western support. As shown in Figure 4-5 the linear branch of the reinforcement reaches to over 400 N/mm^2 and thus modelling the reinforcement linear does not influence the results.

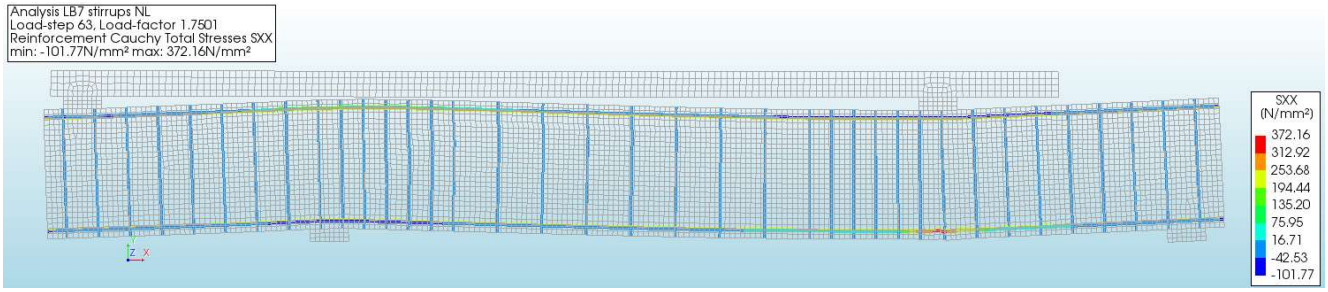

Figure 7-4 σ_{xx} in the reinforcement at failure in specimen LB7

The stirrups however do reach the plasticity and are therefore modelled in a non-linear way. The table below shows the properties of the shear reinforcement.

	f_y $[N/mm^2]$	ϵ_y $[m\epsilon]$	f_u $[N/mm^2]$	ϵ_u $[m\epsilon]$
Shear reinforcement	529	2.65	581	40

These are implemented with Von Mises plasticity as a total yield strain- yield stress relation. This is shown in figure Figure 7-5.

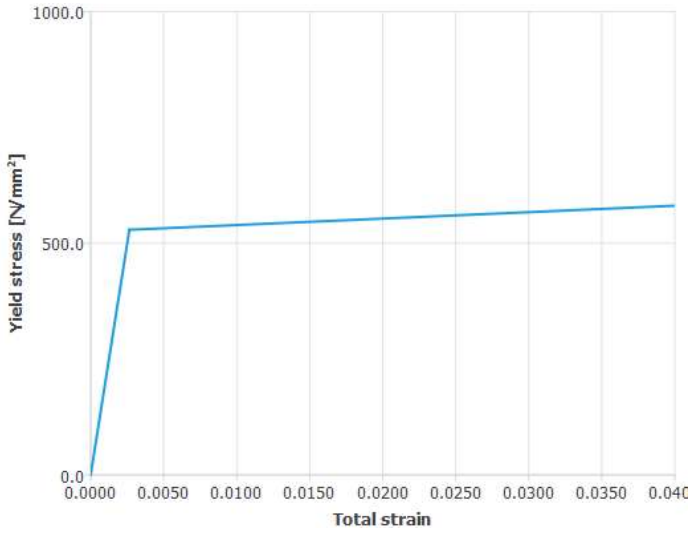

Figure 7-5 Total yield strain - yield stress relation

The only non-linear effect taken into account is the physically non-linear effect, namely the cracking in the concrete. The iteration method used is Newton-Raphson Regular. The convergence norm is set to energy and force with convergence tolerance set to respectively 0.001 and 0.01. The maximum number of iterations is set to 150.

The loads are applied in three phases: first the self-weight than the prestress and than the prescribed displacement, see

Table 7-2. The self-weight and prestress are both applied in one step. The prescribed displacement is added in different step sizes. The prescribed displacement is set to the unit length, which means that a step size of 0.05 is a displacement of 0.05. First a neglectable step of 0.0001 is applied, this is done for post processing reasons. Since without this small step a horizontal line would be present in all force displacement diagrams. The following steps have a step size of 0.05 mm until f_{ctm} is reached in the flange. After reaching f_{ctm} in the flange the step size is halved the path of converging easier.

Table 7-2 Load steps per specimen

		LB6	LB7	LB8
	Step size	**number of steps**	**number of steps**	**number of steps**
Self-weight	1	1	1	1
Prestress	1	1	1	1
Prescribed displacement	0.0001	1	1	1
	0.05	20	10	10
	0.0025	Until no convergence	Until no convergence	Until no convergence

7.2 Results

In this paragraph an overview of the results of NLFEA are given per specimen. The principle tensile stress and the crack width are chosen as output. The principle stress to indicate where cracks are about to occur and to compare with LFEA and the crack width to compare the crack pattern with the experimental results given in chapter 4.3.

LB6

Table 7-3 indicates the steps of interest of the NLFEA. The crucial steps are reaching f_{ctm} in the flange, reaching f_{ctm} in the web and failure of the beam. To get a good insight in the linear behavior between these crucial load-steps every load-step before a crucial moment is added.

Table 7-3 Crucial steps LB6

LB6 *Step*	Prescribed displacement	Reaction force LHS	Shear force	Description
	[mm]	[kN]	[kN]	
3	-0.0001	7.2	3.2	Result of self-weight plus prestress
24	-1.025	354.2	157.4	Last step before reaching f_{ctm} in flange
25	-1.050	362.6	161.2	Reaching f_{ctm} in flange
32	-1.225	420.6	186.9	Last step without reaching f_{ctm} in web
33	-1.250	428.7	190.5	Reaching f_{ctm}in web
45	-1.550	516.7	229.7	Last step of convergence
46	-1.575	394.8	175.5	No convergence

The diagram in Figure 7-6 shows the shear force in relation to the displacement in the middle of the test region at the outer bottom fiber. This shear force- displacement diagram looks bi-linear, it is however the result of a non-linear material properties as given in Table 7-1. The reason this diagram looks bi-linear is that before failure only micro cracks are present in the model. The influence of these cracks on the stiffness is not noticeable.

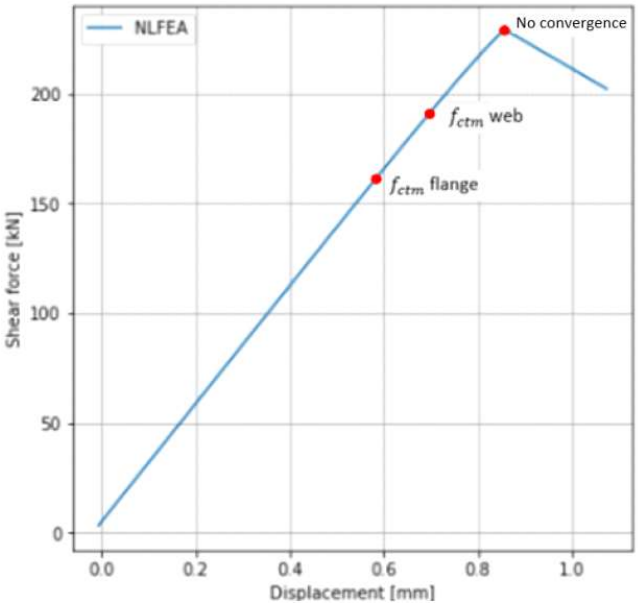

Figure 7-6 FU-diagram at the middle of the test region (LB6)

Figure 7-7 shows the zone of interest, all results are zoomed in at this specific zone. Figure 7-8a to Figure 7-8g show the principle stresses of all crusical steps and Figure 7-9a to Figure 7-9e show the crack width of these steps.

The principle tensile stresses in Figure 7-8a are the principle stresses which are present after prestressing. It shows that the test region, the region between the western support and the eastern load, is under compression as a result of prestressing. A tension field is found at the junction between rectangular cross-section and the I-profile due to redistribution of the prestress. This is the reason why the first part of the I-profile is modelled as linear concrete and thus no cracks appear at that location.

The limit of Figure 7-8b to Figure 7-8g is set in such a way that f_{ctm} is indicated with a red contour. In all these figures the disturbed area above the support is clear. Figure 7-8b shows the priciple stress just before reaching f_{ctm} in the flange. During testing no cracks at the outer fibre were found, yet at the outer fibre the tensile strenght is reached first. This was also predicted by the LFEA and the analytical analysis. Figure 7-8e shows load-step 33 in which f_{ctm} is reached in the junction between the web and the flange.

Load-step 45 in Figure 7-8f shows the last step before the web-shear crack occurs which leads to instant failure. At this step the crack widht in the flange is increased $\frac{9}{1000}$ of a mm, which is not noticeable by the human eye. This explains why no flexural cracks were found during testing. Figure 7-8g the web-shear crack leading to failure. The crack pattern differs from the experimental results shown in Figure 7-10. The NLFEA only shows one large web-shear crack at failure while the experiment shows mulitple web-shear cracks and multiple smaller cracks at the junction between web and flange. The location and the angle are of the main crack in the experiment is comparable to the crack in NLFEA.

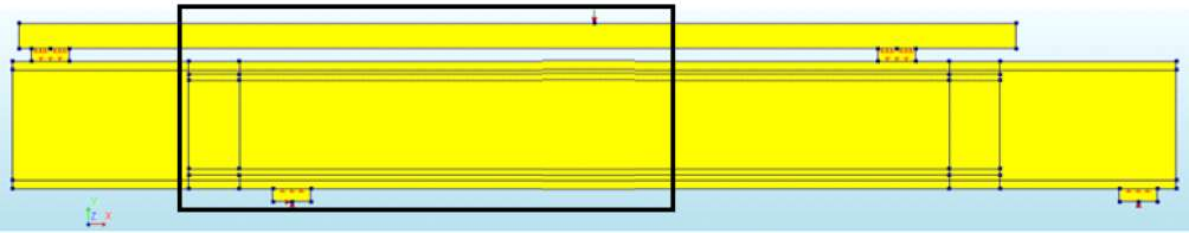

Figure 7-7 Zone of interest

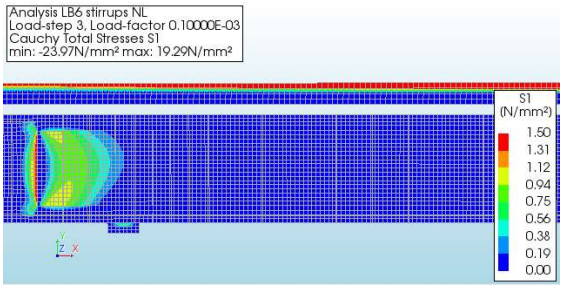

Figure 7-8a σ_1 at load-step 3 (LB6)

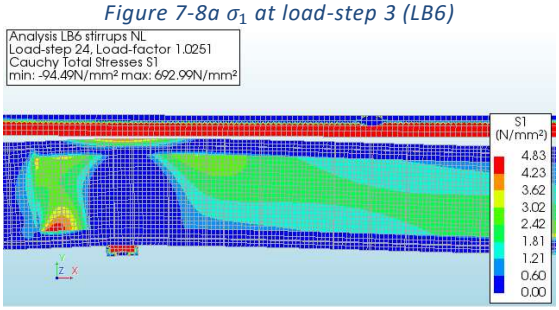

Figure 7-8b σ_1 at load-step 24 (LB6)

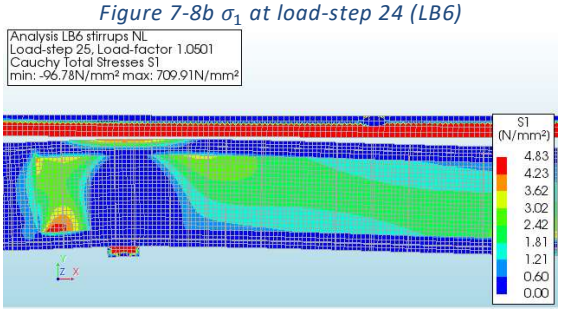

Figure 7-8c σ_1 at load-step 25 (LB6)

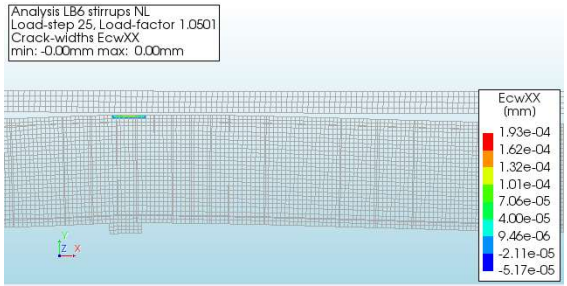

Figure 7-9a Crack width at load-step 25 (LB6)

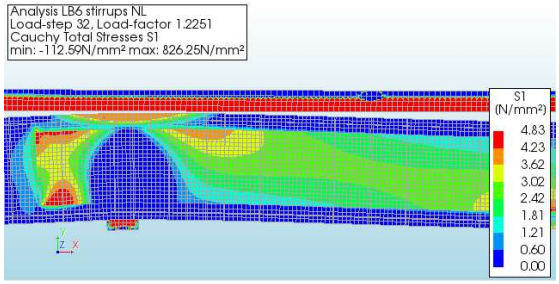

Figure 7-8d σ_1 at load-step 32 (LB6)

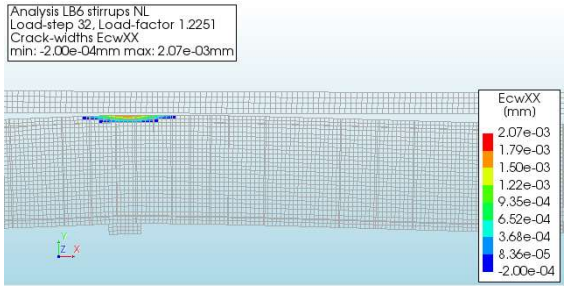

Figure 7-9b Crack width at load-step 25 (LB6)

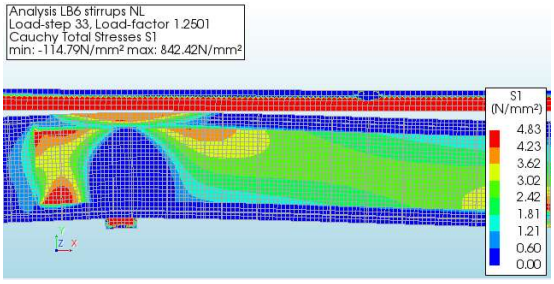

Figure 7-8e σ_1 at load-step 33 (LB6)

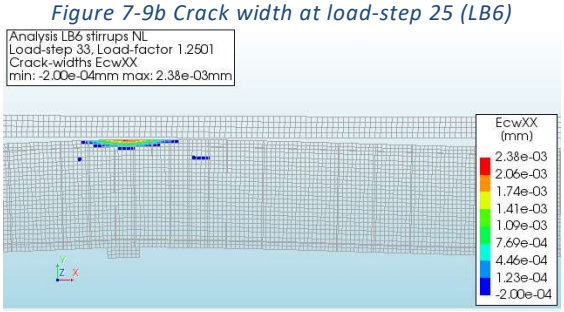

Figure 7-9c Crack width at load-step 33 (LB6)

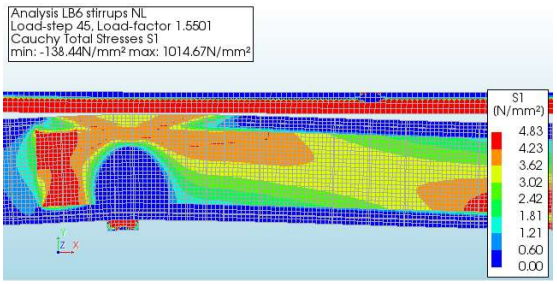

Figure 7-8f σ_1 at load-step 45 (LB6)

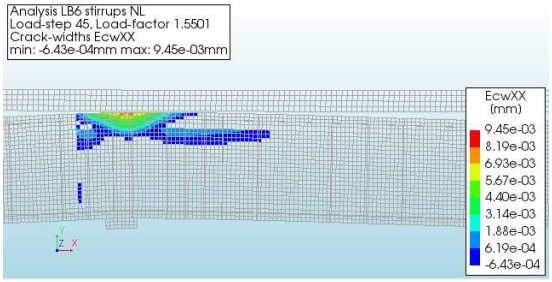

Figure 7-9d Crack width at load-step 45 (LB6)

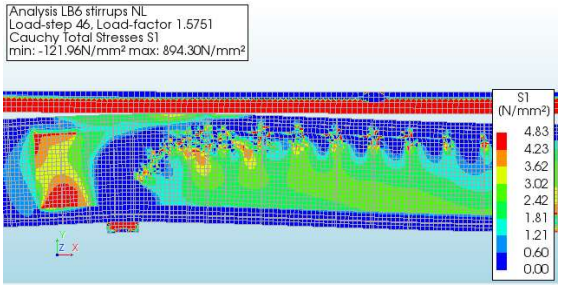

Figure 7-8g σ_1 at load-step 46 (LB6)

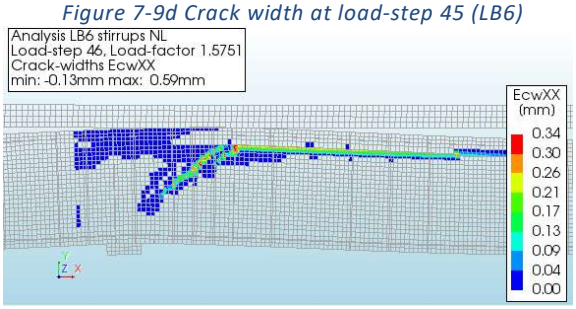

Figure 7-9e Crack width at load-step 46 (LB6)

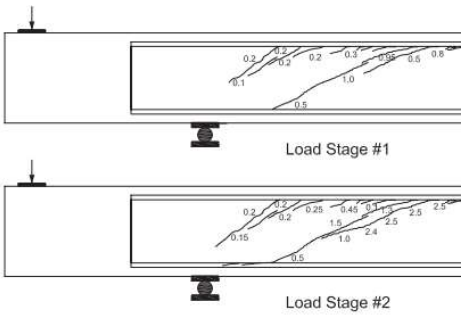

Figure 7-10 Experimental results LB6. Source: Xie (2009)

LB7

Table 7-4 indicates the crucial steps for LB7. Just like LB6 reaching f_{ctm} in flange, reaching f_{ctm} in web and failure are important steps. However during the NLFEA of LB7 flexural- and web-shear cracks occur. These steps are also of importance. To capture the linear process between these load-steps the load-step just before a critical moment is included in the list.

Table 7-4 Crucial steps LB7

LB7 *Step*	Displacement	Reaction force LHS	Shear force	Description
	[mm]	[kN]	[kN]	
3	-0.0001	4.9	2.2	Self-weight plus prestress is applied
14	-0.5251	183.0	81.3	Last step before reaching f_{ctm} in flange
15	-0.5501	191.5	85.1	Reaching f_{ctm} in flange
25	-0.8001	271.4	120.6	Last step without reaching f_{ctm} in web
26	-0.8251	279.2	124.1	Reaching f_{ctm}in web
30	-0.9251	304.0	135.1	Last step before flexural crack
31	-0.9501	294.1	130.7	Occurrence flexural and flexural shear crack
38	-1.1251	331.5	147.3	Last step before web-shear crack
39	-1.1501	329.1	146.3	Occurrence of web-shear crack
43	-1.2501	348.7	155.0	Last step of convergence
44	-1.2751	320.6	142.5	No convergence

The shear-force diagram as displayed in Figure 7-11 shows, just like LB6, a linear branch even after reaching the principle stress of f_{ctm} in the web. However unlike LB6 the non-linear part of the diagram shows more jumps in shear force due to occurrence of a flexure crack and web-shear cracks.

It is interesting to see that after reaching f_{ctm} in the flange and in the web at both locations only micro cracks occur. The difference in shear force between the first significant flexure crack and reaching f_{ctm} in the flange is 53 kN, which is an addition of 60% after reaching f_{ctm} in the first place. For web-shear cracking the difference is smaller with 21kN. An addition of 18% of the shear force between reaching f_{ctm} and the first web-shear crack.

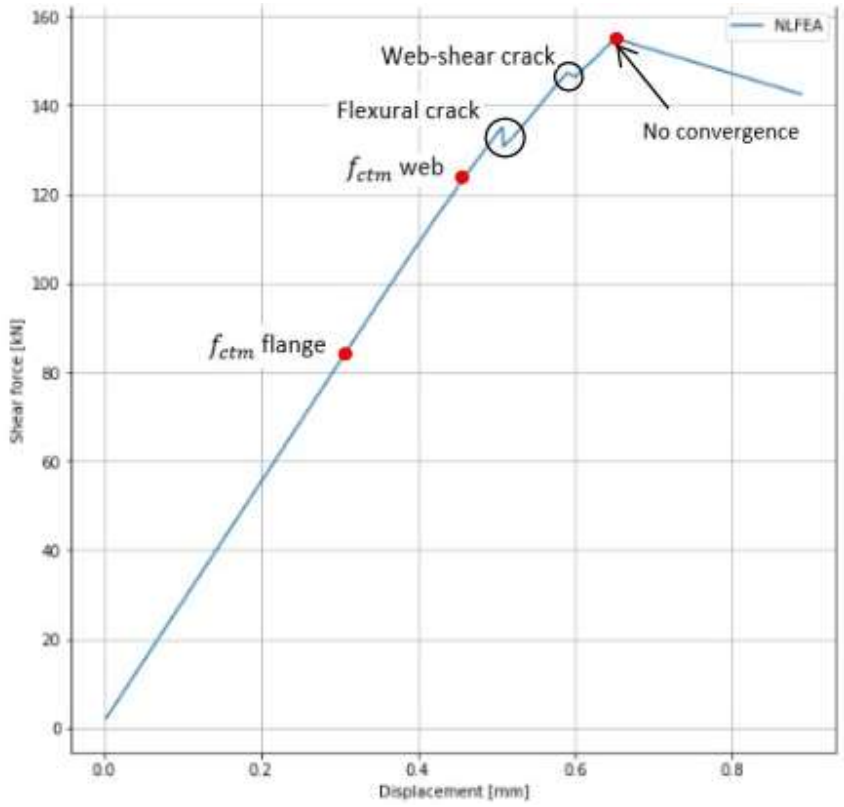

Figure 7-11 FU-diagram at the middle of the test region (LB7)

The contours of the principle stresses for all steps of Table 7-4 are shown in Figure 7-12a to Figure 7-12m. The limit is set that a red contour indicates a principle stress equal or higher than the tensile strength. Figure 7-12a shows the principle stress as a result of self-weight and prestressing. Just like in LB6 a tension area is present at the junction of the rectangular cross-section and the I-profile cross-section. The is due to redistribution of the prestress.

Figure 7-12b show the principle stresses just before reaching f_{ctm} in the outer fiber of the top flange. The area sensitive to web-shear cracking is already visible, this is the green area at the junction between the top flange and the web. The disturbed area above the support is also clearly visible.

With increasing the load the principle stresses increase. Once the principle stresses reach the tensile strength a that specific element is cracked. Therefore the only location where the principle stress is higher than the tensile strength is where the concrete is given linear properties. This is the case at the junction between the rectangular- and I-profile cross-sections and in the bottom fibers on the right hand side, see Figure 7-1. At the later stage the influence of the stirrups is clearly visible, Figure 7-12j to Figure 7-12m.

The crack width for the steps of Table 7-4 are shown in figure Figure 7-13a to Figure 7-13k. First reaching the tensile strength in the outer fiber in the top flange. Than a linear branch until reaching the tensile strength at the junction between flange and web. The cracks are still micro level. The first significant flexure crack occurs in step 31, Figure 7-13e. At this load-step the cracks in the web are still micro cracks. These cracks expand to the first web-shear crack at load-step 39, Figure 7-13g. The crack width at load-

step 43, Figure 7-13g, shows the last step of convergence. One load step later in Figure 7-13h a second web-shear crack occurred and no equilibrium is found.

In Figure 7-14 the experimental result of Xie is given. If this is compared to the results of the NLFEA it can be noted that the location of the web-shear cracks are a bit closer to the support in the NLFEA. Furthermore the angle is steeper in the NLFEA compared to the experiment.

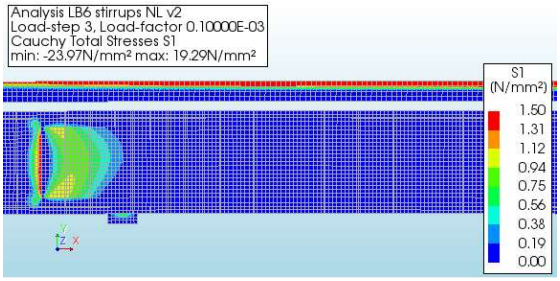

Figure 7-12a σ_1 at load-step 3 (LB7)

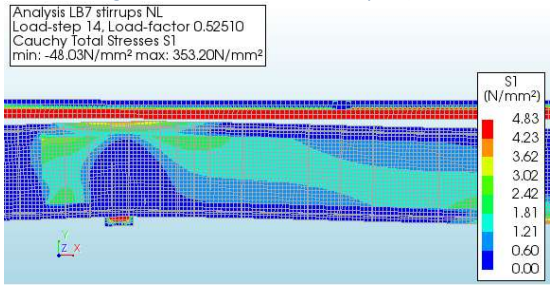

Figure 7-12b σ_1 at load-step 14 (LB7)

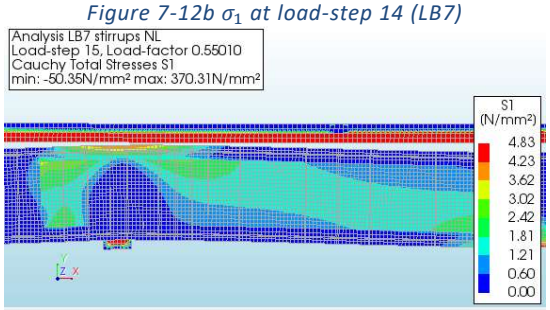

Figure 7-12c σ_1 at load-step 15 (LB7)

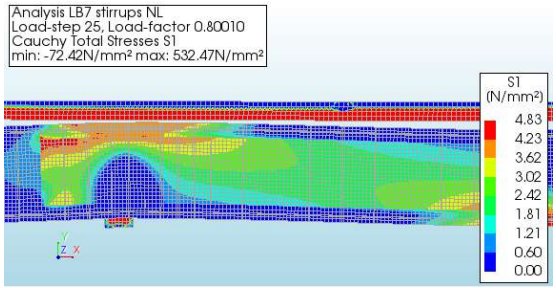

Figure 7-12d σ_1 at load-step 25 (LB7)

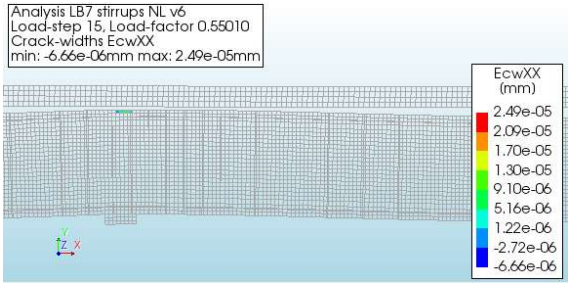

Figure 7-13a Crack width at load-step 15 (LB7)

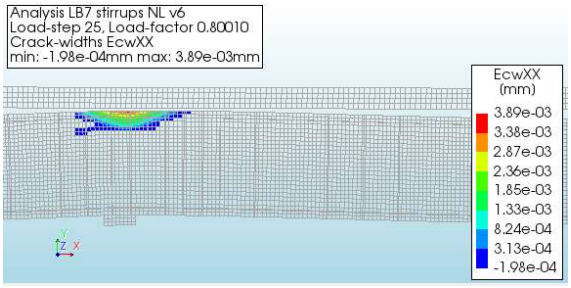

Figure 7-13b Crack width at load-step 25 (LB7)

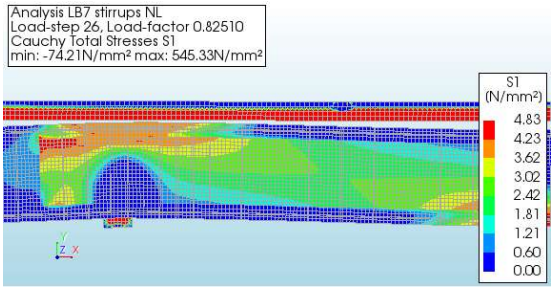

Figure 7-12e σ_1 at load-step 26 (LB7)

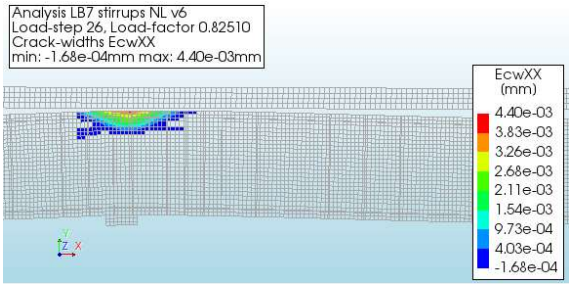

Figure 7-13c Crack width at load-step 26 (LB7)

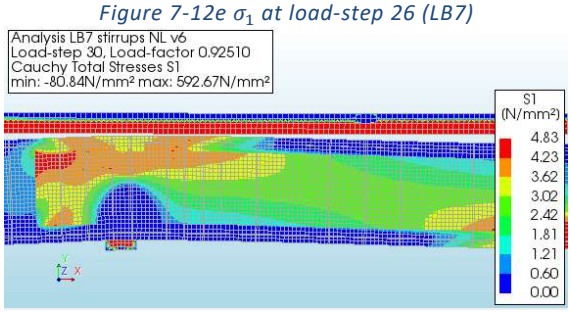

Figure 7-12f σ_1 at load-step 30 (LB7)

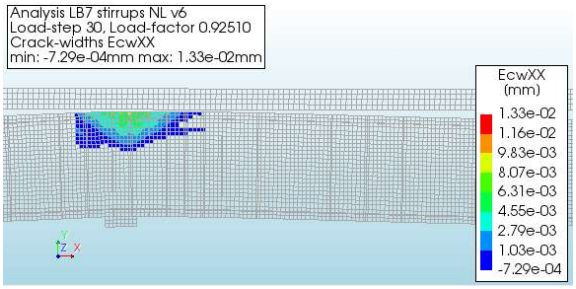

Figure 7-13d Crack width at load-step 30 (LB7)

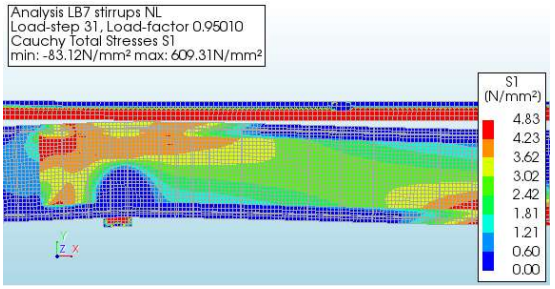

Figure 7-12g σ_1 at load-step 31 (LB7)

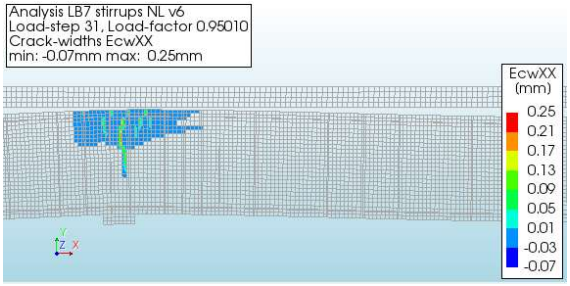

Figure 7-13e Crack width at load-step 31 (LB7)

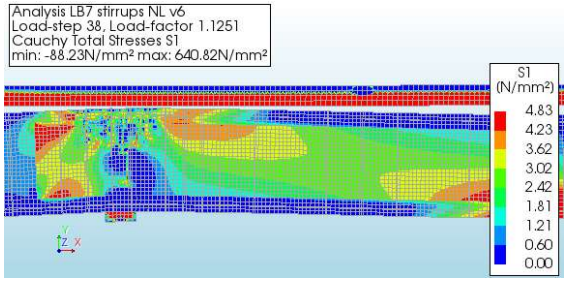

Figure 7-12h σ_1 at load-step 38 (LB7)

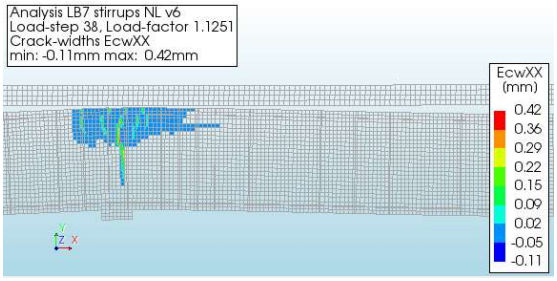

Figure 7-13f Crack width at load-step 38 (LB7)

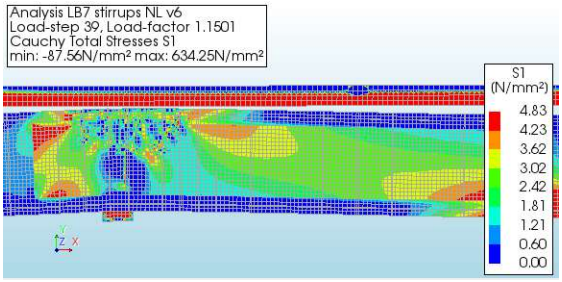

Figure 7-12i σ_1 at load-step 39 (LB7)

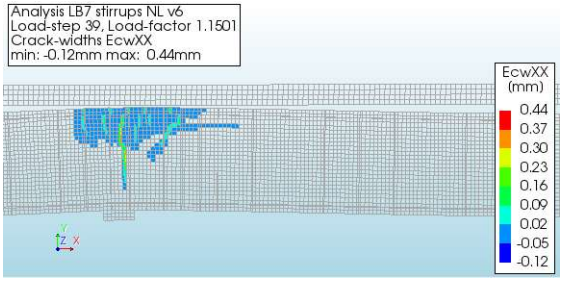

Figure 7-13g Crack width at load-step 39 (LB7)

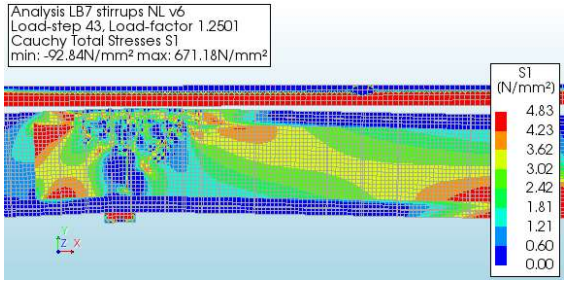

Figure 7-12j σ_1 at load-step 43 (LB7)

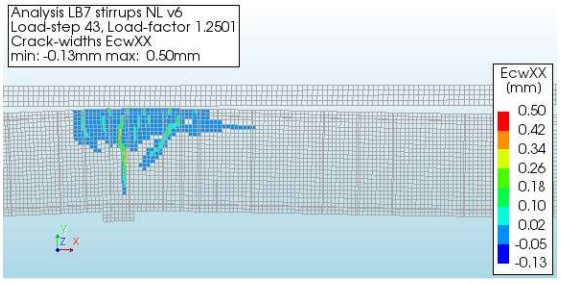

Figure 7-13h Crack width at load-step 43 (LB7)

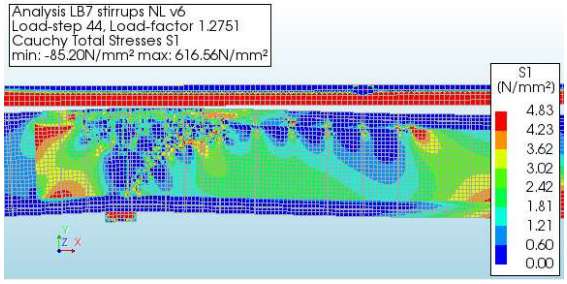

Figure 7-12k σ_1 at load-step 44 (LB7)

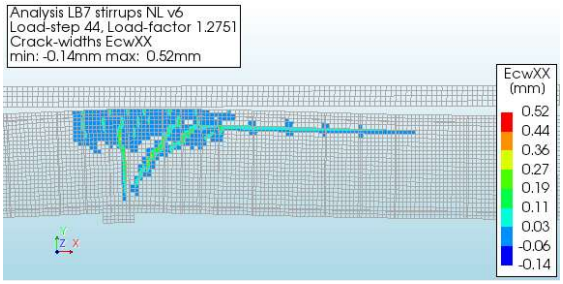

Figure 7-13i Crack width at load-step 44 (LB7)

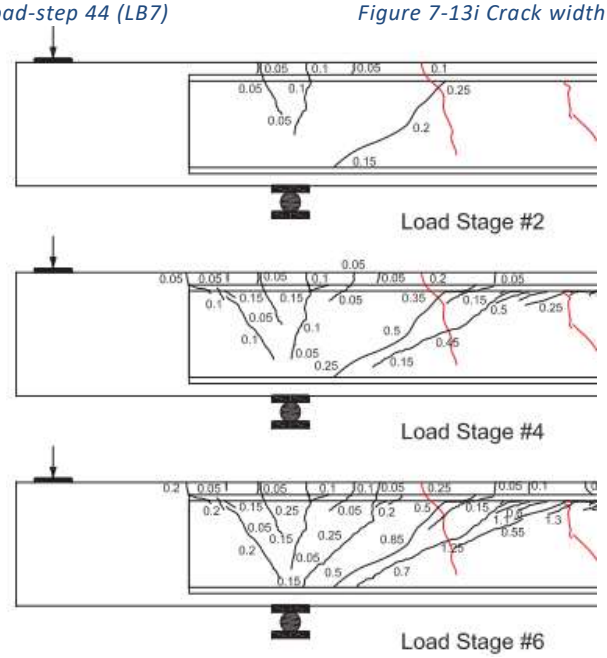

Figure 7-14 Experimental results LB7. Source: Xie (2009)

LB8

Table 7-5 shows the important load-steps of LB8. Starting with the very small load-step to see the result of just self-weight and prestress. Then just as in LB6 and LB7 the load-steps when the principle stress in the outer fiber and in the junction between web and flange reach f_{ctm}. The results of LB8 show that first a flexural crack occurs and later twice a web-shear crack. Finally the last step of convergence and the step without convergence are added. Once again to capture the linear behavior between the events described above the final step before every crucial moment is added as well.

LB8 *Step*	Displacement	Reaction force LHS	Shear force	Description
	[mm]	[kN]	[kN]	
3	-0.0001	5.2	2.3	Self-weight plus prestress is applied
17	-0.6001	204.5	90.9	Last step before reaching f_{ctm} in flange
18	-0.6251	212.8	94.6	Reaching f_{ctm} in flange
28	-0.8751	291.2	129.4	Last step without reaching f_{ctm} in web
29	-0.9001	298.8	132.8	Reaching f_{ctm}in web
34	-1.0251	329.7	146.5	Last step before flexural crack
35	-1.0501	321.0	142.7	Occurrence flexural and flexural shear crack
42	-1.2251	357.7	159.0	Last step before more flexural cracks
43	-1.2501	358.4	159.3	Occurrence of more flexural cracks
46	-1.3251	371.9	165.3	Last step before second web-shear crack
47	-1.3501	373.3	165.9	Occurrence of second web-shear crack
50	-1.4251	388.1	172.5	Last step of convergence
51	-1.4501	363.5	161.5	No convergence

Table 7-5 Crucial steps LB8

Figure 7-15 shows the shear force- displacement diagram for LB8. The displacement is in vertical direction and measured at the outer bottom fiber in the middle of the test region. This diagram shows a lot of similarities to the shear force displacement diagram of LB7. Differences are that LB8 shows two smaller web-shear cracking moments instead of one larger drop in shear force. Furthermore the events all occurred under a higher shear force compared with LB7, this is due the higher prestress present in LB8. It should be noted that also for LB8 a large increment of shear force is needed to create a flexure crack after reaching f_{ctm} in the outer fiber. The tensile strength is reached under a shear force of 94.6 kN however the first significant flexural crack appears at 146.5 kN.

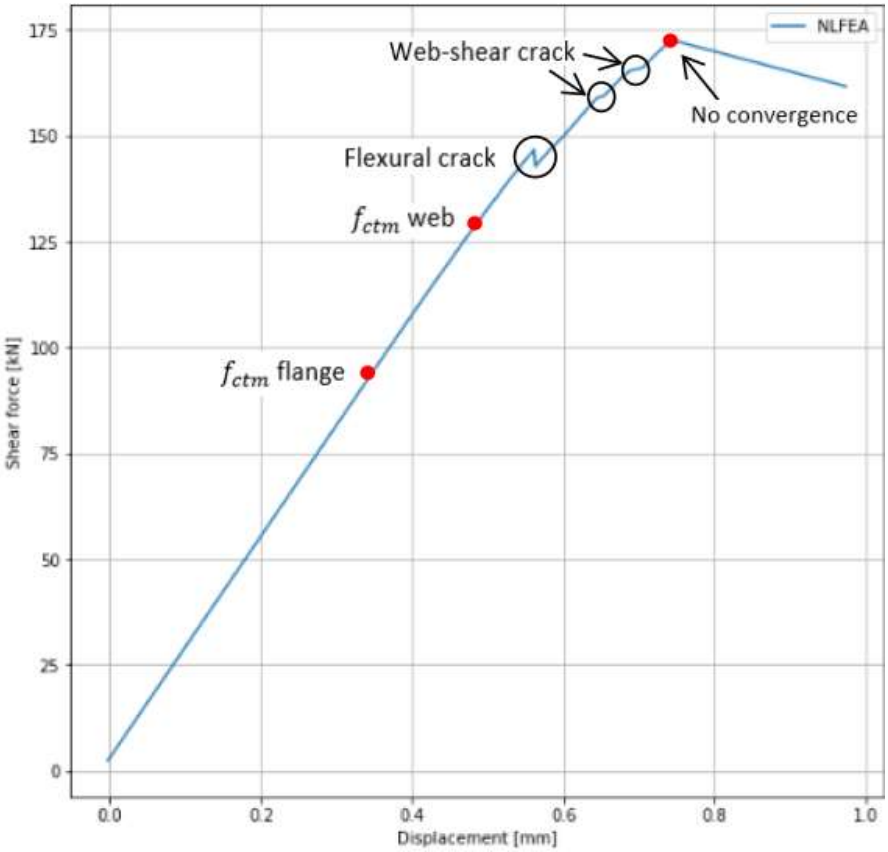

Figure 7-15 FU-diagram at the middle of the test region (LB8)

Figure 7-16a to Figure 7-16m show the development of the principle tensile stress in specimen LB8. The zoomed in area is the same area as used for LB6 and LB7, see Figure 7-7. The principle stresses behave similar as in LB7. From Figure 7-16b to Figure 7-16m the limits are set that a red contour indicates reaching f_{ctm}. The disturbed area is excellently visible. The tensile strength is first reached in the outer fiber, this is corresponding to the shear force- displacement diagram. Then two shear cracks appear and finally no convergence can be made with the occurrence of one large web-shear crack. Figure 7-17a to Figure 7-17k give the corresponding cracking width at the crucial steps described above.

Figure 7-18 shows the experimental results of LB8. All significant cracks of the NLFEA are comparable with the experiment. The angle of the web-shear crack in the NLFEA matches approximately the angle in the experiment.

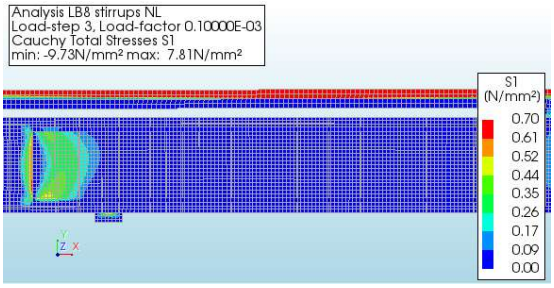

Figure 7-16a σ_1 at load-step 3 (LB8)

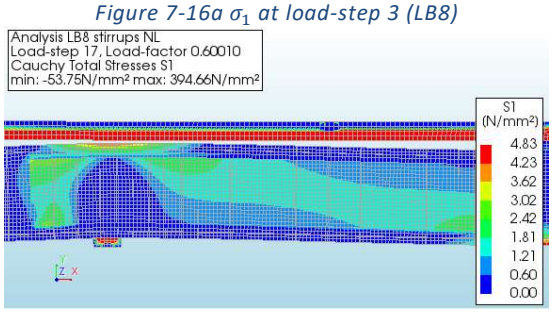

Figure 7-16b σ_1 at load-step 17 (LB8)

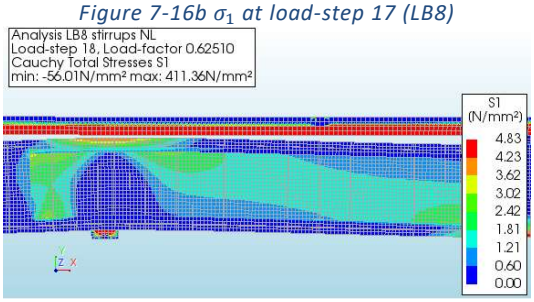

Figure 7-16c σ_1 at load-step 18 (LB8)

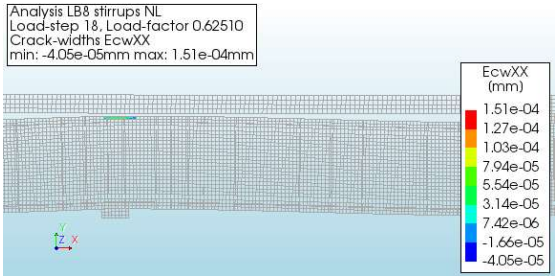

Figure 7-17a Crack width at load-step 18 (LB8)

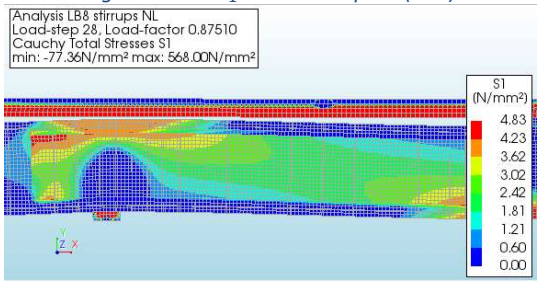

Figure 7-16d σ_1 at load-step 28 (LB8)

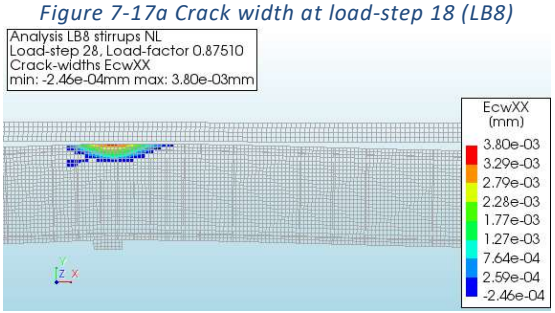

Figure 7-17b Crack width at load-step 28 (LB8)

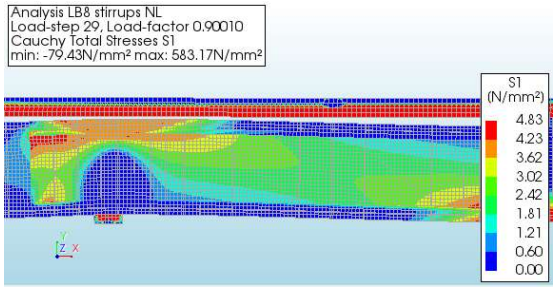

Figure 7-16e σ_1 at load-step 29 (LB8)

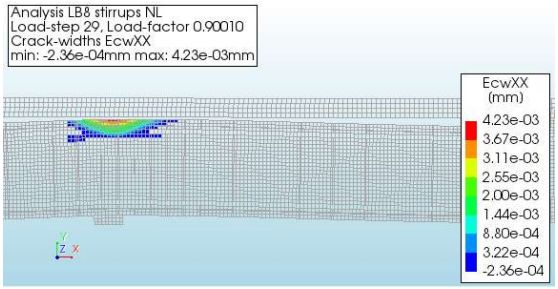

Figure 7-17c Crack width at load-step 29 (LB8)

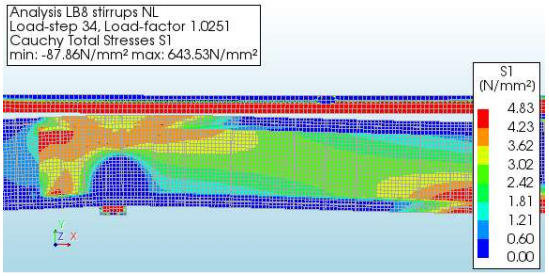

Figure 7-13f σ_1 at load-step 17 (LB8)

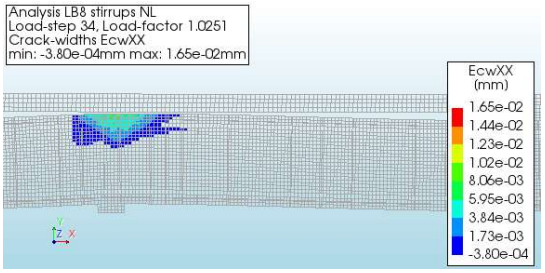

Figure 7-17d Crack width at load-step 34 (LB8)

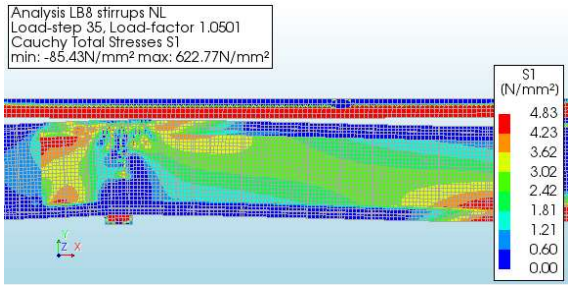

Figure 7-13g σ_1 at load-step 17 (LB8)

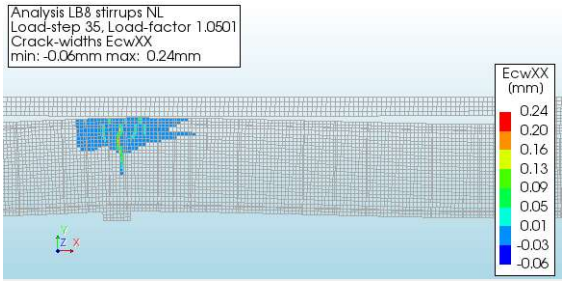

Figure 7-17e Crack width at load-step 35 (LB8)

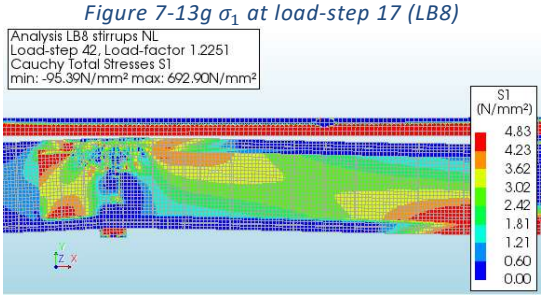

Figure 7-13h σ_1 at load-step 17 (LB8)

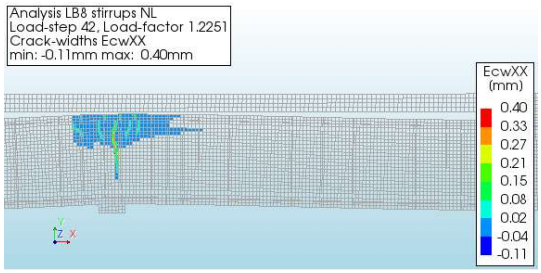

Figure 7-17f Crack width at load-step 42 (LB8)

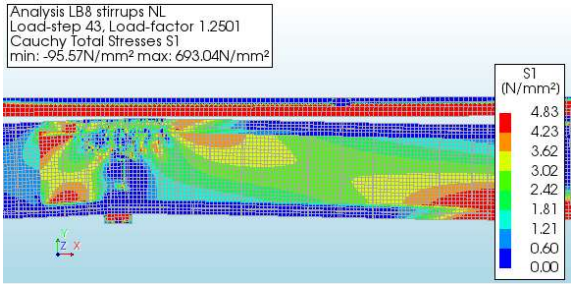

Figure 7-13i σ_1 at load-step 17 (LB8)

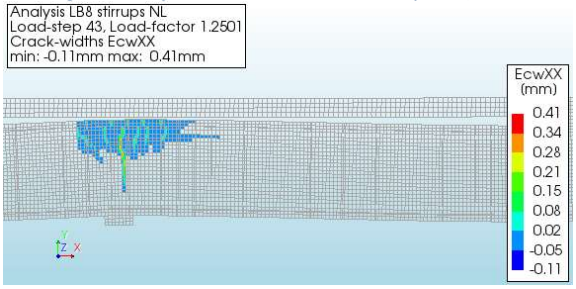

Figure 7-17g Crack width at load-step 43 (LB8)

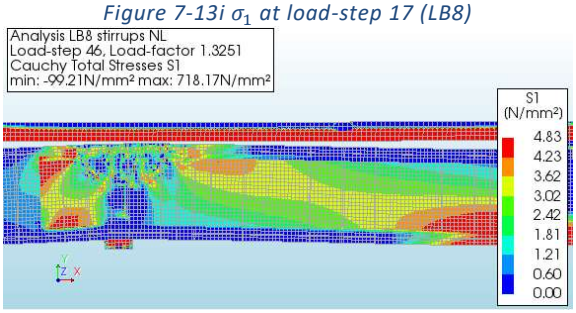

Figure 7-13j σ_1 at load-step 46 (LB8)

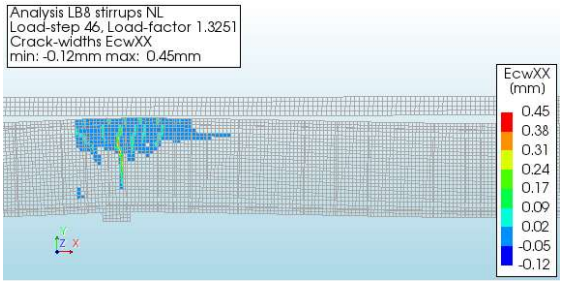

Figure 7-17h Crack width at load-step 46 (LB8)

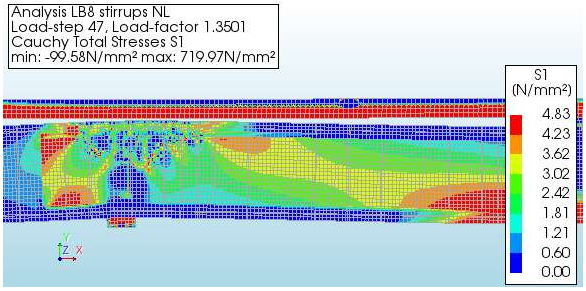

Figure 7-16k σ_1 at load-step 47 (LB8)

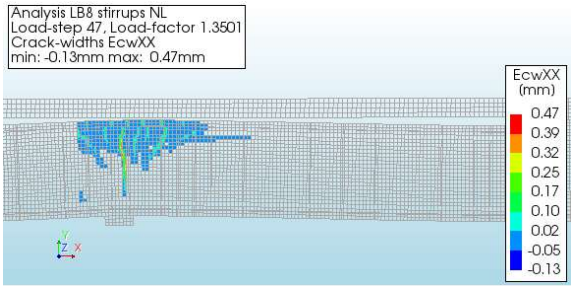

Figure 7-17i Crack width at load-step 47 (LB8)

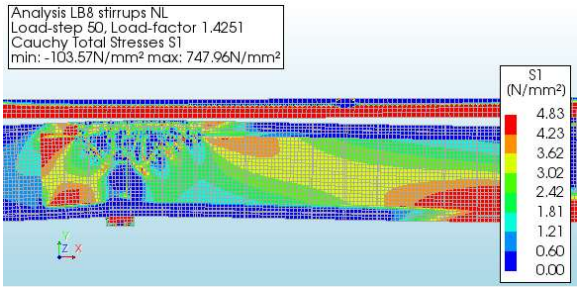

Figure 7-16l σ_1 at load-step 50 (LB8)

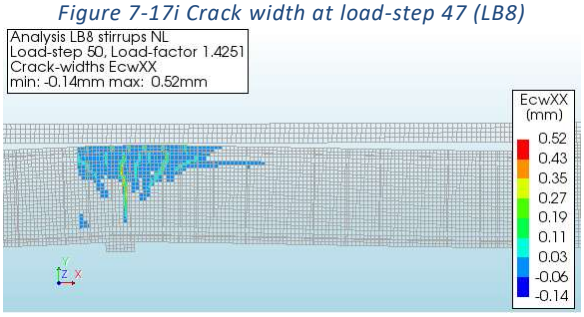

Figure 7-17j Crack width at load-step 50 (LB8)

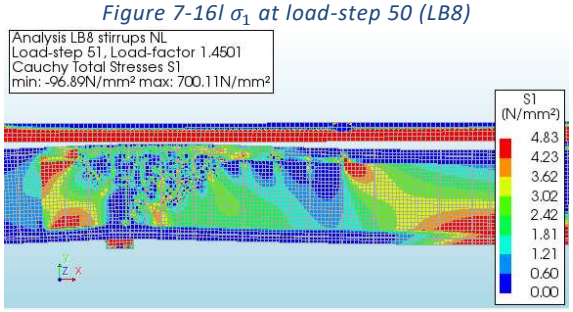

Figure 7-16m σ_1 at load-step 51 (LB8)

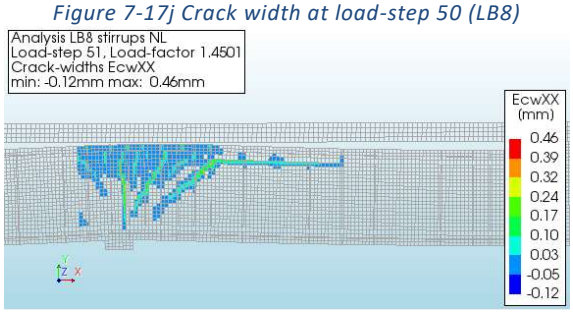

Figure 7-17k Crack width at load-step 51 (LB8)

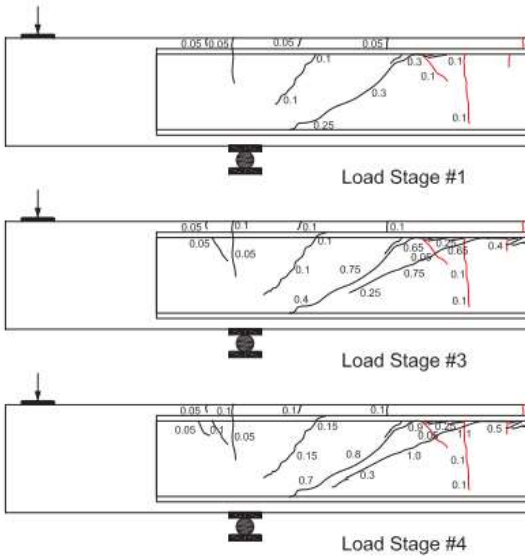

Figure 7-18 Experimental results LB8. Source: Xie (2009)

7.3 Sensitivity analysis

In this paragraph two sensitivity analyses are performed. Namely the influence of shear-reinforcement and the influence of the tensile strength of concrete.

7.3.1 Influence of shear reinforcement

In this paragraph a the influence of the presence of shear reinforcement is researched. Figure 7-19 to Figure 7-21 show the shear force- displacement diagram for a model with and without shear reinforcement. The first interesting result is that after the tensile stress reaches f_{ctm} in the web the specimen modelled without shear reinforcement do not immediately fail due to web-shear cracking. The requirement codes all predict failure when f_{ctm} is reached. However the NLFEA shows a stable path after σ_1 exceeds f_{ctm}. During which micro cracks occur. This can be explained by the tension softening in the concrete, after reaching the tensile strength the concrete stresses are still present. The influence of the fracture energy is looked at in Chapter 7.3.3.

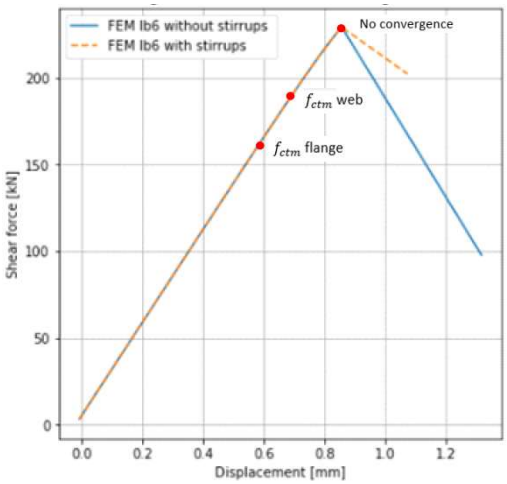

Figure 7-19 FU-diagram at the middle of the test region (LB6)

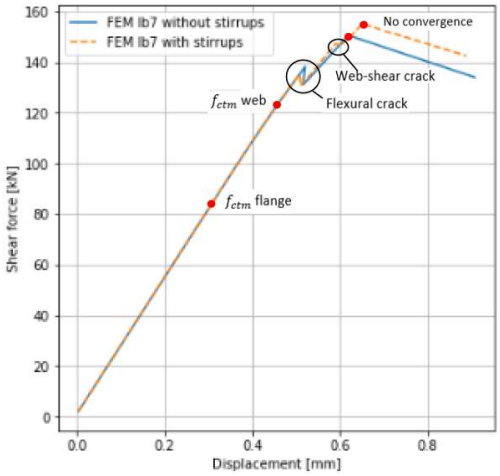

Figure 7-20 FU-diagram at the middle of the test region (LB7)

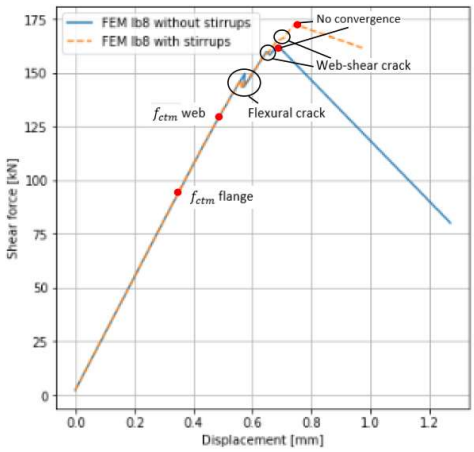

Figure 7-21 FU-diagram at the middle of the test region (LB8)

Table 7-6 Shear force at occurrence of first web-shear crack

	LB6 [kN]	LB7 [kN]	LB8 [kN]
$V_{web-shear\ crack}$ *with stirrups*	230	154	165
$V_{web-shear\ crack}$ *without stirrups*	229	150	153

Table 7-6 shows the shear force present at the occurrence of the first web-shear crack for the NLFEA with and without shear reinforcement for all three specimen. It can be noted that the difference is neglectable for LB6 and LB7. However the difference for LB8 is approximately 8%.

In Figure 7-19 it can be noted that with and without shear reinforcement the beam will follow the same shear force- displacement diagram. The reason was found by Xie, namely that for beams under very high compression the failure becomes extremely violent and it does not matter if more stirrups are added. Figure 7-22a to Figure 7-22c show the crack width at the moment of reaching f_{ctm} in web, last step of convergence and the step without convergence for the model including stirrups. and Figure 7-23a to Figure 7-23c show the crack width for the same events for the model without stirrups.

It can be noted that the steps in which the described events occur are the same. Only noticeable difference is that in that in step 46, the step without convergence, the crack width is larger without the presence of shear reinforcement.

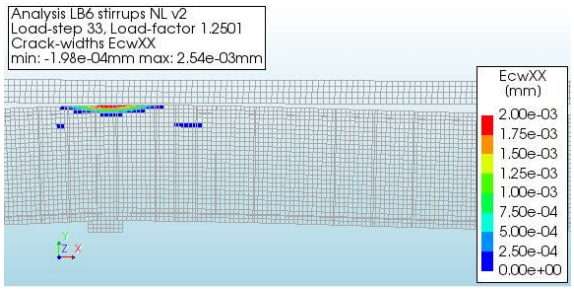

Figure 7-22a Reaching f_{ctm} in web with stirrups, step 33 (LB6)

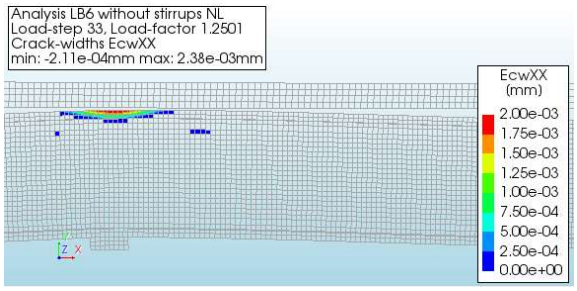

Figure 7-23a Reaching f_{ctm} in web without stirrups, step 33 (LB6)

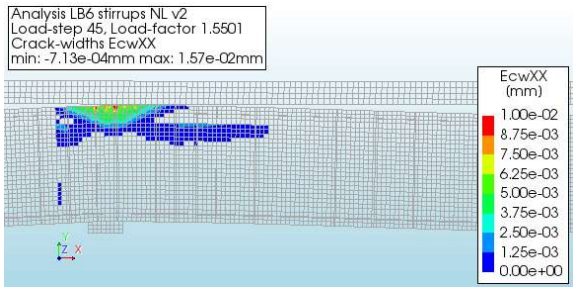

Figure 7-15b last step of convergence with stirrups, step 45 (LB6)

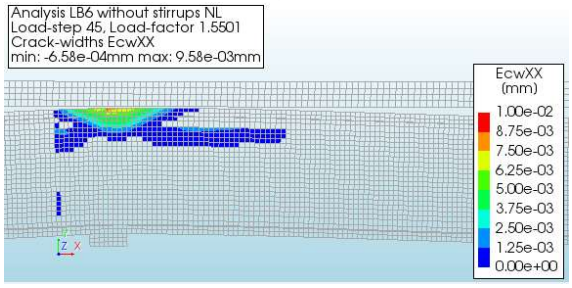

Figure 7-16b last step of convergence without stirrups, step 45 (LB6)

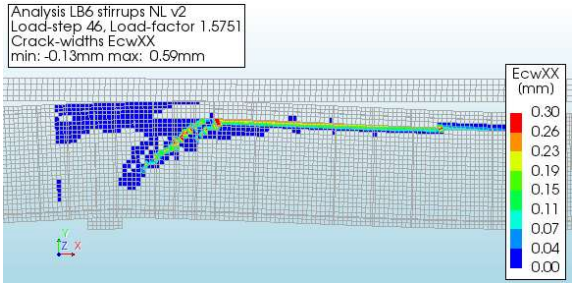

Figure 7-15c No convergence with stirrups, step 46 (LB6)

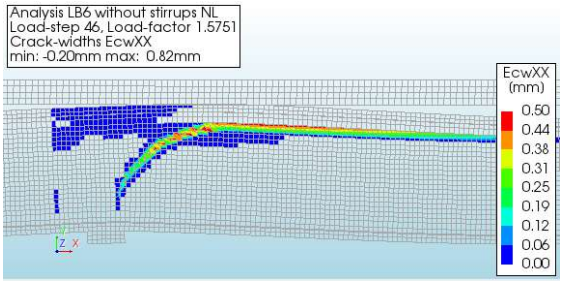

Figure 7-16c No convergence without stirrups, step 46 (LB6)

The shear-force diagram of LB7, Figure 7-20, shows similarities and differences compared to the one of LB6. A similarity is that the presence of shear reinforcement on reaching f_{ctm} in the flange and in the web is not noticeable. This can also be observed by comparing Figure 7-24a and Figure 7-25a, in which the cracking patterns are very similar. The model without stirrups even finds equilibrium at the origin of the web-shear crack, however it fails when this crack increases in width, Figure 7-25b.

The model with stirrups included still finds equilibrium after the first web-shear crack has a substantial width, but can not converge when the second web-shear crack occurs, Figure 7-24c. This leads to a difference in ultimate shear force.

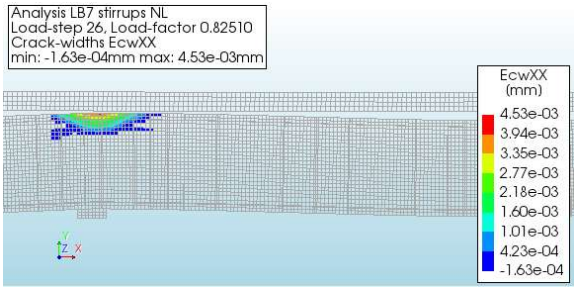

Figure 7-24a Reaching f_{ctm} in web with stirrups, step 26 (LB7)

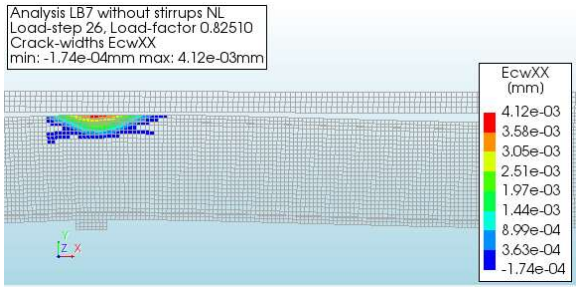

Figure 7-25a Reaching f_{ctm} in web without stirrups, step 26 (LB7)

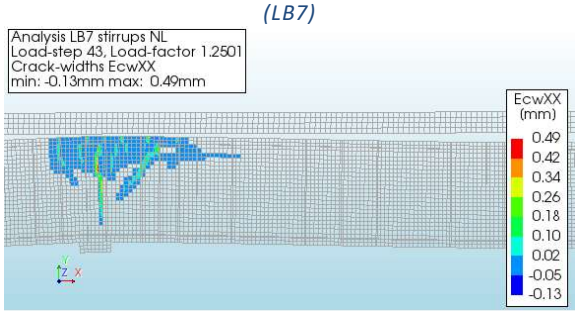

Figure 7-17b last step of convergence with stirrups, step 43 (LB7)

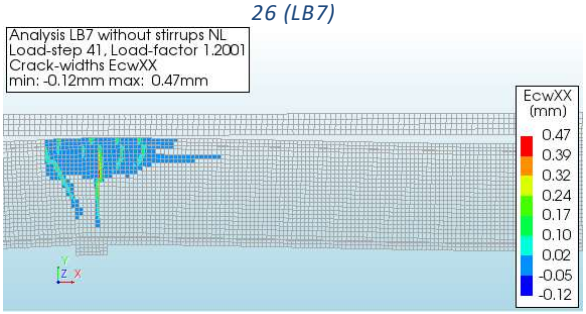

Figure 7-18b last step of convergence without stirrups, step 41 (LB7)

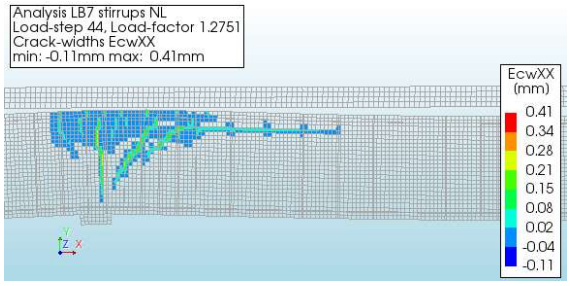

Figure 7-17c No convergence with stirrups, step 44 (LB7)

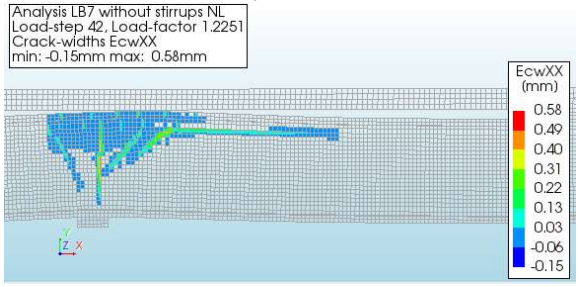

Figure 7-18c No convergence without stirrups, step 42 (LB7)

The shear force- displacement diagram of LB8 as given in Figure 7-21 shows some interesting findings. First of all it shows that until the first flexure crack occurs the path for with and without stirrups is practically the same. Figure 7-26a and Figure 7-27a indicate the moment of reaching f_{ctm} in the web, which is the same for both models. It shows further that even after occurrence of the first web-shear crack even the model without shear reinforcement still converges, also visible in Figure 7-27b.

When the second web-shear crack occurs the model without stirrups can not find equilibrium anymore. The model with shear-reinforcement does find a stable path for another couple of load steps. This is shown in Figure 7-26b and Figure 7-27c. The model with shear reinforcement can not converge on load step 51, ending in a cracking pattern with multiple web-shear cracks.

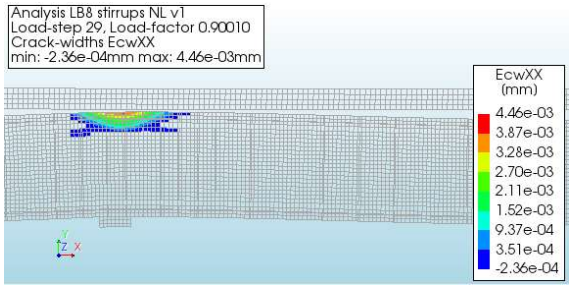

Figure 7-26a Reaching f_{ctm} in web with stirrups, step 29 (LB8)

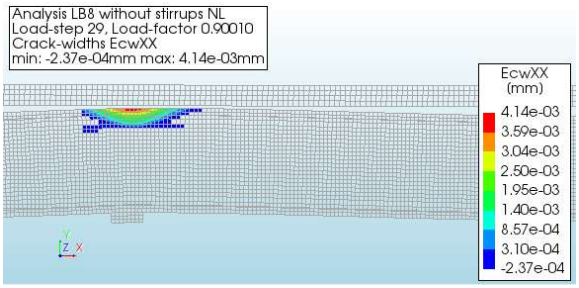

Figure 7-27a Reaching f_{ctm} in web without stirrups, step 29 (LB8)

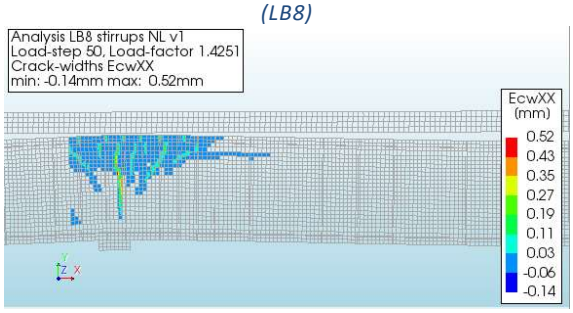

Figure 7-19b last step of convergence with stirrups, step 50 (LB8)

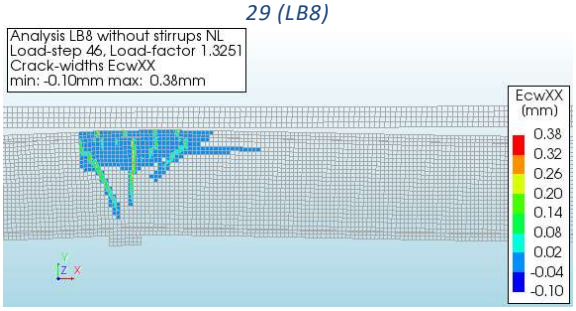

Figure 7-20b last step of convergence without stirrups, step 46 (LB8)

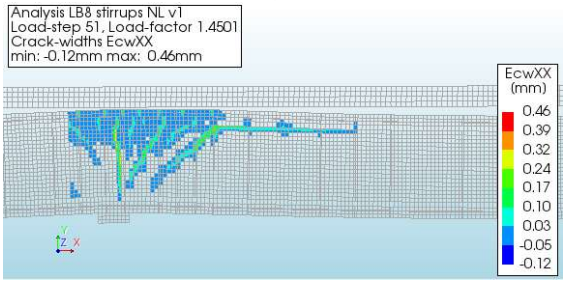

Figure 7-19c No convergence with stirrups, step 51 (LB8)

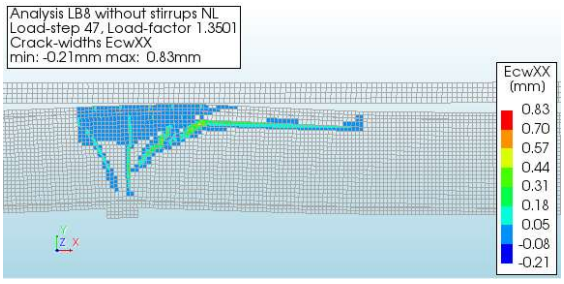

Figure 7-20c No convergence with stirrups, step 47 (LB8)

7.3.2 Influence of tensile strength

The first results of the NLFEA with stirrups show shear forces significantly higher than the shear forces at failure during the experiment. One of the key parameters of which value is not know with certainty is the tensile strength of the concrete. Therefore the shear force displacement diagram for three different tensile strengths is shown in Figure 7-28 to Figure 7-30. The tensile strength is set to $0.6f_{ctm}$, $0.8f_{ctm}$ and to f_{ctm}. The cracking behavior of LB6 remains the same for all tensile strengths. Namely no convergence at originating of the web-shear crack. In LB7 the behavior changes. The analysis with the tensile strength set to 2.54 N/mm^2 does not converge when the first web-shear crack occurs. When the tensile strength is set to 3.39 N/mm^2 the last step of convergence is also the step in which the first web-shear crack occurs. The same phenomena is seen in LB8.

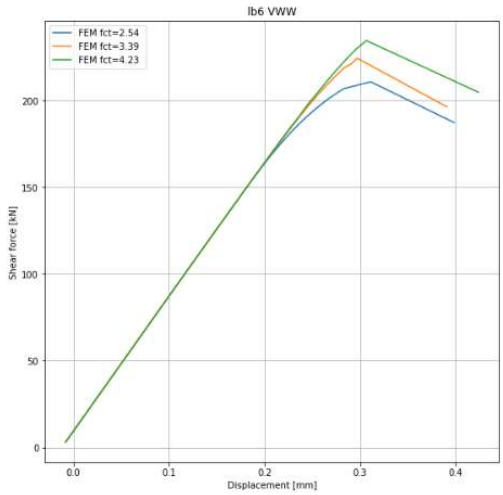

Figure 7-28 Shear force- displacement diagram for different tensile strengths (LB6)

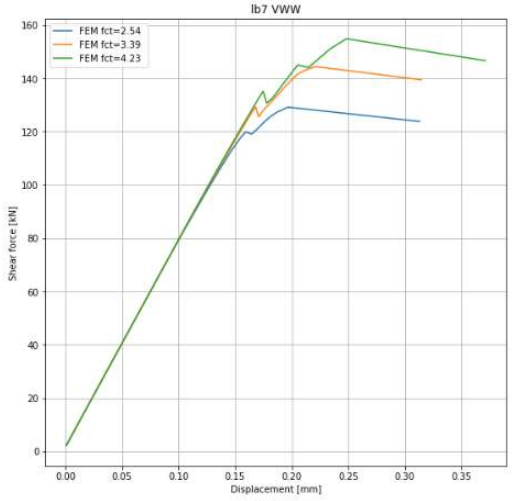

Figure 7-29 Shear force- displacement diagram for different tensile strengths (LB7)

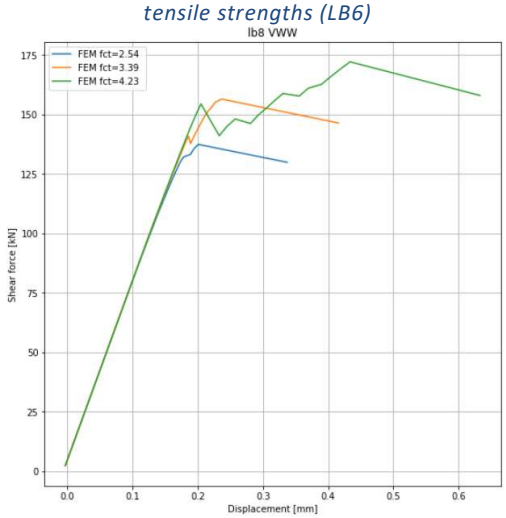

Figure 7-30 Shear force- displacement diagram for different tensile strengths (LB)

Table 7-7 shows the shear force for all three specimen at three different moments. These are reaching f_{ctm} in the web, occurring of web-shear crack and last step of convergence. It can observed that indeed the shear force occurring in the NLFEA is significantly higher than in the experiments when the tensile strength is set to f_{ctm}.

As said before LB6 has no convergence when the first web-shear crack occurs, even though the shear force of the last converging step is a maximum of 55% higher than the shear force at which LB6 forms a web-shear crack in the experiment. The NLFEA with the tensile strength set to $0.6f_{ctm}$ shows a maximum shear stress of 211.5 kN. This is still 42% higher than the shear force at which web-shear cracking occurred during testing.

LB7 shows shear forces from the NLFEA when tensile strength set to f_{ctm} of 35% higher at web-shear cracking compared to the experiment. The shear force of last convergence is only 12% higher than the shear force at failure in the experiment. When the tensile strength is reduced to $0.8f_{ctm}$ the shear forces in the NLFEA are still higher than in the experiment. Even the tensile strength is further reduced to $0.6f_{ctm}$ the shear force at web-shear cracking is higher than the shear force at web-shear cracking in the experiment. However the shear force at last convergence is lower than the shear force at failure with this tensile strength.

LB8 shows similar results to LB7. The shear force according the NLFEA is in all cases higher then the shear force measured during testing. With tensile strength set to f_{ctm} the shear force found in the NLFEA at web-shear cracking is 49% higher than the force found in the experiments. The shear force at last convergence is 28% higher than the ultimate shear force found during testing.

Table 7-7 Shear forces with varying tensile strength

Specimen	Tensile strength $[\mathrm{N/mm^2}]$	$V_{f_{ctm}\_in\_web}$ $[kN]$	$V_{web-shear\_crack}$ $[kN]$	$V_{last\_convergence}$ $[kN]$	V_{cr_exp} $[kN]$	V_{u_exp} $[kN]$
LB6	2.54	190.8	230.2	230.2	148.1	155.8
LB6	3.39	168.7	227.2	227.2	"	"
LB6	4.23	146.3	211.5	211.5	"	"
LB7	2.54	91.4	129.1	129.1	80.1	137.8
LB7	3.39	106.1	144.4	144.4	"	"
LB7	4.23	124.1	144.0	154.8	"	"
LB8	2.54	97.6	138.1	138.1	111.2	134.3
LB8	3.39	115.1	156.5	156.5	"	"
LB8	4.23	132.8	165.9	172.5	"	"

This sensitivity analysis shows that the tensile strength reduction leads to lower shear forces, however the shear forces with the lower tensile strengths are still higher than the shear found in the experiment. If the shear force at last convergence is compared to the ultimate shear force according to the experiment than only the NLFEA of LB7 with tensile strength set to $0.6f_{ctm}$ shows a shear force lower than in the experiment.

7.3.3 Influence of fracture energy

The shear-force diagrams of LB6, LB7 and LB8 are shown in respectively Figure 7-31 to Figure 7-33. The fracture energy is calculated conform equation 7.1. Since the non-linear analyses shows a large difference between reaching the tensile strength and the occurring of cracks. This is the case for both flexure cracks in the flange and for web-shear cracks at the junction of the web and the flange. Therefore it is interesting to see the influence of the fracture energy. This is done by performing the same analysis with a fracture energy half of the calculated fracture energy.

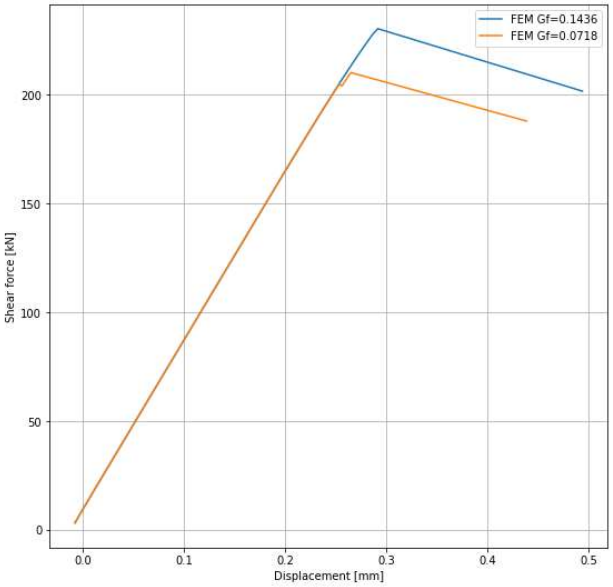

Figure 7-31 Shear force- displacement diagram with reduced fracture energy (LB6)

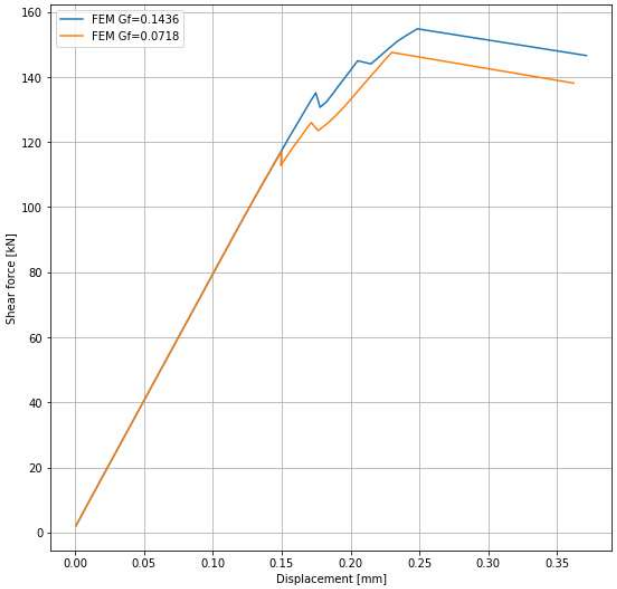

Figure 7-32 Shear force- displacement diagram with reduced fracture energy (LB7)

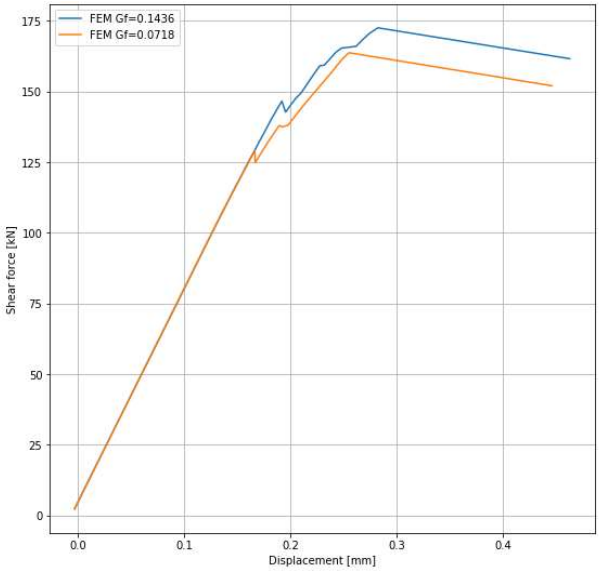

Figure 7-33 Shear force- displacement diagram with reduced fracture energy (LB8)

LB6 shows flexure cracks before the web-shear crack occurs when the fracture energy is reduced. It further shows that the difference between reaching f_{ctm} in the web and the occurring of a web-shear crack is reduced. With the assumed fracture energy of 0.1436 there is a difference of 40 kN between reaching the tensile strength and occurring of a web-shear crack. When the fracture energy is reduced by 50% this difference is also reduced by 50%, thus to 20 kN. This indicates that tension softening is the reason of the difference between reaching f_{ctm} and the occurrence of a crack.

The cracking formation and pattern of LB7 and LB8 remain practically the same with a reduced fracture energy, however the cracks occur at a lower shear force, as can be seen in Table 7-8. The moment that the principle tensile stress reach f_{ctm} in the flange occurs earlier. This is against expectations, since reducing the fracture energy should have zero influence until the tensile strength is reached. However when the tensile strength is reached in the web the flexure micro cracks are already present. These micro cracks have less capacity when the tensile strength is reduced. This explains why the tensile strength in the web is reached under a lower shear force. Just as in LB6 the difference between reaching f_{ctm} in the web and the occurrence of the first web-shear crack is reduced by approximately 50 percent for both LB7 and LB8, respectively from 20 kN to 11 kN and from 33 kN to 14 kN.

Table 7-8 Shear forces with varying fracture energy

Specimen	Fracture energy $[\mathrm{N/mm}]$	$V_{f_{ctm}\_web}$ $[kN]$	$V_{web-shear\_crack}$ $[kN]$
LB6	0.1436	190.8	230.2
LB6	0.0718	190.7	210.1
LB7	0.1436	124.1	144.0
LB7	0.0718	112.8	123.5
LB8	0.1436	132.8	165.9
LB8	0.0718	124.7	138.0

7.4 Comparison of results

LB6

To compare the results of NLFEA of LB6 the shear force- displacement diagram in Figure 7-34 is presented. From this figure it can be noted that the initial stiffness is a good match, however during the experiment the stiffness changed with no apparent reason. This was documented as the uncracked response. Another outstanding difference is that the NLFEA showed a linear process up unto the final step of convergence, at which micro cracks are present leading to a large web-shear crack.

The displacement measured during testing is approximately three times as large as the displacement that follows from the NLFEA. This might be the result of none converging at the first web-shear crack. The largest part of the displacement measured during the experiment happens after the web-shear crack occurred.

Finally it should be noted that the maximum shear force at failure during the experiments is significantly lower than the shear force found in NLFEA. The experiment failed at 153.7 kN while the last step of converging in the NLFEA a shear force of 229.7 is present. This means that the beam failed at 66% of the shear force compared to the NLFEA.

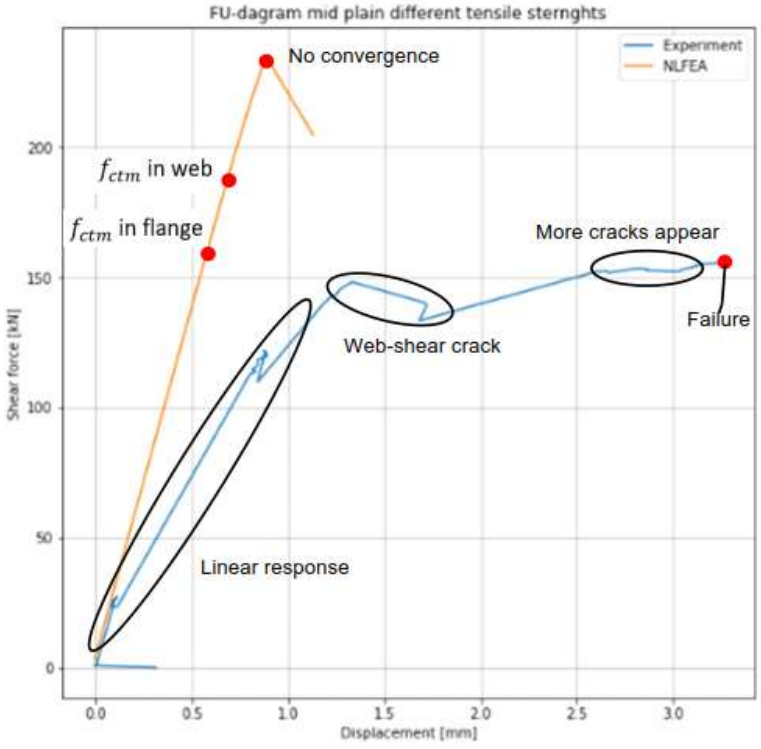

Figure 7-34 Shear force- displacement diagram at mid plain (LB6)

To answer the sub question: ''What is the influence of the presence of bending cracks on the stress distribution in the uncracked zones?'' is the data of the load-step in which f_{ctm} is reached analyzed. The experimental results of LB6 showed no flexure crack up to failure, however the analytical analysis, the LFEA and the NLFEA all indicated principle tensile stresses in the outer fiber higher than f_{ctm}, which suggest that at least micro flexural cracks are present. To find the influence of these micro cracks the

principle tensile stress is compared between the load-step in which f_{ctm} in the flange is reached and the load-step in which f_{ctm} in the web is reached. The shear force present in the NLFEA is applied in the analytical model and in the LFEA. The difference between the analytical model and the experiment is even bigger because of the additional resistance against web-shear cracking after reaching f_{ctm}. The maximum stresses and their locations are given in Table 7-9. Location A is the location where $\sigma_{1\_EC2\_max}$ is found, the location of A is the same for all experiments. Location B is the location where both $\sigma_{1\_LFEA\_max}$ and $\sigma_{1\_NLFEA\_max}$ are located, this is 41 mm to the right of A-A at load-step 25 and 20 mm to the right at load-step 33.

From this table it can be concluded that, as expected, the principle tensile stress at load-step 15 are practically equal for the LFEA and the NLFEA. In load-step 26, first cracked elements in the web, a difference is noticeable between the principle stresses conform the LFEA and NFEA.

This difference is assumed to be the result of the presence of flexural micro cracks, since the rest of the model is the same in both analyses. That the difference is only 3% is probably the result of the fact that the flexure cracks are just $\frac{2}{1000}$ of a mm at this load step. Comparing the principle stress at later load-steps gives unreliable results since the this would mean picking principle stresses of fully cracked elements. The finite element program can give any value due to singularities at that point.

Table 7-9 Maximum principle stresses (LB6)

LB6 EC2	Step	V	Ana	LFEA	NLFEA	x
	[#]	*[kN]*	$[\frac{N}{mm^2}]$	$[\frac{N}{mm^2}]$	$[\frac{N}{mm^2}]$	*[mm]*
A	24	157.5	3.77	3.01	3.01	0
B	24	157.5	3.60	3.04	3.05	41
A	32	190.7	5.54	4.25	4.17	0
B	32	190.7	5.29	4.27	4.20	41

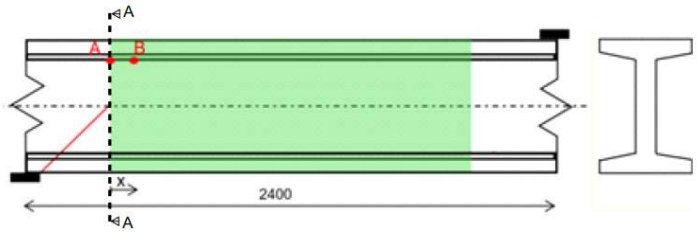

Figure 7-35 Location of maximum principle stresses (LB6)

Table 7-9and Figure 7-37 show the principle tensile stress at A-A at respectively load-step 25 and 33. The blue dotted lines indicate from top to bottom: top of flange, start of inclination of flange, start of web, end of web, end of inclination of flange and bottom of flange. The highest principle tensile stresses are found at the junction between the top flange and the web. It can be seen that the principle stress distribution is almost exactly the same for the NLFEA and the LFEA at load-step 24. The difference between the LFEA and NLFEA compared to the analytical analysis is explained in paragraph 6.4. This has to do with assumptions in the analytical analysis. At load-step 32 a slight difference is found between the LFEA and the NLFEA.

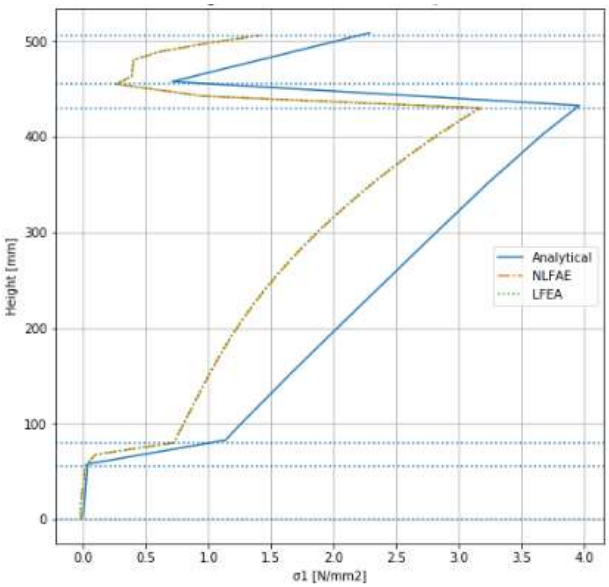

Figure 7-36 σ_1 at the cross-section A-A, load-step 24 (LB6)

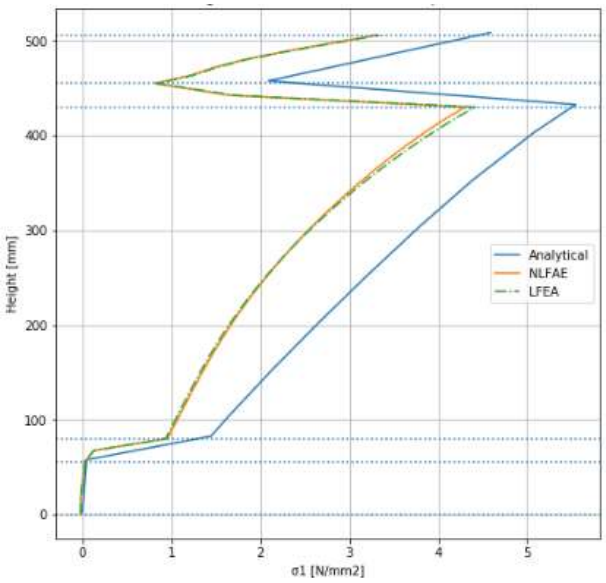

Figure 7-37 σ_1 at the cross-section A-A, load-step 32 (LB6)

The difference is assumed to be caused by the presence of flexure micro cracks. It is known that the principle tensile stress is a calculated with σ_{xx}, σ_{yy} and σ_{xy}, therefore it is of interest to see what the values are at location A. These are given in Table 7-10. The differences are really small, but it can be concluded that due to the micro flexure cracks the shear stress and the stress in vertical direction differ the most and that the horizontal stress remains almost the same in the NLFEA compared to the LFEA.

Table 7-10 Stresses at location A, load-step 32 (LB6)

	σ_{xx} $[N/mm^2]$	σ_{xy} $[N/mm^2]$	σ_{yy} $[N/mm^2]$
LFEA	-1.32	-5.09	-0.11
NLFEA	-1.30	-5.02	-0.20
Difference	0.02	0.07	-0.09

LB7

The shear force- displacement diagram of LB7 at the bottom outer fiber at mid plain is given in Figure 7-38. A shear force of 154 kN is present in the NLFEA in the last step of convergence. This is an increase of just 12% compared to the shear load measured at failure during testing. The stiffness between the experiment and the NLFEA shows some difference. Just like in LB6 the displacements measured during the experiments are way larger than the displacements from NLFEA. However the displacement at first flexure crack and first web-shear crack is comparable. Therefore the difference in displacement at failure is caused by the moment of no convergence in the NLFEA.

The shear force present at web-shear cracking in the experiment results in a completely uncracked response in the NLFEA.

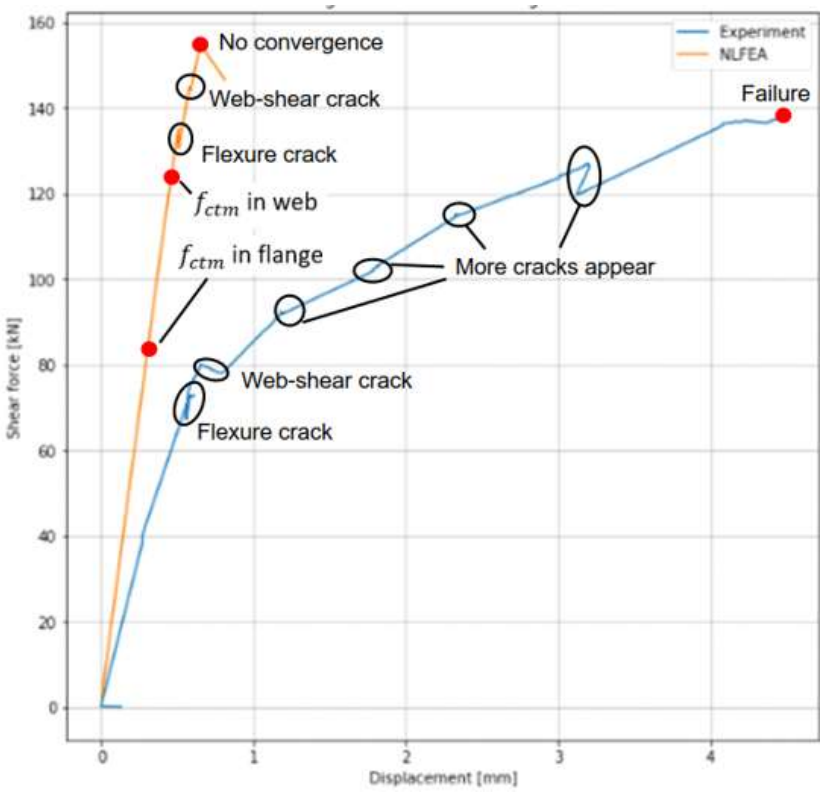

Figure 7-38 Shear force- displacement diagram at mid plain (LB7)

Table 7-11 shows the maximum principle stresses of LB7 as a result of an analytical analysis, LFEA and NLFEA. Location A is again the location where $\sigma_{1\_EC2\_max}$ is found, however for LB7 this is also the location of $\sigma_{1\_LFEA\_max}$ and $\sigma_{1\_NLFEA\_max}$ for load-step 14. In load-step 25 the maximum principle stress conform the NLFEA is found 22 mm to the left, thus outside the region which is evaluated by the EC2.

It can be noted that the analytical analysis results in significantly higher principle stresses at both load-steps. The difference in $\sigma_{1\_LFEA\_max}$ and $\sigma_{1\_NLFEA\_max}$ is almost zero at load-step 14, this is the load-step in which f_{ctm} is reached in the flange. In load-step 25 the difference is 0.26 N/mm^2, which is a 4% reduction of the LFEA. The difference of 0.26 N/mm^2 is more than double the difference at LB6. This can be explained by the size of the micro flexure cracks. LB7 has micro flexure cracks of $\frac{4}{1000}$ of a mm at load-

step 26, which is double the size of the micro cracks at LB6 when reaching f_{ctm} in the web. This confirms the assumption that the difference in principle tensile stress is a consequence of the flexure cracks.

Table 7-11 Maximum principle stresses (LB7)

LB7 EC2	Step	V	Ana	LFEA	NLFEA	x
	[#]	*[kN]*	$[\frac{N}{mm^2}]$	$[\frac{N}{mm^2}]$	$[\frac{N}{mm^2}]$	*[mm]*
A	14	81.3	3.05	2.40	2.39	0
A	25	120.9	5.56	4.45	3.98	0
B	25	120.9	4.57	2.36	4.02	-22

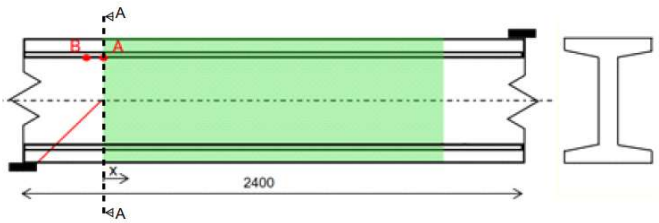

Figure 7-39 Location of maximum principle stresses (LB7)

Figure 7-40 and Figure 7-41 show the principle stress distribution at A-A for respectively load-step 14 and 25. The shift between the analytical analyses compared to the LFEA and NLFEA is again mainly the result of neglecting shear deformation in the analytical analysis. Furthermore it can be seen that at load-step 14 LFEA and NLFEA are approximately the same and at load-step 25 a difference is noticeable. The NLFEA results in slightly smaller values for σ_1 at the crucial location, namely the junction between web and flange.

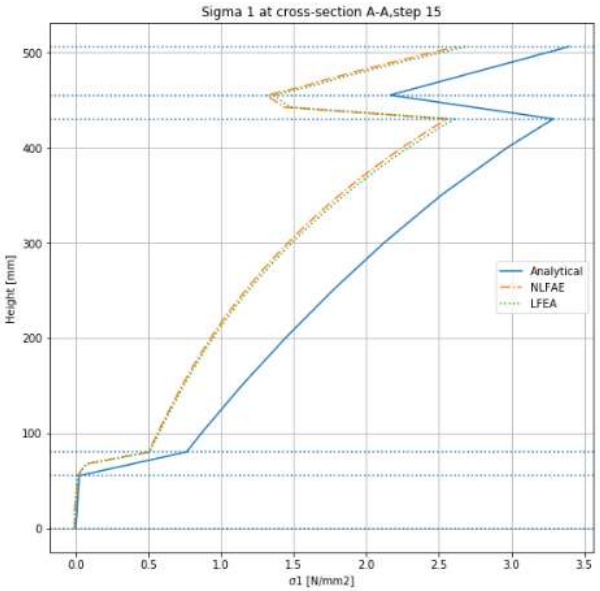

Figure 7-40 σ_1 at the cross-section A-A, load-step 14 (LB7)

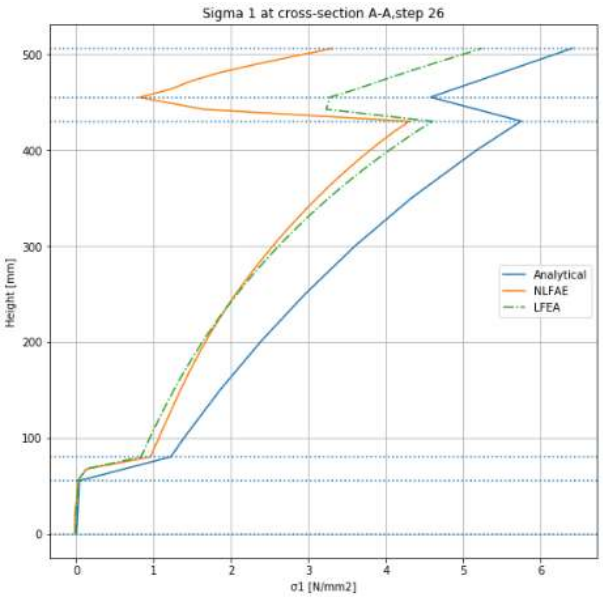

Figure 7-41 σ_1 at the cross-section A-A, load-step 25 (LB7)

Table 7-12 shows the differences of σ_{xx}, σ_{xy} and σ_{yy}. Just as in LB6 it shows that the smallest absolute difference between LFEA and NLFEA is found in σ_{xx}. The values are logically higher than in LB6, since the difference in principle tensile stress is larger. It is interesting to see how the vertical stresses increase to a significant value at the NLFEA. In this specific case the LFEA shows that σ_{yy} is just 2% of σ_{xx} and the NLFEA σ_{yy} is increased to 17% of σ_{xx}, in absolute values.

Table 7-12 Stresses at location A, load-step 25 (LB7)

	σ_{xx} $[N/mm^2]$	σ_{xy} $[N/mm^2]$	σ_{yy} $[N/mm^2]$
LFEA	2.35	3.32	-0.06
NLFEA	2.23	2.95	-0.38
Difference	0.12	0.37	-0.32

LB8

Figure 7-42 shows the shear force- displacement diagram of the outer fiber at mid plane of LB8. Similar trends as in LB6 and LB7 are found. Again the shear force at which the flexure- and web-shear crack occurs in the NLFEA is significantly higher than in the experiment, but the displacement at occurrence of these cracks are comparable. The experiment showed more bending- and web-shear cracks at failure, which explains the difference of displacement at the final step of convergence of the NLFEA with the displacement at failure in the experiment. It can also be observed that after reaching principle tensile stresses of f_{ctm} in the outer fiber and in the web stable paths of equilibrium are found for a significant increase of the shear force.

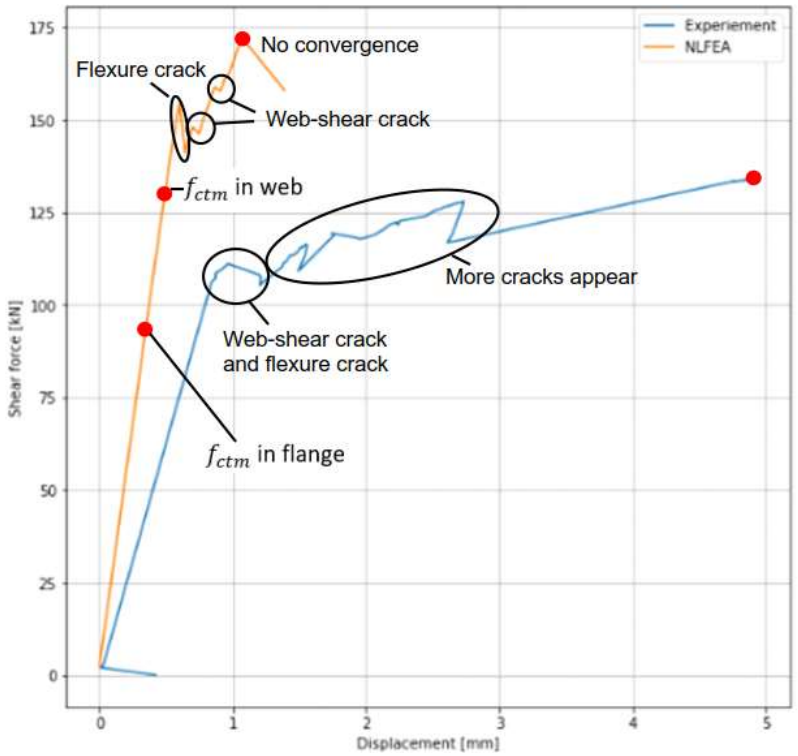

Figure 7-42 Shear force- displacement diagram at mid plain (LB8)

Table 7-13 shows the maximum principle tensile stresses found according to the analytical analyses, the LFEA and the NLFEA for specimen LB8. Figure 7-43 shows the locations. Location A is the location in which at load-step 18 the maximum principle stress is found according the analytical analyses, the LFEA and the NLFEA. At load-step 29, the load-step at which the principle tensile stress reaches the tensile strength in the web, the maximum principle tensile stress according to the NLFEA is found outside the EC2 region. Namely 22 mm to the left of cross-section A-A, this is 1 element of the FEM.

From this table it can be seen that the principle tensile stress at load-step 18 is almost equal according the LFEA compared to the NLFEA. The difference between these two analysis and the analytical analyses is already explained and has to do with the assumptions made in the analytical analyses.

At load-step 29 a difference is noticeable between the LFEA and the NLFEA. Just like in LB6 and LB7 the NLFEA results in a lower maximum principle tensile stress. This is a reduction of 7% compared to the

LFEA. The difference is once again assumed to be caused by the presence of micro flexure cracks which are present at load-step 29. The cracks have a width of $\frac{4}{1000}$ mm. It is expected that if these micro cracks increase that the difference in principle tensile stress between the LFEA and the NLFEA also increases. This is confirmed by the fact that LB6 has the smallest micro cracks when f_{ctm} is reached and also has the smallest difference in σ_1.

Table 7-13 Maximum principle stresses (LB8)

LB8 EC2	Step	V	Ana	LFEA	NLFEA	x
	[#]	*[kN]*	$[\frac{N}{mm^2}]$	$[\frac{N}{mm^2}]$	$[\frac{N}{mm^2}]$	*[mm]*
A	18	94.5	3.42	2.49	2.48	0
A	29	132.8	5.78	4.44	4.08	0
B	29	132,8	5.94	4.43	4.12	-22

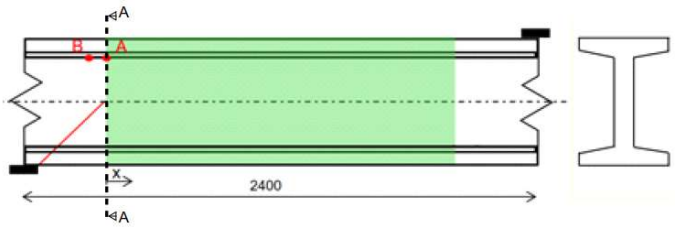

Figure 7-43 Location of maximum principle stresses (LB8)

Figure 7-44 and Figure 7-45 show the stress distribution of the principle tensile stress at respectively load-step 18 and load-step 29. The similar trend as in LB6 and LB7 is found, namely that at the load-step in which $\sigma_1 > f_{ctm}$ in the outer fiber the principle stresses of LFEA and NLFEA are equal and at the load-step in which $\sigma_1 > f_{ctm}$ in the web a difference is noticeable in the principle stresses of LFEA and NLFEA.

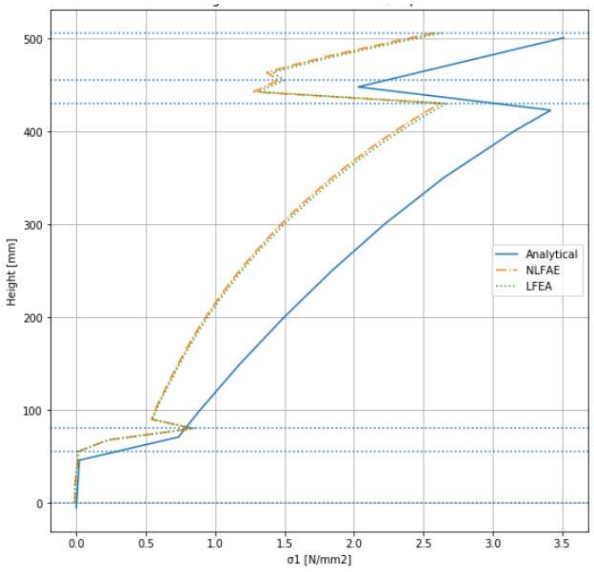

Figure 7-44 σ_1 at the cross-section A-A, load-step 18 (LB8)

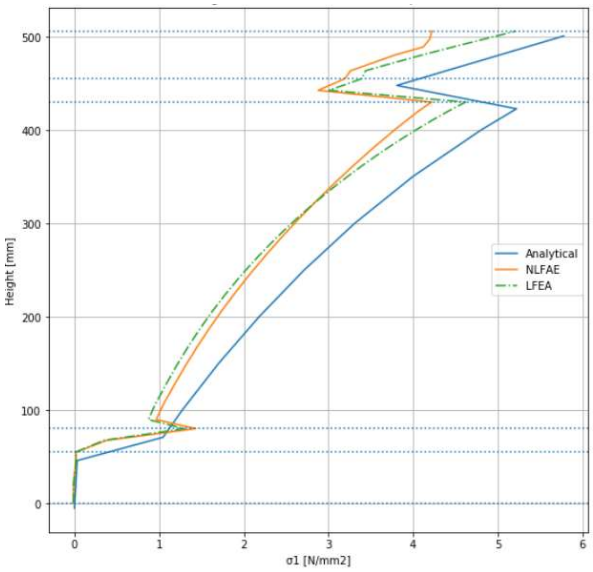

Figure 7-45 σ_1 at the cross-section A-A, load-step 29 (LB8)

Table 7-14 shows how the difference in σ_1 is built up. Just as in LB6 and LB7 the biggest difference follows from differences in the shear stress and in the vertical stress. It is interesting to see how the vertical stresses increase from neglectable to 20% of σ_{xx} in absolute value.

Table 7-14 Stresses at location A, load-step 29 (LB8)

	σ_{xx} $[N/mm^2]$	σ_{xy} $[N/mm^2]$	σ_{yy} $[N/mm^2]$
LFEA	2.04	-3.57	-0.06
NLFEA	1.91	-3.20	-0.40
Difference	0.13	0.37	-0.34

8 Discussion

In this chapter the main results are summarized per research question. The first sub-question is:

''What is the influence of the presence of bending cracks on the stress distribution in the uncracked zones?''

- The analytical analyses, using the assumptions of a Euler-Bernoulli beam, is performed for the three investigated beams. Another assumption in the analytical analyses is neglecting the vertical stresses, which is common in practice. The load used in the analytical analyses is set to the load under which the first web-shear cracks occurred during testing. The analytical analyses show differences compared to the experiments. LB6 had no flexural cracks observed during the experiment, yet the analytical analyses shows the highest principle stress in the outer fiber which indicates bending cracks. Furthermore only LB8 showed $\sigma_1 > f_{ctm}$ at the location of the web-shear crack. Meaning that web-shear cracking occurred in LB6 and LB7 at a stress lower than uniaxial tensile strength.
- The LFEA analyses shows comparable results to the analytical analysis as in where the maximum principle stress occurs. It shows that for all three specimen the principle tensile stress in the outer fiber is larger than f_{ctm_fl} . It further shows that the maximum principle tensile stress occurs in the outer fiber. This indicates that all three specimen have flexural cracks before web-shear cracking, however during the experiment it is observed that only LB7 has flexural cracks before web-shear cracking.
- When the shear force is put to the shear force which is present in the NLFEA just before reaching the tensile strength in the web then the difference between σ_{1_LFEA} and σ_{1_NLFEA} is very small with just 3% for LB6 and 7% for both LB7 and LB8. However at this loading stage only micro flexure cracks are present. The cracking width of the micro cracks in LB7 and LB8 is double the cracking width of LB6 at just before reaching f_{ctm} in the web. This indicates that with an increasing cracking width the influence on the principle tensile stress also increases.

The found results that help answer the second sub question are summarized below. The second sub-question is:

''To which extend can the requirement codes be applied to continuous prestressed reinforced members?

- The area checked by the EC2 and MC2010 level 2 starts where a 45° line out of the support crosses the CoG. The first cross-section shows the highest stresses according to the analytical analyses. The principle tensile stresses at this cross-section show consistently lower values according to the LFEA compared to the analytical analyses. The maximum principle tensile stresses according to the LFEA are all located at the junction between web and flange in cross-section further away than 45° out of the support to the CoG.
- The results of the NLFEA and the LFEA are practically equal up until the tensile strength is reached in the outer fiber, which is logical since the linear parameters are the same. The σ_1 after micro flexure cracks occurred start to deviate from the LFEA. The order of maximum principle tensile stress is consistent: $\sigma_{ana} > \sigma_{1\_LFEA} \geq \sigma_{1\_NLFEA}$. Both LB7 and LB8 showed maximum principle stresses according to the NLFEA closer to the support than the cross-section where a

45° line out of the support crosses CoG. These maximum stresses were located 22 mm, only 1 finite element. See Table 7-11 and Table 7-13.

The found results which are of interest to the main question are given below. The main question is:

''How can the shear tension resistance of concrete members without shear reinforcement be predicted in the most accurate way?''

- The σ_{1_max} according to the analytical analyses are between 24% and 27% higher than the σ_{1_max} according to the LFEA, see Table 6.6, Table 6.8 and Table 6.10. These differences are the result of the simplification made in the analytical analyses, mainly the neglection of shear deformation.
- It is concluded that neglecting the vertical stresses in the analytical analyses is not the cause of the difference between the σ_{1_LFEA} and σ_{1_ana}. Neglecting the vertical stresses in the analytical analysis is only the cause of approximately 5% of the difference between σ_{1_LFEA} and σ_{1_ANA}. The largest part of the difference between the σ_{1_LFEA} and σ_{1_ana} is caused by the difference in σ_{xx_ana} and σ_{xx_LFEA}.
- The NLFEA shows that between σ_1 reaching f_{ctm} and the occurring of a significant crack the stiffness of the specimen remains practically unchanged. This is the case for both flexural- and web-shear cracks. In this path only micro cracks are formed. This explains how it is possible that during testing no flexural cracks were observed, but the analytical analysis and the LFEA does show principle stresses higher than the tensile strength at the outer fiber, because the micro cracks were, with a width of 9/1000, too small to notice by the human eye.
- The sensitivity analysis about the influence of shear reinforcement shows that until the first web-shear crack the behavior is similar with and without stirrups. Furthermore it shows that even the model without stirrups has a path of equilibrium after the principle tensile stresses have reached the tensile strength of the concrete.
- It can be concluded on the basis of the sensitivity analysis to fracture energy that the difference between reaching the tensile strength and the occurrence of a crack is mainly caused by tension softening. In this analysis the fracture energy is reduced by 50 percent and this results in a reduction of also roughly 50 percent in the difference between reaching the tensile strength and the occurrence of a crack.
- The sensitivity analysis about the influence of the tensile strength of the concrete shows that even when the tensile strength is set to $0.6f_{ctm}$ the shear forces found in the last step of converging in the NLFEA are higher than the shear force at failure in the experiment. Also when the moment of originating of the web-shear crack is compared it follows that the shear force in the NLFEA is higher than in the experiments.

9 Conclusion

In this chapter the research questions are answered. Starting with the sub-questions:

''What is the influence of the presence of bending cracks on the stress distribution in the uncracked zones?''

It is concluded that the influence of bending cracks on the stress distribution in the cross-section where web-shear cracking occurs is present. This is concluded by comparing the results of the LFEA and the NLFEA under the shear force which is present just before flexural cracking occurs and just before web-shear cracking occurs. The principle stress distribution of the NLFEA and the FLEA are equal until the principle tensile stress reaches the tensile strength in the outer fibre. At a later stage, just before the tensile strength is reached in the junction between web and flange, there is a difference in the principle tensile stress that follows from the NLFEA and the LFEA. This difference is due to the presence of micro flexural cracks. It is also concluded that the presence of larger micro bending cracks result in a larger reduction of the principle tensile stress when the NLFEA is compared to the LFEA.

At the moment when the first bending cracks are originated a large part of the web has already reached the tensile strength. Therefore it not possible to compare the principle tensile stresses between LFEA and NLFEA at this moment, since the principle tensile stresses of the NLFEA are capped at f_{ctm}. It can only be assumed that bending cracks have a increasing influence on the stress distribution and result in a larger reduction of the principle tensile stress compared to the analytical analyses and the LFEA.

''To which extend can the requirement codes be applied to continuous prestressed reinforced members?''

Both the EC2 and the MC2010 are meant to only be applicable to single span prestressed concrete members. However during this thesis the design codes are used on continuous prestressed concrete members and no indications were found that this results in unreliable results. The EC2 and MC2010 both indicate an disturbed area above the support which has not to be checked. This area is applied in a similar fashion to the continuous beams, above the support and under the loads. The stress distribution at the cross-section where web-shear cracking occurs are comparable.

However when the results of single span and continuous prestressed members are compared it shows that the continuous members, unlike the single span members, underestimate the resistance to web-shear cracking. This indicates that the resistance of continuous beams differs to the resistance of single span members.

With the now answered sub-question the main question can be answered:

''How can the shear tension resistance of concrete members without shear reinforcement be predicted in the most accurate way?''

To predict the shear tension resistance of concrete members without shear reinforcement for continuous prestressed members it is concluded that the influence of the presence of micro bending cracks on the principle tensile stress in the uncracked region is present. This means that the shear tension resistance is underestimated when calculated with a analytical analyses and with a LFEA. Therefore a NLFEA results in a higher resistance to web-shear cracking. It can only be assumed that the

reduction on the principle tensile stress due to the presence micro bending cracks increases when the micro bending cracks evolve to significant flexure cracks.

However the experiments showed failure at a significantly lower load than the NLFEA show web-shear cracking. This indicates that the resistance to shear tension is overestimated. Even when the tensile strength is reduced by 40% an overestimation follows.

The analytical analyses, LFEA and the NLFEA overestimate the resistance to web-shear cracking for the considered specimen. There is no clear reason found in this thesis. It is however concluded that an overestimation of the tensile strength is not the main cause.

10 Recommendations for future work

This thesis only used a single case study, which is far too little to draw conclusions. Therefore it is needed to perform more NLFEA on more experiments. It is also recommended to do this for both single span and continuous beams.

The used case study had specimen in which no flexural cracks were observed during testing, however the analytical, LFEA and NLFEA indicate a principle tensile stress higher than the tensile strength of concrete in the outer fibre. This indicates that at least micro cracks were present during testing. To get a guideline for concrete members uncracked in bending it is therefore important to create an experiment in which the principle tensile stresses in the outer fibre are smaller than the tensile strength.

Furthermore it is interesting to do more research on the capacity of the concrete in prestressed reinforced members after reaching the tensile strength. It is normally assumed that when the tensile strength is reached the influence of the concrete is neglectable. However this thesis shows a large difference between reaching the tensile strength and the occurrence of a significant crack. It is expected that this difference is there due to tension softening of concrete.

Bibliography

[1] Xie L. ,,The influence of axial load and prestress on the shear strength of web-shear critical reinforced concrete elements''. Degree of Ph. D. at University Toronto, 2009.

[2] Kroeze SJ. ,, Resistance to diagnol tension cracking in prestressed beams''. MSc Thesis at TU Delft, 2018.

[3] Sugianto A. ,, Seize effect study on uniaxial tensile strength. By investigating shear tension crack at prestressed concrete beams''. Additional MSc thesis at TU Delft, 2019.

[4] Bentz E.C. ,, Sectional analysis of reinforced concrete members''. Degree of Ph. D. at University Toronto, 2000.

[5] Paper by M. Roosen, C. van der Veen and D. Hordijk ,, Suitability of shear tension code requirements for assessment of existing structures build-up with prestressed I- and T-shape girders'', 2019.

[6] Paper by M. Roosen, C. van der Veen and D. Hordijk ,, Resistance to diagonal tension cracking of single span prestressed girders''.

[7] FÉDÉRATION INTERNATIONALE DU BÉTON (fib) Model Code 2010 - final draft (2012). Vol. 1, Bulletin 65, and Vol. 2, Bulletin 66, Lausanne, Switzerland.

[8] EUROCODE 2 (2005). EN 1992-1-1:2004: Design of concrete structures - Part l - 1: General rules and rules for buildings. CEN European Committee for Standardization, Brussels, Belgium.

[9] ACI Committee 318 (2008). Building Code Requirements for Structural Concrete (ACI 318-08) and Commentary (318R-08), American Concrete Institute, Farmington Hills

[10] Walraven J.C. ,,Background document for prENC 1992-1-1:2002 6.2 shear. TU Delft 2002.

[11] Rijkswaterstaat technical document ''Guidelines for nonlinear finite element analysis of concrete structures'', 2017.

Apendix A: Python script LB6

```
newProject( "../Desktop", 1000 )
setModelAnalysisAspects( [ "STRUCT" ] )
setModelDimension( "2D" )
setDefaultMeshOrder( "QUADRATIC" )
setDefaultMesherType( "HEXQUAD" )

setUnit( "LENGTH", "MM" )
setUnit( "MASS", "LB" )
setUnit( "MASS", "G" )
setUnit( "FORCE", "N" )

##Geometry

createSheet( "left rectangular", [[ 0, 0, 0 ],[ 700, 0, 0 ],[ 700, 506, 0 ],[ 0, 506, 0 ]] )
createSheet( "right rectangular", [[ 3920, 0, 0 ],[ 4620, 0, 0 ],[ 4620, 506, 0 ],[ 3920, 506, 0 ]] )

createSheet( "top flange lin 1", [[ 700, 455, 0 ],[ 900, 455, 0 ],[ 900, 506, 0 ],[ 700, 506, 0 ]] )
createSheet( "web lin 1", [[ 700, 80, 0 ],[ 900, 80, 0 ],[ 900, 430, 0 ],[ 700, 430, 0 ]] )
createSheet( "bottom flange lin 1", [[ 700, 0, 0 ],[ 900, 0, 0 ],[ 900, 55, 0 ],[ 700, 55, 0 ]] )
createSheet( "Inclined bot lin 1", [[ 700, 55, 0 ],[ 900, 55, 0 ],[ 900, 80, 0 ],[ 700, 80, 0 ]] )
createSheet( "Inclined top lin 1", [[ 700, 430, 0 ],[ 900, 430, 0 ],[ 900, 455, 0 ],[ 700, 455, 0 ]] )

createSheet( "top flange non-lin", [[ 900, 455, 0 ],[ 2310, 455, 0 ],[ 2310, 506, 0 ],[ 900, 506, 0 ]] )
createSheet( "web non-lin", [[ 900, 80, 0 ],[ 2310, 80, 0 ],[ 2310, 430, 0 ],[ 900, 430, 0 ]] )
createSheet( "bottom flange non-lin", [[ 900, 0, 0 ],[ 2310, 0, 0 ],[ 2310, 55, 0 ],[ 900, 55, 0 ]] )
createSheet( "Inclined bot non-lin", [[ 900, 55, 0 ],[ 2310, 55, 0 ],[ 2310, 80, 0 ],[ 900, 80, 0 ]] )
createSheet( "Inclined top non-lin", [[ 900, 430, 0 ],[ 2310, 430, 0 ],[ 2310, 455, 0 ],[ 900, 455, 0 ]] )

createSheet( "top flange lin 2", [[ 2310, 455, 0 ],[ 3920, 455, 0 ],[ 3920, 506, 0 ],[ 2310, 506, 0 ]] )
createSheet( "web lin 2", [[ 2310, 80, 0 ],[ 3920, 80, 0 ],[ 3920, 430, 0 ],[ 2310, 430, 0 ]] )
createSheet( "bottom flange lin 2", [[ 2310, 0, 0 ],[ 3920, 0, 0 ],[ 3920, 55, 0 ],[ 2310, 55, 0 ]] )
createSheet( "Inclined bot lin 2", [[ 2310, 55, 0 ],[ 3920, 55, 0 ],[ 3920, 80, 0 ],[ 2310, 80, 0 ]] )
createSheet( "Inclined top lin 2", [[ 2310, 430, 0 ],[ 3920, 430, 0 ],[ 3920, 455, 0 ],[ 2310, 455, 0 ]] )

createSheet( "load1", [[ 75, 506, 0 ],[ 225, 506, 0 ],[ 225, 556, 0 ],[ 150, 556, 0 ],[ 75, 556, 0 ]] )
createSheet( "load2", [[ 3435, 506, 0 ],[ 3585, 506, 0 ],[ 3585, 556, 0 ],[ 3510, 556, 0 ],[ 3435, 556, 0 ]] )
createSheet( "support1", [[ 1035, -50, 0 ],[ 1110, -50, 0 ],[ 1185, -50, 0 ],[ 1185, 0, 0 ],[ 1035, 0, 0 ]] )
createSheet( "support2", [[ 4395, -50, 0 ],[ 4470, -50, 0 ],[ 4545, -50, 0 ],[ 4545, 0, 0 ],[ 4395, 0, 0 ]] )

createLine( "lower reinforcement", [ 0, 33, 0 ], [ 4620, 33, 0 ] )
createLine( "upper reinforcement", [ 0, 473, 0 ], [ 4620, 473, 0 ] )
createLine( "lower prestress tendon", [ 0, 33, 0 ], [ 4620, 33, 0 ] )
createLine( "upper prestress tendon", [ 0, 473, 0 ], [ 4620, 473, 0 ] )

createSheet( "spreader beam", [[ 25, 556, 0 ],[ 25, 656, 0 ],[ 2310, 656, 0 ],[ 3985, 656, 0 ],[ 3985, 556, 0 ]] )

#stirrups
createLine( "Line 1", [ 75, 0, 0 ], [ 75, 506, 0 ] )
createLine( "Line 2", [ 200, 0, 0 ], [ 200, 506, 0 ] )
createLine( "Line 3", [ 325, 0, 0 ], [ 325, 506, 0 ] )
createLine( "Line 4", [ 450, 0, 0 ], [ 450, 506, 0 ] )
createLine( "Line 5", [ 575, 0, 0 ], [ 575, 506, 0 ] )
createLine( "Line 6", [ 700, 0, 0 ], [ 700, 506, 0 ] )
```

```
createLine( "Line 7", [ 825, 0, 0 ], [ 825, 506, 0 ] )
createLine( "Line 8", [ 950, 0, 0 ], [ 950, 506, 0 ] )
createLine( "Line 9", [ 1075, 0, 0 ], [ 1075, 506, 0 ] )
createLine( "Line 10", [ 1162.5, 0, 0 ], [ 1162.5, 506, 0 ] )
createLine( "Line 11", [ 1250, 0, 0 ], [ 1250, 506, 0 ] )
createLine( "Line 12", [ 1337.5, 0, 0 ], [ 1337.5, 506, 0 ] )
createLine( "Line 13", [ 1425, 0, 0 ], [ 1425, 506, 0 ] )
createLine( "Line 14", [ 1512.5, 0, 0 ], [ 1512.5, 506, 0 ] )
createLine( "Line 15", [ 1600, 0, 0 ], [ 1600, 506, 0 ] )
createLine( "Line 16", [ 1775, 0, 0 ], [ 1775, 506, 0 ] )
createLine( "Line 17", [ 1950, 0, 0 ], [ 1950, 506, 0 ] )
createLine( "Line 18", [ 2125, 0, 0 ], [ 2125, 506, 0 ] )
createLine( "Line 19", [ 2300, 0, 0 ], [ 2300, 506, 0 ] )
createLine( "Line 20", [ 2475, 0, 0 ], [ 2475, 506, 0 ] )
createLine( "Line 21", [ 2650, 0, 0 ], [ 2650, 506, 0 ] )
createLine( "Line 22", [ 2825, 0, 0 ], [ 2825, 506, 0 ] )
createLine( "Line 23", [ 3000, 0, 0 ], [ 3000, 506, 0 ] )
createLine( "Line 24", [ 3087.5, 0, 0 ], [ 3087.5, 506, 0 ] )
createLine( "Line 25", [ 3175, 0, 0 ], [ 3175, 506, 0 ] )
createLine( "Line 26", [ 3262.5, 0, 0 ], [3262.5, 506, 0 ] )
createLine( "Line 27", [ 3350, 0, 0 ], [ 3350, 506, 0 ] )
createLine( "Line 28", [ 3437.5, 0, 0 ], [ 3437.5, 506, 0 ] )
createLine( "Line 29", [ 3525, 0, 0 ], [ 3525, 506, 0 ] )
createLine( "Line 30", [ 3650, 0, 0 ], [ 3650, 506, 0 ] )
createLine( "Line 31", [ 3775, 0, 0 ], [ 3775, 506, 0 ] )
createLine( "Line 32", [ 3900, 0, 0 ], [ 3900, 506, 0 ] )
createLine( "Line 33", [ 4025, 0, 0 ], [ 4025, 506, 0 ] )
createLine( "Line 34", [ 4150, 0, 0 ], [ 4150, 506, 0 ] )
createLine( "Line 35", [ 4275, 0, 0 ], [ 4275, 506, 0 ] )
createLine( "Line 36", [ 4400, 0, 0 ], [ 4400, 506, 0 ] )
createLine( "Line 37", [ 4525, 0, 0 ], [ 4525, 506, 0 ] )

#Functions for inclined part of flanges
setFunctionValues( "inclined bot", [  ], [ 55, 80 ], [  ], [ 175, 36.5 ] )
setFunctionValues( "inclined top", [  ], [ 430, 455 ], [  ], [ 36.5, 175 ] )

##Materials
#manual input of concrete material, hordijk and thorenfeldt
addMaterial( "concrete", "CONCR", "TSCR", [] )
setParameter( "MATERIAL", "concrete", "LINEAR/ELASTI/YOUNG", 40300 )
setParameter( "MATERIAL", "concrete", "LINEAR/ELASTI/POISON", 0.2 )
setParameter( "MATERIAL", "concrete", "TENSIL/TENSTR", 4.23 )
setParameter( "MATERIAL", "concrete", "TENSIL/TENCRV", "HORDYK" )
setParameter( "MATERIAL", "concrete", "TENSIL/GF1", 0.1436 )
setParameter( "MATERIAL", "concrete", "MODTYP/TOTCRK", "ROTATE" )
setParameter( "MATERIAL", "concrete", "COMPRS/COMCRV", "PARABO" )
setParameter( "MATERIAL", "concrete", "COMPRS/COMSTR", 63.5 )
setParameter( "MATERIAL", "concrete", "COMPRS/GC", 35.9 )
setParameter( "MATERIAL", "concrete", "LINEAR/MASS/DENSIT", 2.4e-09 )
#manual input of concrete material - linear
addMaterial( "concrete linear", "CONCR", "TSCR", [] )
setParameter( "MATERIAL", "concrete linear", "LINEAR/ELASTI/YOUNG", 40300 )
setParameter( "MATERIAL", "concrete linear", "LINEAR/ELASTI/POISON", 0.2 )
```

```
setParameter( "MATERIAL", "concrete linear", "TENSIL/TENCRV", "ELASTI" )
setParameter( "MATERIAL", "concrete linear", "LINEAR/MASS/DENSIT", 2.4e-09 )
#longitudinal reinforcement
addMaterial( "reinforcement", "REINFO", "LINEAR", [] )
setParameter( "MATERIAL", "reinforcement", "LINEAR/ELASTI/YOUNG", 210000 )
#sup/load plate
addMaterial( "sup/load plate", "MCSTEL", "ISOTRO", [] )
setParameter( "MATERIAL", "sup/load plate", "LINEAR/ELASTI/YOUNG", 200000 )
setParameter( "MATERIAL", "sup/load plate", "LINEAR/ELASTI/POISON", 0.2 )
setParameter( "MATERIAL", "sup/load plate", "LINEAR/MASS/DENSIT", 0 )
#prestress
addMaterial( "prestress", "REINFO", "VMISES", [] )
setParameter( "MATERIAL", "prestress", "LINEAR/ELASTI/YOUNG", 2e+11 )
setMaterialAspects( "prestress", [ "NOBOND" ] )
setParameter( "MATERIAL", "prestress", "PLASTI/YLDTYP", "KAPSIG" )
setParameter( "MATERIAL", "prestress", "PLASTI/YLDTYP", "NONE" )
setParameter( "MATERIAL", "prestress", "PLASTI/HARDI1/YLDSTR", 972 )
#interface
addMaterial( "Interface material", "INTERF", "ELASTI", [] )
setParameter( "MATERIAL", "Interface material", "LINEAR/IFTYP", "LIN2D" )
setParameter( "MATERIAL", "Interface material", "LINEAR/ELAS2/DSNY", 2015000 )
setParameter( "MATERIAL", "Interface material", "LINEAR/ELAS2/DSNY", 2015000 )
setParameter( "MATERIAL", "Interface material", "LINEAR/ELAS2/DSSX", 2.015 )
setParameter( "MATERIAL", "Interface material", "LINEAR/ELAS2/DSSX", 2.015 )
#Spreader Beam
addMaterial( "spreader beam", "MCSTEL", "ISOTRO", [] )
setParameter( "MATERIAL", "spreader beam", "LINEAR/ELASTI/YOUNG", 2.1e+08 )
setParameter( "MATERIAL", "spreader beam", "LINEAR/ELASTI/POISON", 0.2 )
setParameter( "MATERIAL", "spreader beam", "LINEAR/MASS/DENSIT", 0 )
#Stirrups
addMaterial( "stirrups", "REINFO", "VMISES", [] )
setParameter( "MATERIAL", "stirrups", "LINEAR/ELASTI/YOUNG", 195800 )
setParameter( "MATERIAL", "stirrups", "PLASTI/YLDTYP", "EPSSIG" )
setParameter( "MATERIAL", "stirrups", "PLASTI/HARDI4/EPSSIG", [] )
setParameter( "MATERIAL", "stirrups", "PLASTI/HARDI4/EPSSIG", [ 0, 0, 0.00265, 529, 0.04, 581 ] )

##Geometries
addGeometry( "beam fl top", "SHEET", "MEMBRA", [] )
setParameter( "GEOMET", "beam fl top", "THICK", 350 )
addGeometry( "beam fl bot", "SHEET", "MEMBRA", [] )
setParameter( "GEOMET", "beam fl bot", "THICK", 350 )
addGeometry( "rectangles", "SHEET", "MEMBRA", [] )
setParameter( "GEOMET", "rectangles", "THICK", 350 )
addGeometry( "beam web", "SHEET", "MEMBRA", [] )
setParameter( "GEOMET", "beam web", "THICK", 73 )
addGeometry( "inclined top", "SHEET", "MEMBRA", [] )
setParameter( "GEOMET", "inclined top", "LOCAXS", True )
setParameter( "GEOMET", "inclined top", "LOCAXS", False )
setParameter( "GEOMET", "inclined top", "THICK", [] )
setGeometryFunction( "inclined top", "THICK", "inclined top" )
setParameter( "GEOMET", "inclined top", "THICK", 2 )
addGeometry( "inclined bot", "SHEET", "MEMBRA", [] )
setParameter( "GEOMET", "inclined bot", "LOCAXS", True )
```

```
setParameter( "GEOMET", "inclined bot", "LOCAXS", False )
setParameter( "GEOMET", "inclined bot", "THICK", [] )
setGeometryFunction( "inclined bot", "THICK", "inclined bot" )
setParameter( "GEOMET", "inclined bot", "THICK", 2 )
addGeometry( "Sup/load plates", "SHEET", "MEMBRA", [] )
setParameter( "GEOMET", "Sup/load plates", "THICK", 350 )
addGeometry( "Interface geometry", "LINE", "STLIIF", [] )
setParameter( "GEOMET", "Interface geometry", "LIFMEM/THICK", 350 )
addGeometry( "prestress", "RELINE", "REBAR", [] )
setParameter( "GEOMET", "prestress", "REIEMB/CROSSE", 507 )
addGeometry( "As", "LINE", "TRUSS", [] )
setParameter( "GEOMET", "As", "CROSSE", 800          )
addGeometry( "spreader beam", "SHEET", "MEMBRA", [] )
setParameter( "GEOMET", "spreader beam", "THICK", 350 )
addGeometry( "stirrups", "LINE", "TRUSS", [] )
setParameter( "GEOMET", "stirrups", "CROSSE", 24.2 )

##Loads and load combinations
createPointLoad( "prescribed deformation", "prescribed deformation" )
setParameter( "GEOMETRYLOAD", "prescribed deformation", "LODTYP", "DEFORM" )
setParameter( "GEOMETRYLOAD", "prescribed deformation", "DEFORM/TR/VALUE", -1 )
setParameter( "GEOMETRYLOAD", "prescribed deformation", "DEFORM/TR/DIRECT", 2 )
attach( "GEOMETRYLOAD", "prescribed deformation", "spreader beam", [[ 2310, 656, 0 ]] )
#prestressing force
addSet( "GEOMETRYLOADSET", "prestressing load case" )
createBodyLoad( "prestress 1 side", "prestressing load case" )
setParameter( "GEOMETRYLOAD", "prestress 1 side", "LODTYP", "POSTEN" )
setParameter( "GEOMETRYLOAD", "prestress 1 side", "POSTEN/TENTYP", "ONEEND" )
setParameter( "GEOMETRYLOAD", "prestress 1 side", "POSTEN/ONEEND/FORCE1", 398500 )
setParameter( "GEOMETRYLOAD", "prestress 1 side", "POSTEN/SHEAR", 0 )
attachTo( "GEOMETRYLOAD", "prestress 1 side", "POSTEN/ONEEND/PNTS1", "lower prestress tendon", [[ 4620, 66,
0 ]] )
attachTo( "GEOMETRYLOAD", "prestress 1 side", "POSTEN/ONEEND/PNTS1", "upper prestress tendon", [[ 4620,
433, 0 ]] )
attach( "GEOMETRYLOAD", "prestress 1 side", [ "lower prestress tendon", "upper prestress tendon" ] )
#dead weight
addSet( "GEOMETRYLOADSET", "dead weight" )
createModelLoad( "dead weight", "dead weight" )
#load combinations
setDefaultGeometryLoadCombinations(  )
setGeometryLoadCombinationFactor( "Geometry load combination 1", "prescribed deformation", 1 )
setGeometryLoadCombinationFactor( "Geometry load combination 3", "dead weight", 1 )
addGeometryLoadCombination( "" )
setGeometryLoadCombinationFactor( "Geometry load combination 4", "prescribed deformation", 1 )
setGeometryLoadCombinationFactor( "Geometry load combination 4", "prestressing load case", 1 )
setGeometryLoadCombinationFactor( "Geometry load combination 4", "dead weight", 1 )

##Supports
addSet( "GEOMETRYSUPPORTSET", "supports" )
createPointSupport( "bc left", "supports" )
setParameter( "GEOMETRYSUPPORT", "bc left", "AXES", [ 1, 2 ] )
setParameter( "GEOMETRYSUPPORT", "bc left", "TRANSL", [ 1, 1, 0 ] )
setParameter( "GEOMETRYSUPPORT", "bc left", "ROTATI", [ 0, 0, 0 ] )
```

```
attach( "GEOMETRYSUPPORT", "bc left", "support1", [[ 1110, -50, 0 ]] )
createPointSupport( "bc right", "supports" )
setParameter( "GEOMETRYSUPPORT", "bc right", "AXES", [ 1, 2 ] )
setParameter( "GEOMETRYSUPPORT", "bc right", "TRANSL", [ 0, 1, 0 ] )
setParameter( "GEOMETRYSUPPORT", "bc right", "ROTATI", [ 0, 0, 0 ] )
attach( "GEOMETRYSUPPORT", "bc right", "support2", [[ 4470, -50, 0 ]] )
createPointSupport( "predescribed displacement", "supports" )
setParameter( "GEOMETRYSUPPORT", "predescribed displacement", "AXES", [ 1, 2 ] )
setParameter( "GEOMETRYSUPPORT", "predescribed displacement", "TRANSL", [ 0, 1, 0 ] )
setParameter( "GEOMETRYSUPPORT", "predescribed displacement", "ROTATI", [ 0, 0, 0 ] )
attach( "GEOMETRYSUPPORT", "predescribed displacement", "spreader beam", [[ 2310, 656, 0 ]] )

##assigning materials, element class to geometry
#Concrete
setElementClassType( "SHAPE", [ "bottom flange lin 1", "bottom flange lin 2" ], "MEMBRA" )
assignMaterial( "concrete linear", "SHAPE", [ "bottom flange lin 1", "bottom flange lin 2" ] )
assignGeometry( "beam fl bot", "SHAPE", [ "bottom flange lin 1", "bottom flange lin 2" ] )
setElementClassType( "SHAPE", [ "bottom flange non-lin" ], "MEMBRA" )
assignMaterial( "concrete", "SHAPE", [ "bottom flange non-lin" ] )
assignGeometry( "beam fl bot", "SHAPE", [ "bottom flange non-lin" ] )
setElementClassType( "SHAPE", [ "Inclined bot lin 1", "Inclined bot lin 2" ], "MEMBRA" )
assignMaterial( "concrete linear", "SHAPE", [ "Inclined bot lin 1", "Inclined bot lin 2" ] )
assignGeometry( "inclined bot", "SHAPE", [ "Inclined bot lin 1", "Inclined bot lin 2" ] )
setElementClassType( "SHAPE", [ "Inclined bot non-lin" ], "MEMBRA" )
assignMaterial( "concrete", "SHAPE", [ "Inclined bot non-lin" ] )
assignGeometry( "inclined bot", "SHAPE", [ "Inclined bot non-lin" ] )
setElementClassType( "SHAPE", [ "Inclined top lin 2", "Inclined top lin 1" ], "MEMBRA" )
assignMaterial( "concrete linear", "SHAPE", [ "Inclined top lin 2", "Inclined top lin 1" ] )
assignGeometry( "inclined top", "SHAPE", [ "Inclined top lin 2", "Inclined top lin 1" ] )
setElementClassType( "SHAPE", [ "Inclined top non-lin" ], "MEMBRA" )
assignMaterial( "concrete", "SHAPE", [ "Inclined top non-lin" ] )
assignGeometry( "inclined top", "SHAPE", [ "Inclined top non-lin" ] )
setElementClassType( "SHAPE", [ "left rectangular", "right rectangular" ], "MEMBRA" )
assignMaterial( "concrete linear", "SHAPE", [ "left rectangular", "right rectangular" ] )
assignGeometry( "rectangles", "SHAPE", [ "left rectangular", "right rectangular" ] )
setElementClassType( "SHAPE", [ "support2", "support1", "load2", "load1", "spreader beam" ], "MEMBRA" )
assignMaterial( "sup/load plate", "SHAPE", [ "support2", "support1", "load2", "load1", "spreader beam" ] )
assignGeometry( "beam fl top", "SHAPE", [ "support2", "support1", "load2", "load1", "spreader beam" ] )
setElementClassType( "SHAPE", [ "top flange lin 1", "top flange lin 2" ], "MEMBRA" )
assignMaterial( "concrete linear", "SHAPE", [ "top flange lin 1", "top flange lin 2" ] )
assignGeometry( "beam fl top", "SHAPE", [ "top flange lin 1", "top flange lin 2" ] )
setElementClassType( "SHAPE", [ "top flange non-lin" ], "MEMBRA" )
assignMaterial( "concrete", "SHAPE", [ "top flange non-lin" ] )
assignGeometry( "beam fl top", "SHAPE", [ "top flange non-lin" ] )
setElementClassType( "SHAPE", [ "web lin 1", "web lin 2" ], "MEMBRA" )
assignMaterial( "concrete linear", "SHAPE", [ "web lin 1", "web lin 2" ] )
assignGeometry( "beam web", "SHAPE", [ "web lin 1", "web lin 2" ] )
setElementClassType( "SHAPE", [ "web non-lin" ], "MEMBRA" )
assignMaterial( "concrete", "SHAPE", [ "web non-lin" ] )
assignGeometry( "beam web", "SHAPE", [ "web non-lin" ] )
#Reinforcement and prestress
setReinforcementAspects( [ "upper reinforcement", "lower reinforcement" ] )
assignMaterial( "reinforcement", "SHAPE", [ "upper reinforcement", "lower reinforcement" ] )
```

```
assignGeometry( "As", "SHAPE", [ "upper reinforcement", "lower reinforcement" ] )
resetElementData( "SHAPE", [ "upper reinforcement", "lower reinforcement" ] )
setReinforcementDiscretization( [ "upper reinforcement", "lower reinforcement" ], "ELEMENT" )
setReinforcementAspects( [ "upper prestress tendon", "lower prestress tendon" ] )
assignMaterial( "prestress", "SHAPE", [ "upper prestress tendon", "lower prestress tendon" ] )
assignGeometry( "prestress", "SHAPE", [ "upper prestress tendon", "lower prestress tendon" ] )
resetElementData( "SHAPE", [ "upper prestress tendon", "lower prestress tendon" ] )
setReinforcementDiscretization( [ "upper prestress tendon", "lower prestress tendon" ], "ELEMENT" )
setReinforcementAspects( [ "Line 1", "Line 2", "Line 3", "Line 4", "Line 5", "Line 6", "Line 7", "Line 8", "Line 9", "Line
10", "Line 11", "Line 12", "Line 13", "Line 14", "Line 15", "Line 16", "Line 17", "Line 18", "Line 19", "Line 20", "Line
21", "Line 22", "Line 23", "Line 24", "Line 25", "Line 26", "Line 27", "Line 28", "Line 29", "Line 30", "Line 31", "Line
32", "Line 33", "Line 34", "Line 35", "Line 36", "Line 37" ] )
assignMaterial( "stirrups", "SHAPE", [ "Line 1", "Line 2", "Line 3", "Line 4", "Line 5", "Line 6", "Line 7", "Line 8", "Line
9", "Line 10", "Line 11", "Line 12", "Line 13", "Line 14", "Line 15", "Line 16", "Line 17", "Line 18", "Line 19", "Line
20", "Line 21", "Line 22", "Line 23", "Line 24", "Line 25", "Line 26", "Line 27", "Line 28", "Line 29", "Line 30", "Line
31", "Line 32", "Line 33", "Line 34", "Line 35", "Line 36", "Line 37" ] )
assignGeometry( "stirrups", "SHAPE", [ "Line 1", "Line 2", "Line 3", "Line 4", "Line 5", "Line 6", "Line 7", "Line 8",
"Line 9", "Line 10", "Line 11", "Line 12", "Line 13", "Line 14", "Line 15", "Line 16", "Line 17", "Line 18", "Line 19",
"Line 20", "Line 21", "Line 22", "Line 23", "Line 24", "Line 25", "Line 26", "Line 27", "Line 28", "Line 29", "Line 30",
"Line 31", "Line 32", "Line 33", "Line 34", "Line 35", "Line 36", "Line 37" ] )
resetElementData( "SHAPE", [ "Line 1", "Line 2", "Line 3", "Line 4", "Line 5", "Line 6", "Line 7", "Line 8", "Line 9",
"Line 10", "Line 11", "Line 12", "Line 13", "Line 14", "Line 15", "Line 16", "Line 17", "Line 18", "Line 19", "Line 20",
"Line 21", "Line 22", "Line 23", "Line 24", "Line 25", "Line 26", "Line 27", "Line 28", "Line 29", "Line 30", "Line 31",
"Line 32", "Line 33", "Line 34", "Line 35", "Line 36", "Line 37" ] )
setReinforcementDiscretization( [ "Line 1", "Line 2", "Line 3", "Line 4", "Line 5", "Line 6", "Line 7", "Line 8", "Line 9",
"Line 10", "Line 11", "Line 12", "Line 13", "Line 14", "Line 15", "Line 16", "Line 17", "Line 18", "Line 19", "Line 20",
"Line 21", "Line 22", "Line 23", "Line 24", "Line 25", "Line 26", "Line 27", "Line 28", "Line 29", "Line 30", "Line 31",
"Line 32", "Line 33", "Line 34", "Line 35", "Line 36", "Line 37" ], "ELEMENT" )
#Interface
createConnection( "Interface", "INTER", "SHAPEEDGE" )
setParameter( "GEOMETRYCONNECTION", "Interface", "MODE", "AUTO" )
attachTo( "GEOMETRYCONNECTION", "Interface", "SOURCE", "support1", [[ 1110, 0, 0 ]] )
attachTo( "GEOMETRYCONNECTION", "Interface", "SOURCE", "support2", [[ 4470, 0, 0 ]] )
attachTo( "GEOMETRYCONNECTION", "Interface", "SOURCE", "load2", [[ 3510, 506, 0 ]] )
attachTo( "GEOMETRYCONNECTION", "Interface", "SOURCE", "load1", [[ 150, 506, 0 ]] )
setElementClassType( "GEOMETRYCONNECTION", "Interface", "STLIIF" )
assignMaterial( "Interface material", "GEOMETRYCONNECTION", "Interface" )
assignGeometry( "Interface geometry", "GEOMETRYCONNECTION", "Interface" )
setParameter( "GEOMETRYCONNECTION", "Interface", "FLIP", False )
resetElementData( "GEOMETRYCONNECTION", "Interface" )
createConnection( "interface spreader beam", "INTER", "SHAPEEDGE" )
setParameter( "GEOMETRYCONNECTION", "interface spreader beam", "MODE", "AUTO" )
attachTo( "GEOMETRYCONNECTION", "interface spreader beam", "SOURCE", "load1", [[ 187.5, 556, 0 ]] )
attachTo( "GEOMETRYCONNECTION", "interface spreader beam", "SOURCE", "load1", [[ 112.5, 556, 0 ]] )
attachTo( "GEOMETRYCONNECTION", "interface spreader beam", "SOURCE", "load2", [[ 3547.5, 556, 0 ]] )
attachTo( "GEOMETRYCONNECTION", "interface spreader beam", "SOURCE", "load2", [[ 3472.5, 556, 0 ]] )
setElementClassType( "GEOMETRYCONNECTION", "interface spreader beam", "STLIIF" )
assignMaterial( "Interface material", "GEOMETRYCONNECTION", "interface spreader beam" )
assignGeometry( "Interface geometry", "GEOMETRYCONNECTION", "interface spreader beam" )
setParameter( "GEOMETRYCONNECTION", "interface spreader beam", "FLIP", False )
resetElementData( "GEOMETRYCONNECTION", "interface spreader beam" )

## Mesh properties
```

setElementSize(["left rectangular", "right rectangular", "top flange lin 1", "web lin 1", "bottom flange lin 1", "Inclined bot lin 1", "Inclined top lin 1", "top flange non-lin", "web non-lin", "bottom flange non-lin", "Inclined bot non-lin", "Inclined top non-lin", "top flange lin 2", "web lin 2", "bottom flange lin 2", "Inclined bot lin 2", "Inclined top lin 2", "load1", "load2", "support1", "support2", "lower reinforcement", "upper reinforcement", "lower prestress tendon", "upper prestress tendon", "spreader beam", "Line 1", "Line 2", "Line 3", "Line 4", "Line 5", "Line 6", "Line 7", "Line 8", "Line 9", "Line 10", "Line 11", "Line 12", "Line 13", "Line 14", "Line 15", "Line 16", "Line 17", "Line 18", "Line 19", "Line 20", "Line 21", "Line 22", "Line 23", "Line 24", "Line 25", "Line 26", "Line 27", "Line 28", "Line 29", "Line 30", "Line 31", "Line 32", "Line 33", "Line 34", "Line 35", "Line 36", "Line 37"], 20, -1, True)
setMesherType(["left rectangular", "right rectangular", "top flange lin 1", "web lin 1", "bottom flange lin 1", "Inclined bot lin 1", "Inclined top lin 1", "top flange non-lin", "web non-lin", "bottom flange non-lin", "Inclined bot non-lin", "Inclined top non-lin", "top flange lin 2", "web lin 2", "bottom flange lin 2", "Inclined bot lin 2", "Inclined top lin 2", "load1", "load2", "support1", "support2", "lower reinforcement", "upper reinforcement", "lower prestress tendon", "upper prestress tendon", "spreader beam", "Line 1", "Line 2", "Line 3", "Line 4", "Line 5", "Line 6", "Line 7", "Line 8", "Line 9", "Line 10", "Line 11", "Line 12", "Line 13", "Line 14", "Line 15", "Line 16", "Line 17", "Line 18", "Line 19", "Line 20", "Line 21", "Line 22", "Line 23", "Line 24", "Line 25", "Line 26", "Line 27", "Line 28", "Line 29", "Line 30", "Line 31", "Line 32", "Line 33", "Line 34", "Line 35", "Line 36", "Line 37"], "HEXQUAD")
clearMidSideNodeLocation(["left rectangular", "right rectangular", "top flange lin 1", "web lin 1", "bottom flange lin 1", "Inclined bot lin 1", "Inclined top lin 1", "top flange non-lin", "web non-lin", "bottom flange non-lin", "Inclined bot non-lin", "Inclined top non-lin", "top flange lin 2", "web lin 2", "bottom flange lin 2", "Inclined bot lin 2", "Inclined top lin 2", "load1", "load2", "support1", "support2", "lower reinforcement", "upper reinforcement", "lower prestress tendon", "upper prestress tendon", "spreader beam", "Line 1", "Line 2", "Line 3", "Line 4", "Line 5", "Line 6", "Line 7", "Line 8", "Line 9", "Line 10", "Line 11", "Line 12", "Line 13", "Line 14", "Line 15", "Line 16", "Line 17", "Line 18", "Line 19", "Line 20", "Line 21", "Line 22", "Line 23", "Line 24", "Line 25", "Line 26", "Line 27", "Line 28", "Line 29", "Line 30", "Line 31", "Line 32", "Line 33", "Line 34", "Line 35", "Line 36", "Line 37"])
generateMesh([])

##Analyses
addAnalysis("Analysis LB6 stirrups L")
addAnalysisCommand("Analysis LB6 stirrups L", "LINSTA", "Structural linear static")
setAnalysisCommandDetail("Analysis LB6 stirrups L", "Structural linear static", "OUTPUT(1)/SELTYP", "USER")
addAnalysisCommandDetail("Analysis LB6 stirrups L", "Structural linear static", "OUTPUT(1)/USER")
addAnalysisCommandDetail("Analysis LB6 stirrups L", "Structural linear static",
"OUTPUT(1)/USER/STRESS(1)/TOTAL/CAUCHY/GLOBAL")
addAnalysisCommandDetail("Analysis LB6 stirrups L", "Structural linear static",
"OUTPUT(1)/USER/STRESS(2)/TOTAL/CAUCHY/PRINCI")
addAnalysisCommandDetail("Analysis LB6 stirrups L", "Structural linear static",
"OUTPUT(1)/USER/FORCE(1)/REACTI/TRANSL")
addAnalysisCommandDetail("Analysis LB6 stirrups L", "Structural linear static",
"OUTPUT(1)/USER/DISPLA(1)/TOTAL/TRANSL/GLOBAL")
addAnalysisCommandDetail("Analysis LB6 stirrups L", "Structural linear static",
"OUTPUT(1)/USER/STRAIN(1)/TOTAL/GREEN/GLOBAL")

addAnalysis("Analysis LB6 stirrups NL")
addAnalysisCommand("Analysis LB6 stirrups NL", "NONLIN", "Structural nonlinear")
setAnalysisCommandDetail("Analysis LB6 stirrups NL", "Structural nonlinear", "EXECUT/EXETYP", "LOAD")
setAnalysisCommandDetail("Analysis LB6 stirrups NL", "Structural nonlinear", "EXECUT/EXETYP", "LOAD")
addAnalysisCommandDetail("Analysis LB6 stirrups NL", "Structural nonlinear", "EXECUT(1)/LOAD/LOADNR")
setAnalysisCommandDetail("Analysis LB6 stirrups NL", "Structural nonlinear", "EXECUT(1)/LOAD/LOADNR", 3)
addAnalysisCommandDetail("Analysis LB6 stirrups NL", "Structural nonlinear", "EXECUT(2)/LOAD/LOADNR")
setAnalysisCommandDetail("Analysis LB6 stirrups NL", "Structural nonlinear", "EXECUT(2)/LOAD/LOADNR", 2)
setAnalysisCommandDetail("Analysis LB6 stirrups NL", "Structural nonlinear",
"EXECUT(3)/LOAD/STEPS/EXPLIC/SIZES", "0.000100000 0.0500000(20) 0.025 (75)")
addAnalysisCommandDetail("Analysis LB6 stirrups NL", "Structural nonlinear", "EXECUT(3)/LOAD/LOADNR")

```
setAnalysisCommandDetail( "Analysis LB6 stirrups NL", "Structural nonlinear", "EXECUT(3)/LOAD/LOADNR", 1 )
setAnalysisCommandDetail( "Analysis LB6 stirrups NL", "Structural nonlinear", "EXECUT(3)/ITERAT/MAXITE", 10 )
setAnalysisCommandDetail( "Analysis LB6 stirrups NL", "Structural nonlinear",
"EXECUT(3)/ITERAT/CONVER/DISPLA", False )
addAnalysisCommandDetail( "Analysis LB6 stirrups NL", "Structural nonlinear",
"EXECUT(3)/ITERAT/CONVER/ENERGY" )
setAnalysisCommandDetail( "Analysis LB6 stirrups NL", "Structural nonlinear",
"EXECUT(3)/ITERAT/CONVER/ENERGY", True )
setAnalysisCommandDetail( "Analysis LB6 stirrups NL", "Structural nonlinear",
"EXECUT(3)/ITERAT/CONVER/ENERGY/TOLCON", 0.001 )
setAnalysisCommandDetail( "Analysis LB6 stirrups NL", "Structural nonlinear", "EXECUT(3)/ITERAT/MAXITE", 150 )
setAnalysisCommandDetail( "Analysis LB6 stirrups NL", "Structural nonlinear", "OUTPUT(1)/SELTYP", "USER" )
addAnalysisCommandDetail( "Analysis LB6 stirrups NL", "Structural nonlinear", "OUTPUT(1)/USER" )
addAnalysisCommandDetail( "Analysis LB6 stirrups NL", "Structural nonlinear",
"OUTPUT(1)/USER/DISPLA(1)/TOTAL/TRANSL" )
addAnalysisCommandDetail( "Analysis LB6 stirrups NL", "Structural nonlinear",
"OUTPUT(1)/USER/STRESS(1)/TOTAL/CAUCHY/GLOBAL" )
addAnalysisCommandDetail( "Analysis LB6 stirrups NL", "Structural nonlinear",
"OUTPUT(1)/USER/STRESS(2)/TOTAL/CAUCHY/PRINCI" )
addAnalysisCommandDetail( "Analysis LB6 stirrups NL", "Structural nonlinear",
"OUTPUT(1)/USER/FORCE(1)/REACTI/TRANSL" )
addAnalysisCommandDetail( "Analysis LB6 stirrups NL", "Structural nonlinear",
"OUTPUT(1)/USER/STRAIN(1)/CRACK" )
addAnalysisCommandDetail( "Analysis LB6 stirrups NL", "Structural nonlinear",
"OUTPUT(1)/USER/STRAIN(2)/CRKWDT" )
addAnalysisCommandDetail( "Analysis LB6 stirrups NL", "Structural nonlinear",
"OUTPUT(1)/USER/STRAIN(3)/CRKSUM" )
addAnalysisCommandDetail( "Analysis LB6 stirrups NL", "Structural nonlinear",
"OUTPUT(1)/USER/STRAIN(4)/TOTAL/GREEN/GLOBAL" )
```